Performance Analysis of Space-Time Block Coded Systems with Channel Estimation

Shan Cheng

M.Eng, Zhejiang University, P.R. China

A THESIS SUBMITTED

FOR THE DEGREE OF DOCTOR OF PHILOSOPHY

DEPARTMENT OF ELECTRICAL AND COMPUTER ENGINEERING

NATIONAL UNIVERSITY OF SINGAPORE

May 2006

Ackowledgements

I would like to express my profound gratitude to my supervisors: Dr. A. Nallanathan and Prof. P. Y. Kam, for their invaluable guidance and endless patience throughout the entire duration of my Ph.D course.

I would like to thank my parents and other family members. Their love, patience and understanding have accompanied me all the way along. Special regards to my beloved grandfather, who departed us in 2004.

I am also thankful to my labmates and friends, not only for their resourceful discussion in research, but their friendship that makes my life pleasant and joyful.

Abstract

The capacity of a wireless communication system can be increased considerably by using multiple transmit and receive antennas. The high-data rate provided by such Multiple-input-multiple-output (MIMO) communication systems make them promising for next-generation wireless communication. Among these MIMO techniques, space-time block coding (STBC) has attracted much research interests. The orthogonal structure of STBC allows every symbol transmitted to be decoupled at the receiver using only linear processing. Such a symbol-by-symbol receiver is simple yet efficient in implementation to achieve the gain provided by both transmit and receive diversities.

To coherently decode the STBC, ideally perfect channel state information (CSI) would be used at the receiver. As the channel information is not readily available at the receiver in practice, channel estimates are used to perform coherent detection. The optimum maximum likelihood detector with imperfect channel estimation is far more computationally complicated than the optimum symbol-by-symbol detector when perfect CSI is available. In this dissertation, we propose a symbol-by-symbol channel estimation receiver for STBC systems, which is sub-optimal but computationally efficient for implementation and can be applied to many channel models with their corresponding estimators. In particular, we analyze the bit error probability (BEP) performance of this receiver when minimum mean-square-error estimates are available.

We first derive the BEP performance of the receiver with maximum ratio combining. The BEP result is given in an exact closed-form expression, which shows the direct dependence on the mean square error of the channel estimator and the signal-to-noise ratio. An upper bound is derived to show the maximum diversity order achievable, which is determined by the product of the numbers of transmit and receive antennas. We then extend the work to a system with selection combining schemes, where the receiver

selects the received signal from one or several antennas with best quality according to the channel estimates. Exact closed-form BEP expressions are derived. The results show that the selection combining systems achieve the diversity gain provided by the total number of available receive antennas, but independent of the number of antennas chosen.

Transmit antenna selection (TAS) is a technique to exploit the transmit diversity other than space-time coding. We propose a TAS/STBC system based on the channel estimation receiver structure. Through a feedback link, the receiver informs the transmitter which antennas to be used for STBC transmission. This TAS/STBC system has a simple yet energy-saving structure, while exhibits the full diversity order provided by the total number of transmit antennas. An BEP upper bound is obtained in closed-form for the TAS/STBC systems. Particularly, exact BEP expressions are derived for TAS/STBC systems with single receive antenna, which is important in down-link communication scenarios.

The designs of orthogonal STBC so far known are limited. Unitary space-time modulation (USTM) treats the whole transmission block as one constellation, and thus provides many more possible designs while maintaining the orthogonality of signals. However, there is no systematic method for optimal USTM constellation design. Thus we propose a systematic algorithm to search for sub-optimal differential unitary space-time modulation. The constellations generated by the proposed simple algorithm exhibits better performance than the well-known cyclic codes.

In summary, in this dissertation, space-time block coded communication systems with imperfect channel estimation are extensively studied and BEP performances are obtained in closed-forms. Improved algorithms for constellation search are also proposed for differential unitary space-time modulation systems.

Contents

List of Figures

List of Tables

List of Abbreviations

1BTW	first-order Butterworth
2G	second-generation
3BTW	third-order Butterworth
3G	third-generation
4G	fourth-generation
ADF	actual decision feedback
AWGN	additive white Gaussian noise
BEP	bit error probability
BLAST	Bell-lab Layered Architecture of Space-Time
COD	complex orthogonal designs
CSI	channel state information
DD	differential detection
DF	decision-feedback
DSC	dual selection combining
DUSTM	differential unitary space-time modulation
EGC	equal gain combining
EM	expectation-maximization
GSC	generalized selection combing
i.i.d.	independent, identically distributed
IDF	ideal decision feedback
KF	Kalman filter
MGF	moment generating function
MIMO	multiple-input-multiple-output
MISO	multi-input-single-output
ML	maximum-likelihood
MMSE	minimum mean squared error
MRC	maximum ratio combining
MSE	mean square error
p.d.f.	probability density function
PEP	pair-wise error probability
PSAM	pilot-symbol assisted modulation
PSD	power spectrum density
PSK	phase-shift keying
r.v.	random variable
Rx	receive antenna
SBS	symbol-by-symbol
SEP	symbol error probability
SIMO	single-input-multi-output
SNR	signal-to-noise ratio
SSC	single selection combining
STBC	space-time block codes
STTC	space-time trellis codes
TAS	transmit antenna selection
TCM	trellis coded modulation
Tx	transmit antenna
USTM	unitary space-time modulation
WF	Wiener filter
WLAN	wireless local-area network

Chapter 1

Introduction

The ability to communicate with people on the move has evolved remarkably ever since 1897, when Guglielmo Marconi first demonstrated continuous contacts with ships sailing the English Channel using a radio. More recently, the technical breakthroughs in digital and radio frequency circuit fabrication, new large-scaled circuit integration and other miniaturization technologies have made the portable radio equipment smaller, cheaper by orders of magnitude for the past several decades, and will continue at an even greater pace for the coming decade.

1.1 Introduction to Wireless Communication Systems

More than 20 years have passed since the first-generation mobile communication services using analog technology started in the early 1980s. From the early 1990s, digital cellular and cordless systems (e.g. PDC/GSM/IS54 and IS95) have been introduced around the world as the second-generation (2G) mobile communication systems capable of voice and short message communications. The 2G services have been integrated into our everyday life and society extensively after explosive growth for more than ten

years. Meanwhile, research and standardization have been carried out toward the third-generation (3G) mobile communication systems for the past decade, which is capable of mobile multimedia services and international seamless roaming. Telecommunication companies worldwide are now beginning to deploy 3G systems for commercial service and we will soon be in the era of 3G. As for researchers and engineers, they have already put their sight to a highly reliable and higher capacity wireless digital system, which is to be called as the fourth-generation (4G) mobile radio communication systems. The next-generation requires high speed reliable wireless systems for multimedia communications services, including voice, data, and image.

The tremendous growth in demand for higher data rates is now out of the range of current radio technology. Given a limited radio spectrum, the only way to support high data rates is to develop new spectrally efficient radio communication techniques.

1.2 A Literature Review of Space-Time Coding

Wireless transmission under fading channel suffers from attenuation due to destructive addition of multipaths in the propagation media and due to the reflections,scatterings, interference from other users, etc.. Severe attenuation makes it impossible for the receiver to determine the transmitted signal unless some less-attenuated replica of the transmitted signal is provided to the receiver. This resource is called diversity and it is the single most important contributor to reliable wireless communications. Examples of diversity techniques are, but not restricted to, *temporal diversity*, *frequency diversity*, and *antenna diversity*. Conventionally, to exploit the receive antenna diversity, multiple antennas are deployed at the receiver side to increase the link capacity. Recently, researchers have found ways to deploy multiple antennas at the transmit side to further increase the communication capacity. Thus a communication system with multiple transmit and multiple receive antennas is formed, and we call it a

multiple-input-multiple-output (MIMO) communication system. A brief historic review of MIMO systems is given as following

1.2.1 Simulcast

The concept of MIMO system can be traced back to 1987, when Winters proposed two basic communication systems in [1]: communication between multiple mobiles and a base station with multiple antennas, and communication between two mobiles each with multiple antenna. This is the first paper that discusses the use of multiple antennas at both ends of the radio link and gives the capacity expression in terms of the eigenvalues of the channel matrix. In [2] and [3], the authors considered a communication network where several adjacent base station simultaneously transmit the same message. Later, and independently, a similar scheme was suggested by Seshadri and Winters for a single base station in which copies of the same symbol are transmitted through multiple antennas at different times [4], hence creating an artificial multipath distortion. Then a maximum likelihood sequence estimator or a minimum mean squared error (MMSE) equalizer is used to resolve multipath distortion and obtain diversity gain.

1.2.2 BLAST

Subsequently, Foschini presented the analytical basis of MIMO systems in [5, 6], where he proposed key expressions for the enhanced capacity of MIMO systems. Reference [5] is the first paper in which Bell Lab proposed BLAST (Bell-lab Layered Architecture of Space-Time) as communication architecture for the transmission of high data rates using multiple antennas at the transmitter and receiver. In the proposed BLAST system the data stream is divided into blocks which are distributed among the transmit antennas. In vertical BLAST sequential data blocks are distributed among consecutive antenna elements, whereas in diagonal BLAST, they are circularly rotated among the antenna elements. The BLAST signal processing algorithms used at the receiver are

the heart of the technique. At the bank of receiving antennas, high-speed signal processors look at the signals from all the receive antennas simultaneously, first extracting the strongest substream and then proceeding with the remaining weaker signals, which are easier to recover once the stronger signals have been removed as a source of interference. Again, the ability to separate the substreams depends on the slight differences in the way the different substreams propagate through the environment.

Under the widely used theoretical assumption of independent Rayleigh scattering, the theoretical capacity of the BLAST architecture grows roughly linearly with the number of antennas, even when the total transmitted power is held constant. The laboratory prototype [7] has already demonstrated spectral efficiencies of 20 - 40 bits per second per Hertz of bandwidth, numbers which are simply unattainable using standard techniques.

1.2.3 Space-Time Trellis Codes

Although the first attempt to jointly encode multiple transmit antennas was presented in [4], the key development of the space-time coding concept was originally revealed in [8] in the form of trellis codes. Somehow, space-time trellis codes (STTC) can be viewed as an improvement of the delay diversity scheme. The example trellis diagram of delay diversity is shown below in Figure 1.1. By simply swapping the odd row of the delay-diversity trellis diagram, 2.5-dB coding gain can be achieved in (b), which is a typical STTC. Note that the STTC is also a delay scheme except the delayed PSK symbol is π-shifted on the constellation plane if it is an odd symbol, and kept the same if even symbol.

The STTC requires a multidimensional Viterbi algorithm at the receiver for decoding. It was shown in [8, 9] that the STTC provides a diversity gain equal to the number of transmit antennas, and a coding gain which depends on the complexity of the code, i.e., number of states in the trellis, without any loss in the bandwidth efficiency. Still

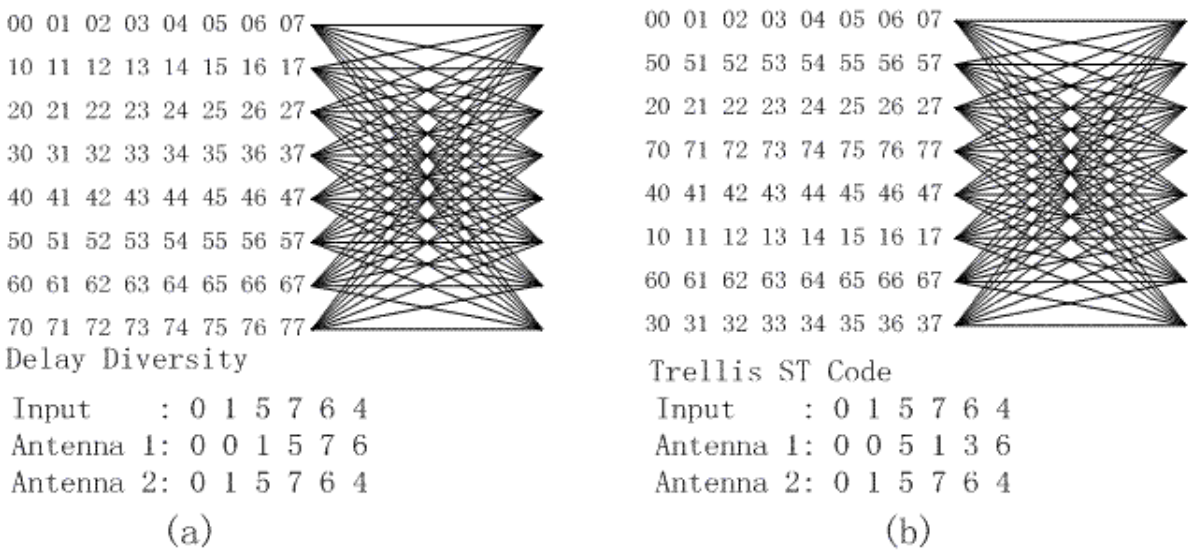

Fig. 1.1: Delay Diversity and Trellis Space-Time Code (Figure partially taken from [8])

the gain of STTC is achieved at the expense of a complex receiver. Since the debut of STTC in [8], there has been extensive research aiming at improving the performance of the original STTC designs. Numerous works have been proposed for new code construction and designs of STTC systems, e.g., [10–14]. However, only marginal gains over the original scheme by Tarokh *et al.* were obtained in most cases.

1.2.4 Space-Time Block Codes

The receiver complexity of STTC increases exponentially with the dimensions of code, trellis, etc., thus making the receiver structure quite complex in implementation. The popularity of space-time coding really took off with the discovery of the so-called space-time block codes (STBC) . In [15], Alamouti presented a perfectly beautiful code that exploits the transmit diversity with two transmit antennas. The orthogonal construction of the code allows simple linear processing at the receiver, in contrast to the multi-dimensional Viterbi decoder at the STTC receiver. Later, Tarokh *et al.* generalized this scheme for an arbitrary number of transmit antennas[16, 17]. While STBC

provides the same diversity gain as STTC, it gives none or minimal coding gain.

The coherent detection in both [15] and [17] requires perfect channel state information (CSI) at the receiver. In [18] and [19], differential STBC schemes were presented, respectively, for Alamouti's code and generalized STBC with an arbitrary number of transmit antennas. The authors use some mapping skills to determine the next block to be sent. Similar topics were also addressed in [20–22]. More complicated differential designs can also be found in [23, 24] to combat the fading.

1.2.5 Unitary Space-Time Modulation

More recently, a new scheme called unitary space-time modulation (USTM) [25] was proposed to achieve channel capacity. The key idea of the USTM is that the whole transmitting matrix is treated as one constellation signal. By constraining the signal matrix to be unitary, it is proved that the USTM is still capacity-achieving. Moreover, there are more available designs compared to the limited designs of STBC, since the entry of USTM signal matrix is no longer restricted to the combination of certain symbols from a given constellation set. In [25] and [26], it is pointed out that the ultimate capacity of a multiple-antenna wireless link is determined by the number of symbol periods between fades. The diversity gain achievable is constrained by the coherent symbol periods. For example, in the extreme case where the channel fluctuates every symbol period, only one transmitter antenna can be usefully employed. Theoretically speaking, one could increase the capacity indefinitely by employing a greater number of transmit antennas, but the capacity appears to increase only logarithmically in this number - not a very effective way to boost capacity. So, actually, there is no point in making the number of transmitter antennas greater than the length of the coherence interval.

When the coherence interval becomes large compared with the number of transmitter antennas, the normalized capacity approaches the capacity obtained as if the receiver knew the propagation coefficients. The magnitudes of the time-orthogonal signal vectors

become constants that are equal for all transmitter antennas. In this regime, all of the signaling information is contained in the directions of the random orthogonal vectors, the receiver learns the propagation coefficients, and the channel becomes similar to the classical Gaussian channel.

1.2.6 MIMO Applications in 3G Wireless Systems and Beyond

The 3G mobile communications standards are expected to provide a wide range of bearer services, spanning from voice to high-rate data services, supporting rates of at least 144 kb/s in vehicular, 384 kb/s in outdoor-to-indoor and 2 Mb/s in indoor as well as pico-cellular applications. In work beyond 3G the target is to achieve data rates in the order of 1Gbps for low-mobility solutions, and 100 Mbps for full coverage and mobility.

Some techniques like turbo coding have brought the utilization of a single link very close to Shannon limits of channel capacity. The next step is the creation of multiple links between a terminal and a base station,which is fulfilled by MIMO systems. So far there is little commercial implementation of MIMO in cellular systems and deployed 3G systems. The existing MIMO applications include the Lucent's BLAST chip, which is demonstrated to be capable of high data rate transmissions. Recently, the third-generation partnership project has standardized the MIMO models in IEEE 802.16. Also in the standard IEEE 802.11n for wireless local-area network (WLAN) , MIMO techniques have been adopted to boost the data rate. Multiple commercialized models with MIMO techniques have recently been released [27], which demonstrate impressive performances gains against the existing products. With the potential communication capacity provided by the multiple links, it is predictable that MIMO systems will be incorporated into wireless communications of most kinds: cellular, WLAN, or even satellite in the near future.

1.3 Research Objective

As addressed above, the MIMO system is an attractive solution for the next-generation wireless communication. In our research, we have concentrated on the performance analysis of STBC systems and differential unitary space-time modulation (DUSTM) .

In STBC system designs,it is assumed that the receiver knows perfectly the CSI for coherent detection. Although differential schemes have been proposed which do not need CSI, they actually require the channel coherence interval to be long enough for efficient detection. When the channel fluctuates faster, the performance of differential schemes degrades considerably. This makes an STBC system that is incorporated with channel estimation more preferable in practice. The objective of our research is to develop such a receiver with channel estimation and analyze its performance under fading channels.

Space-time coding provides us with transmit diversity additional to those diversities conventionally used. In receive antenna diversity, we have several combining schemes to utilize those received signals undergoing more-or-less independent fading, e.g., equal gain combining (EGC) , maximum ratio combining (MRC) , selection combining, etc. Those schemes can all be independently adopted at the receiver for MIMO systems. Thus, it also aroused our interest in what the performance will be if we introduce these receive diversity combining techniques together with the transmit diversity provided by the space-time coding. Also, for a communication system with multiple transmit antennas, if the transmitter knows the channel fading, it can choose the best one or several antennas to transmit. The design and performance of such an adaptive transmit system is also within our research interests.

Furthermore, finding good constellation sets is always of interest for MIMO systems. This problem is still open since so far there is no systematic optimum solution. We also put our effort into this approach to find simple yet efficient constellation designs.

1.4 Structure of the Dissertation

In the next chapter, we present some basic background on MIMO systems and the channel model adopted in this dissertation.

In Chapter 3, we propose a symbol-by-symbol channel-estimation receiver structure for STBC systems. Based on the receiver structure, we analyze the performance of the receiver with imperfect channel estimation.

In Chapter 4, we concentrate on the receiver structure developed in Chapter 3 together with selection combining. Bit error probability (BEP) performance analysis is carried out based on the order statistics of estimated SNR.

We further extend the work by feeding back the channel estimation information to the transmitter to optimize the performance. We present an adaptive transmit antenna selection system. System structure and performance analysis are presented.

In Chapter 5, two new methods for DUSTM constellation design are proposed. The algorithms are described in detail. The new methods provide better performance than the known cyclic codes, yet with limited increase in computational complexity.

1.5 Research Contributions

We develop a receiver structure for STBC system with imperfect channel estimation in Chapter 3. As the optimal maximum-likelihood receiver is rather computationally complex, we use a symbol-by-symbol receiver for its simplicity. Based on this symbol-by-symbol receiver structure, performance analysis is carried out to predict its BEP with phase-shift keying modulations. A closed-form BEP expression is obtained for those STBC's where energy is uniformly distributed along time. For those STBC's where energy is not uniform along time, upper and lower bounds are obtained to predict the performance. These two bounds are in most cases so close to each other that they provide good approximation to the exact BEP. Simulations conducted validate our theoretical

predictions.

Based on the results obtained in Chapter 3, we further extend our work to channel estimation STBC systems with receive antenna selection combining and transmit antenna selection in Chapter 4 and 5, respectively. In both receive antenna selection and transmit antenna selection schemes, the choice of the transmit/receive antennas are based on the channel estimates, i.e., it is a channel-estimation based system, so that no expensive and complex signal-to-noise ratio (SNR) evaluation is needed at the receiver, which reduces the complexity of the receiver to a large extent. Based on the system structures, BEP performances are derived and presented in closed-form expressions.

We improved the cyclic code presented in [28, 29] for DUSTM. To utilize the space-time diversity more than the cyclic code does, we introduce a rotation matrix in code construction. The proposed constellations are in quasi-diagonal matrix forms. Detailed diversity product calculations are analyzed to simplify the search process. The final algorithm improves the diversity product significantly compared to the cyclic codes, with limited increase or even reduced computational complexity.

Chapter 2

MIMO Communication Systems in Wireless Fading Channels

In this Chapter, we present the information theoretic basis for MIMO systems and derive their ultimate capacity. We then introduce the MIMO channel models adopted in this dissertation, and detailed simulation algorithms for multiple channel models are described and then verified. The principles of Kalman Filter and Wiener Filter are also described for state-space and Jakes' channel model, respectively. The PSK signaling used in this dissertation is defined at the end.

2.1 Capacity of MIMO Systems

2.1.1 MIMO Communication System

We consider a MIMO system with M_T transmit and N_R receive antennas as shown in Figure 2.1.

The transmitted signal at time p is represented by an $1 \times M_T$ row vector $\boldsymbol{S} = [s_{p1}, s_{p2}, \ldots, s_{pM_T}]$. The total transmitted power is constrained to E_0, regardless of the

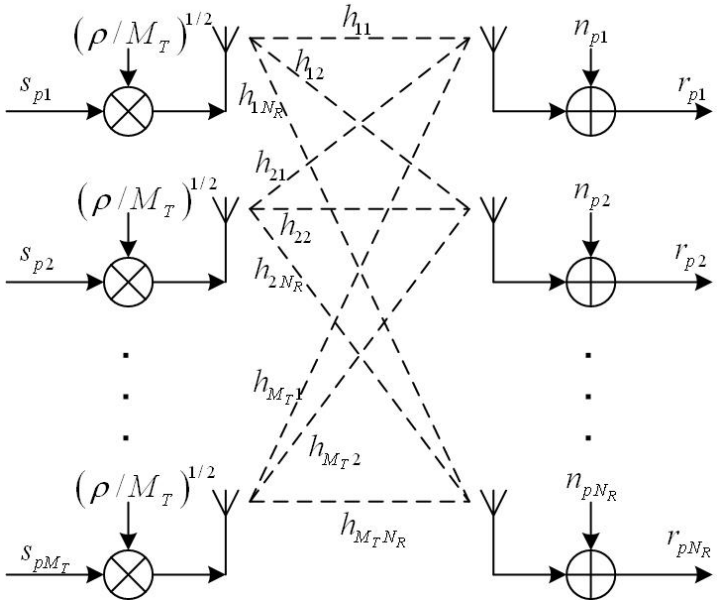

Fig. 2.1: Wireless link with M_T transmitter and N_R receiver antennas. Every receiver antenna is connected to every transmitter antenna through an independent, random, unknown propagation coefficient having Rayleigh distributed magnitude and uniformly distributed phase. Normalization ensures that the total expected transmitted power is independent of M_T for a fixed ρ

number of transmit antennas M_T. This power constraint gives

$$\mathrm{E}\left[\sum_{i=1}^{M_T} |s_{pi}|^2\right] = E_0. \tag{2.1}$$

If we assume that the signals transmitted from individual transmit antennas have equal power, then the power from each single transmit antenna is given by E_0/M_T.

The transmitted signal bandwidth is narrow enough, so its frequency response can be considered as flat.

The channel is described by an $M_T \times N_R$ complex matrix, denoted by $\boldsymbol{H}$, whose element h_{il} represents the propagation coefficient between the i-th transmit antenna and the l-th receive antenna. For normalization purposes we assume that the received power for each of the N_R receive antennas is equal to the total transmitted power, i.e., E_0.

Thus we obtain the normalization constraint for the elements of $\boldsymbol{H}$, in a channel with fixed coefficients, as

$$\mathrm{E}\left[\sum_{i=1}^{M_T}|h_{il}|^2\right] = M_T,\ l = 1, 2, \ldots, N_R. \tag{2.2}$$

We assume that the channel matrix is known to the receiver when using a method such as transmitting training preamble. On the other hand, in most situations we assume that the channel parameters are not known at the transmitter.

At the receiver, the additive noise is described by an $1 \times N_R$ row matrix $\boldsymbol{N} = [n_{p1}, n_{p2}, \ldots, n_{pN_R}]$, whose components are statistically independent, complex, zero-mean Gaussian variables. The receive antennas have identical noise powers of N_0.

The received signal is represented by an $1 \times N_R$ row matrix, denoted by $\boldsymbol{R} = [r_{p1}, r_{p2}, \ldots, r_{pN_R}]$, where each complex component refers to a receive antenna.

The average SNR at each receiver branch is given by

$$\rho = E_0/N_0. \tag{2.3}$$

Normalizing the transmitted signal with (2.3), we can re-define the power constraints (2.1) as

$$\frac{1}{M_T}\mathrm{E}\left[\sum_{i=1}^{M_T}|s_{pi}|^2\right] = 1 \tag{2.4}$$

and the received vector can then be represented as

$$\boldsymbol{R} = \sqrt{\rho/M_T}\boldsymbol{H}\boldsymbol{S} + \boldsymbol{N}. \tag{2.5}$$

2.1.2 Capacity Analysis of MIMO Communication System

The channel capacity is defined as the maximum possible transmission rate such that the probability of error is arbitrarily small. The well-known Shanon capacity is

given by

$$C = W \log_2(1 + \rho), \tag{2.6}$$

where W is the bandwidth of the communication channel and ρ is the SNR. In the system mentioned above, according to the singular value decomposition, the channel matrix $\boldsymbol{H}$ can be written as

$$\boldsymbol{H} = \boldsymbol{V}\boldsymbol{D}\boldsymbol{U}^{\dagger}, \tag{2.7}$$

where $\boldsymbol{U}$ and $\boldsymbol{V}$ are $M_T \times M_T$ and $N_R \times N_R$ unitary matrices, respectively, and $\boldsymbol{D}$ is an $M_T \times N_R$ non-negative diagonal matrix given by

$$\boldsymbol{D} = \begin{bmatrix} \sum_{\boldsymbol{r}} & \mathbf{0} \\ \mathbf{0} & \mathbf{0} \end{bmatrix}, \tag{2.8}$$

where $\sum_{\boldsymbol{r}} = diag\,[\sigma_1, \sigma_2, \ldots, \sigma_\tau]$, σ_i are the singular values of matrix $\boldsymbol{H}$ (also the non-negative square roots of the eigenvalues of $\boldsymbol{H}^{\dagger}\boldsymbol{H}$) and τ is the rank of $\boldsymbol{H}$.

We define $m = \min(M_T, N_R)$, and

$$\boldsymbol{Q} = \begin{cases} \boldsymbol{H}^{\dagger}\boldsymbol{H} & N_R < M_T \\ \boldsymbol{H}\boldsymbol{H}^{\dagger} & N_R \geq M_T \end{cases}. \tag{2.9}$$

Thus we calculate the eigenvalues of $\boldsymbol{H}^{\dagger}\boldsymbol{H}$ by finding the roots of the characteristic polynomial

$$\det(\lambda \boldsymbol{I}_{\boldsymbol{m}} - \boldsymbol{Q}) = 0. \tag{2.10}$$

Substituting (2.7) into (2.5) and right-multiplying with $\boldsymbol{U}$, we get

$$\boldsymbol{R}' = \sqrt{\rho}\boldsymbol{D}\boldsymbol{S}' + \boldsymbol{N}', \tag{2.11}$$

where $\boldsymbol{R}' = \boldsymbol{R}\boldsymbol{U}$, $\boldsymbol{S}' = \boldsymbol{S}\boldsymbol{V}$ and $\boldsymbol{N}' = \boldsymbol{N}\boldsymbol{U}$.

Since $\tau = \text{rank}(\boldsymbol{H}) = \text{rank}(\boldsymbol{H}^{\dagger}\boldsymbol{H})$, for the $M_T \times N_R$ matrix $\boldsymbol{H}$, the rank τ is at

most $m = \min(M_T, N_R)$, which means that at most m of its singular values are non-zero. By substituting the entries σ_i in (2.11) we get for the received components

$$\begin{aligned} r'_l &= \sigma_l s'_{pl} + n'_l,\ l = 1, 2, \ldots, \tau \\ r'_l &= n'_l,\ l = \tau + 1, \tau + 2, \ldots, N_R \end{aligned} . \tag{2.12}$$

(2.12) indicates that the received components r'_l, $l = \tau+1, \tau+2, \ldots, N_R$, do not depend on the transmitted signal, i.e., the channel gain is zero. On the other hand, received components r'_{pl}, for $l = 1, 2, \ldots, \tau$ depend only on the transmitted component s'_{pl}. Thus the equivalent MIMO channel from (2.11) can be considered as consisting of τ uncoupled parallel channels. For example, if $M_T > N_R$, as the rank of $\boldsymbol{H}$ cannot be higher than N_R, (2.12) shows that there will be at most N_R non-zero gain sub-channels in the equivalent MIMO channel. On the other hand if $N_R > M_T$, there will at most M_T non-zero gain sub-channels in the equivalent MIMO channel.

Note that in the above models the sub-channels are uncoupled and thus their capacities are summed up. Assuming that transmit power from each antenna is identical, from (2.1), we can estimate the overall channel capacity as

$$C = W \sum_{i=1}^{\tau} \log_2 \left(1 + \frac{\rho}{M_T} \sigma_i^2\right). \tag{2.13}$$

(2.13) can also be written as

$$C = W \log_2 \left[\det \left(\boldsymbol{I_m} + \frac{\rho}{M_T} \boldsymbol{Q}\right)\right]. \tag{2.14}$$

As the non-zero eigenvalues of $\boldsymbol{H}^\dagger \boldsymbol{H}$ and $\boldsymbol{H}\boldsymbol{H}^\dagger$ are the same, the capacity of a channel with matrix $\boldsymbol{H}$ and $\boldsymbol{H}^\dagger$ are the same. When the channel parameters are known at the transmitter, the capacity given by (2.14) can be increased by assigning the transmitting power to various antennas according to the "water-filling" rule. The power allocated to channel i is given by

$$E_i = \left(\mu - \frac{E_0/\rho}{\sigma_i^2}\right)^+ \quad i = 1, 2, ..., \tau, \tag{2.15}$$

where a^+ denotes $\max(a, 0)$ and μ is determined so that

$$\sum_{i=1}^{r} E_i = E_0. \tag{2.16}$$

The MIMO channel capacity is then

$$C = W \sum_{i=1}^{\tau} \log_2 \left[1 + \frac{\rho}{E_0} (\sigma_i^2 \mu - E_0/\rho)^+ \right] = W \sum_{i=1}^{\tau} \left(\log_2 \frac{\rho \mu \sigma_i^2}{E_0} \right)^+. \tag{2.17}$$

For example, let's consider a transmit-diversity system with M_T transmit antennas and one receive antenna. The channel matrix is

$$\boldsymbol{H} = (h_1, h_2, ...h_{M_T})^T. \tag{2.18}$$

As $\boldsymbol{H}^\dagger \boldsymbol{H} = \sum_{i=1}^{M_T} |h_i|^2$, by applying formula (2.14) we get for the capacity

$$C = W \log_2 \left(1 + \sum_{i=1}^{M_T} |h_i|^2 \frac{\rho}{M_T} \right). \tag{2.19}$$

This capacity corresponds to that of linear maximum ratio combining at the receiver. In the case when the channel matrix elements are equal and normalized as follows:

$$|h_1|^2 = |h_2|^2 = ...|h_{M_T}|^2 = 1, \tag{2.20}$$

then the capacity becomes

$$C = W \log_2 (1 + \rho). \tag{2.21}$$

This expression applies to the case when the transmitter does not know the channel. For coordinated transmissions, when the transmitter knows the channel, we can apply the capacity formula from (2.17). As the rank of the channel matrix is one, there is only one term in the sum in (2.17) and only one non-zero eigenvalue given by

$$\sigma^2 = \sum_{i=1}^{M_T} |h_i|^2. \tag{2.22}$$

And from the normalization condition, we have

$$\mu = E_0(1 + \frac{1}{\rho\sigma^2}). \tag{2.23}$$

So we get for the capacity

$$C = W \log_2 \left(1 + \sum_{i=1}^{M_T} |h_i|^2 \cdot \rho\right). \tag{2.24}$$

For $M_T = 8$ and SNR of 20dB, the capacity is 9.646bps/Hz.

2.2 Mobile Radio Channels and MMSE Channel Estimation

The communication channel is the physical medium that connects the transmitter and the receiver. It can be a pair of wires or an optical fiber for wired communication. In wireless communication environment, the channel is the free space between the transmit and the receive antennas. The presence of reflecting objects and scatterers in the space creates a constantly changing environment that dissipates the signal energy in amplitude, phase, and time. These effects result in multiple versions of the transmitted signal that arrive at the receiving antenna, displaced with respect to one another in time and spatial orientation. The random phases and amplitudes of the different multipath components cause fluctuations in strength of the received signal. There are many channel models in the literature. Here, in this dissertation, we consider the non frequency-selective Rayleigh channel models, where the received signal is a summation of many reflected signals and the signal with maximum delay does not exceed the symbol duration. Assume that the multipaths are independent and statistically identical, and the number of multipaths is large enough, the fading gain can then be modeled as a complex symmetric Gaussian random variable. The absolute value of the complex Gaussian gain follows the Rayleigh distribution. This non frequency-selective slow Rayleigh fading channel is the most

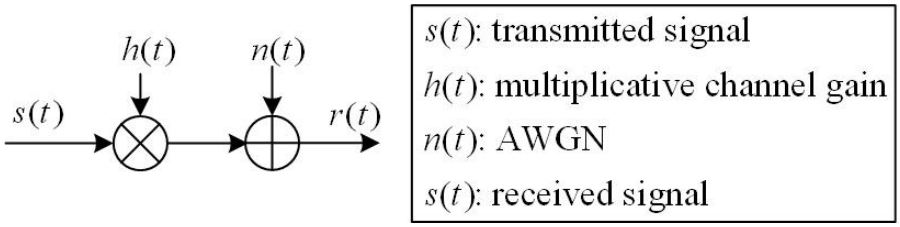

Fig. 2.2: Communication channel model

widely accepted channel model for narrowband transmission systems.

Fig.2.2 depicts the baseband channel model we used in this dissertation. The multiplicative channel gain is introduced by the medium while the additive white Gaussian noise (AWGN) arises from the electronic circuitry in the receiver.

At the receiver, perfect sampling is assumed and thus the multiplicative channel gain is assumed to be piecewise constant for a symbol duration. The model in Fig. 2.2 can be expressed in a discrete-time representation for the m -th symbol duration $[mT_s, (m+1)T_s]$ where T_s is the symbol duration time

$$r(m) = s(m)h(m) + n(m). \tag{2.25}$$

2.2.1 Rayleigh Fading Channel with Butterworth power spectrum density

In this section, we consider non-frequency-selective slow Rayleigh fading channels with first-order Butterworth, and third-order butterworth models. The Butterworth spectrum [30] is commonly used to model the fading process on mobile satellite channels or other channels where the fading process is exponentially correlated. Here, the in-phase component $x_c(m) = \mathrm{Re}\,[h(m)]$ and the quadrature-phase component $x_s(m) = \mathrm{Im}\,[h(m)]$ of each fading process is the output of a state-space model, i.e., $x_c(m)$ or $x_s(m) = \boldsymbol{B}\boldsymbol{x}(m)$, where the state vector $\boldsymbol{x}(m)$ evolves according to a model.

$$\boldsymbol{x}(m+1) = \boldsymbol{F}\,\boldsymbol{x}(m) + \boldsymbol{G}\,\boldsymbol{w}(m) \tag{2.26}$$

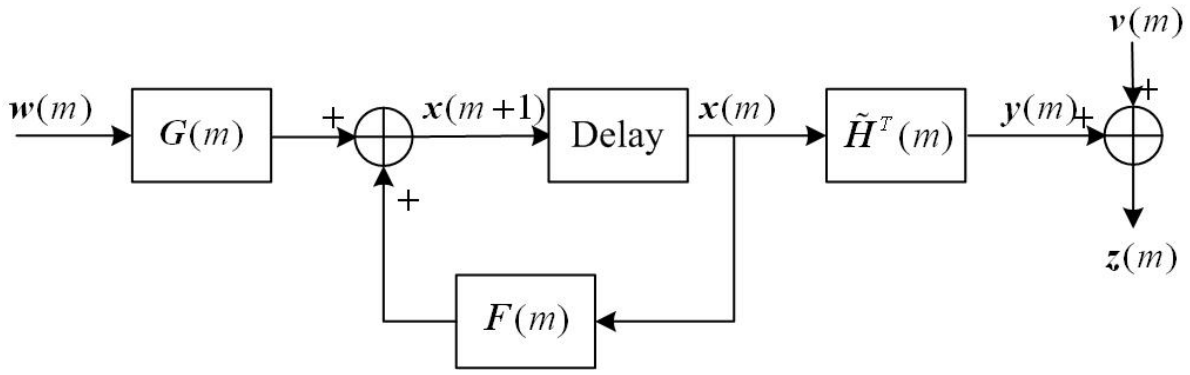

Fig. 2.3: Markov signal model for Kalman filter

of appropriate dimension. Substituting (2.26) into the communication channel model (2.25), one get the received signal model depicted in Fig. 2.3, where $\{\boldsymbol{w}(m)\}_{m=0}^{\infty}$ and $\{\boldsymbol{v}(m)\}_{m=0}^{\infty}$ are zero mean, independent Gaussian processes with covariance matrices given by

$$\mathrm{E}[\boldsymbol{w}(m)\boldsymbol{w}^T(m')] = \boldsymbol{W}\delta_{mm'} \tag{2.27a}$$

$$\mathrm{E}[\boldsymbol{v}(m)\boldsymbol{v}^T(m')] = \boldsymbol{V}\delta_{mm'} \tag{2.27b}$$

$$\mathrm{E}[\boldsymbol{w}(m)\boldsymbol{v}^T(m')] = 0 \tag{2.27c}$$

After $\boldsymbol{x}(m)$ has been generated according to 2.26, it is sent to a multiplicative channel with gain $\tilde{\boldsymbol{H}}^T(m)$; a sample $\boldsymbol{z}(m)$ is obtained by further disturbing the so generated $\boldsymbol{y}(m)$ with an additive noise $\boldsymbol{v}(m)$. $\boldsymbol{z}(m)$ is the noisy sample available to the filter to recover $\boldsymbol{x}(m)$, which will be discussed in the next section. We consider here in particular the case of a first-order Butterworth (1BTW) and a third-order Butterworth (3BTW) model for the channel.

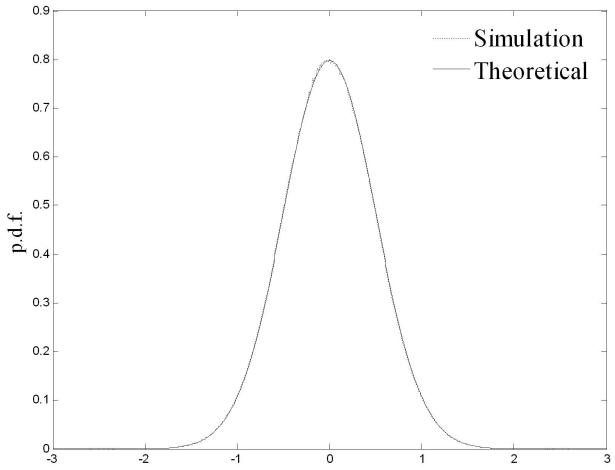

Fig. 2.4: Theoretical and simulated PDF's of the real part of the first-order Butterworth channel model with $\omega_d T_s = 0.01$ and $\sigma^2 = 0.25$. The simulated PDF is obtained by averaging 1000 repeated trials

2.2.1.1 First-Order Butterworth Channel Model

The first-order Butterworth fading process has the following power spectrum density (PSD) function:

$$S(\omega) = \frac{2\sigma^2/\omega_d}{1 + (\omega/\omega_d)^2}, \tag{2.28}$$

where ω_d is the 3dB radian frequency of the Butterworth power spectrum. The state-space realization for the Rayleigh fading channel with first-order Butterworth PSD is obtained by transforming (2.28) into time domain and solving its first order differential equation. The processes $\{x_c(m)\}_{m=0}^{\infty}$ and $\{x_s(m)\}_{m=0}^{\infty}$ are each given by a one-dimensional version of (2.26) with

$$F = \exp\left[-\omega_d T_s\right], \quad G = 1, \quad B = 1, \quad \text{and} \quad W = \sigma^2(1 - e^{-2\omega_d T_s}), \tag{2.29}$$

where T_s is the interval between discrete time points.

The output probability density function (p.d.f.) of the simulator given in (2.26) and

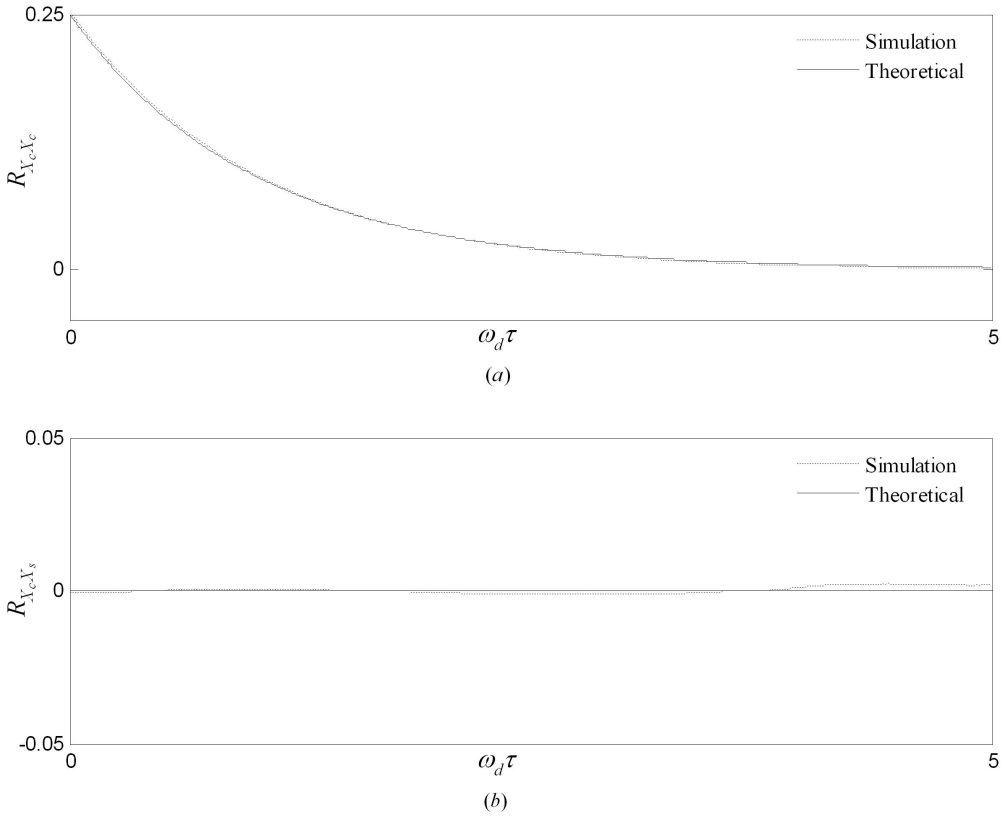

Fig. 2.5: (a)Theoretical and simulated autocorrelation function of the real part;
(b) Theoretical and simulated crosscorrelation function between the real and imaginary part ; of the first-order Butterworth channel model with $\omega_d T_s = 0.01$ *and* $\sigma^2 = 0.25$. *The simulated results are obtained by averaging 1000 repeated trials*

(2.29) is plotted in Fig. 2.4. Compared to the theoretical one, the output samples have a perfect Gaussian distribution as designed. In this dissertation, we are more interested in the channel autocorrelation function than the PSD, since the autocorrelation function would be used to evaluate the mean square error(MSE) of channel estimator. According to the 1BTW's PSD function in (2.28), the autocorrelation function is obtained by inverse Fourier transforming

$$\mathcal{R}_{x_c x_c}(\Delta m) = \mathcal{R}_{x_s x_s}(\Delta m) = \sigma^2 e^{-\omega_d T_s |\Delta m|} \tag{2.30}$$

and the cross-correlation $\mathcal{R}_{x_s x_c}(\Delta m)$ or $\mathcal{R}_{x_c x_{s(\Delta m)}}$ between the real and imaginary parts should be zero as they are zero-mean independent processes. In Fig. 2.5, we plot the simulated correlation function $\mathcal{R}_{x_c x_c}(\Delta m)$ and $\mathcal{R}_{x_c x_{s(\Delta m)}}$ for example. It is shown that they match the theoretical prediction quite well.

2.2.1.2 Third-Order Butterworth Channel Model

In the 3BTW model, the quadrature components of the continuous-time fading process each have a power density spectrum

$$S(\omega) = \frac{3\sigma^2}{\omega_d \left[1 + (\omega/\omega_d)^6\right]}. \tag{2.31}$$

The processes $\{x_c(m)\}_{k=0}^{\infty}$ and $\{x_s(m)\}_{k=0}^{\infty}$ can each be generated using a three-dimensional version of the model (2.26) with

$$\begin{aligned} \boldsymbol{x}(m) &= \begin{pmatrix} x^{(1)}(m) \\ x^{(2)}(m) \\ x^{(3)}(m) \end{pmatrix}, \boldsymbol{F} = \begin{pmatrix} 1 & \omega_d T & 0 \\ 0 & 1 & \omega_d T \\ -\omega_d T & -2\omega_d T & 1 - 2\omega_d T \end{pmatrix}, \boldsymbol{G} = \begin{pmatrix} 0 \\ 0 \\ 1 \end{pmatrix}, \\ \boldsymbol{B} &= \begin{bmatrix} 1 & 0 & 0 \end{bmatrix}, \boldsymbol{W} = 3\sigma^2 \, \omega_d T \end{aligned} \tag{2.32}$$

Note that in achieving the Markov model given in (2.26) and (2.32), approximation $\omega_d T_s << 1$ must been taken. Therefore, the simulation model is only fine for slow fading. The p.d.f of 3BTW with $\omega_d T_s = 0.001$ is plotted in 2.6. The simulated result still matches theoretical one quite well. It is reported through simulation that the simulation output has a 5% greater variance than the desired one. As the $\omega_d T_s$ further increase, the deviation from theoretical becomes more and more obvious, and thus makes the simulator deviate from theory under fast fading situations. So the usage of 3BTW is refrained to slow fading scenarios. The 3BTW PSD in (2.31) has an autocorrelation

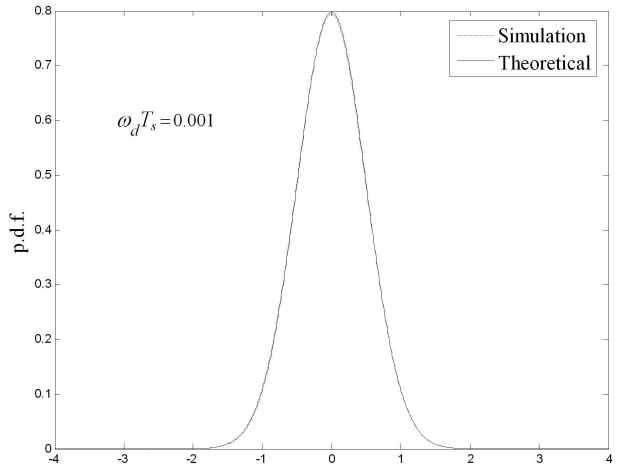

Fig. 2.6: Theoretical and simulated PDF's of the real part of the third-order Butterworth channel model with $\omega_d T_s = 0.001$ and $\sigma^2 = 0.25$. The simulated PDF is obtained by averaging 1000 repeated trials

function given by [31]

$$\mathcal{R}_{x_c x_c}(\Delta m) = \mathcal{R}_{x_s x_s}(\Delta m) = \frac{\sigma^2}{2} \sum_{l=1}^{3} e^{-\omega_d T_s |\Delta m| \cdot \sin\left(\frac{2l-1}{6}\pi\right)} \cdot \sin\left[\frac{2l-1}{6}\pi + \omega_d T_s |\Delta m| \cos\left(\frac{2l-1}{6}\pi\right)\right]. \tag{2.33}$$

The theoretical correlation functions together with simulated ones are illustrated in Fig. 2.7. Perfect matches are observed, which validates that the 3BTW simulator is still quite good under slow fading.

2.2.2 Kalman Filtering for State-Space Channel Model

When a state-space channel model is available, the Kalman filter (KF) is the optimum channel estimator. The KF is more suitable for the decision-feedback (DF) channel estimation scheme since it can operate recursively in time as symbol decisions are made. According to the state-space signal model in Fig. 2.3, the correspondent Kalman filter structure is shown in Fig. 2.8. The principle of KF is described by the following

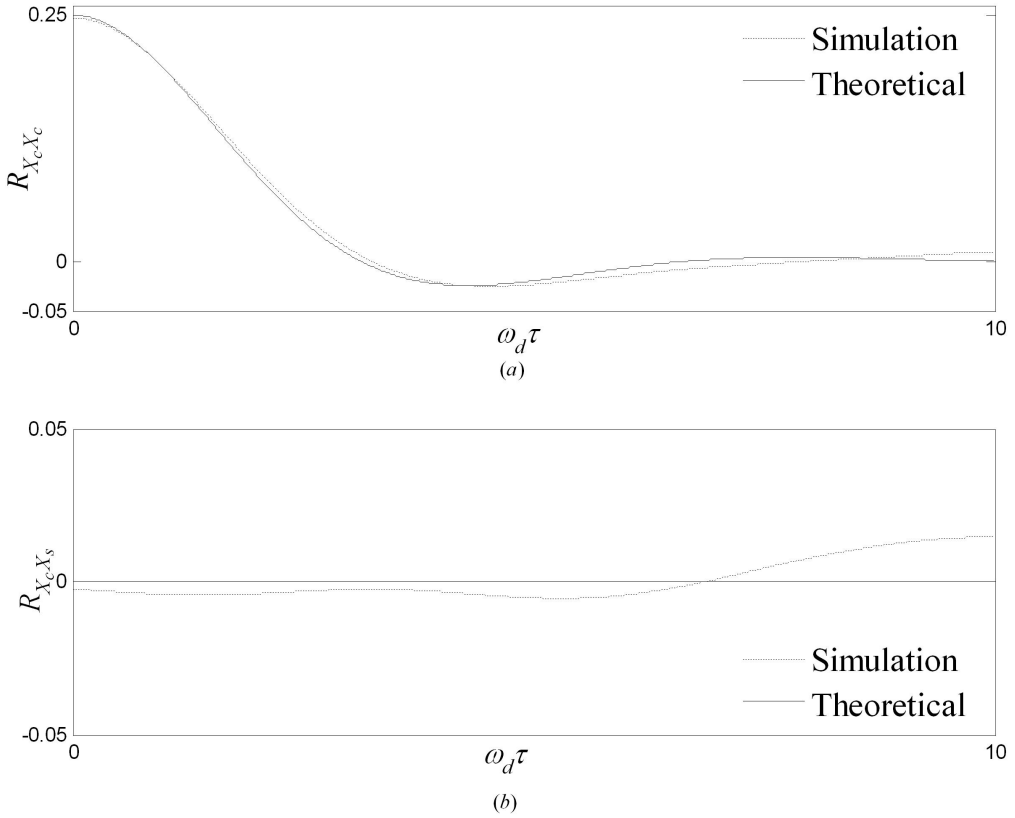

Fig. 2.7: (a)Theoretical and simulated autocorrelation function of the real part;
(b) Theoretical and simulated crosscorrelation function between the real and imaginary part ;
of the third-order Butterworth channel model with $\omega_d T_s = 0.001$ and $\sigma^2 = 0.25$. The simulated results are obtained by averaging 1000 repeated trials

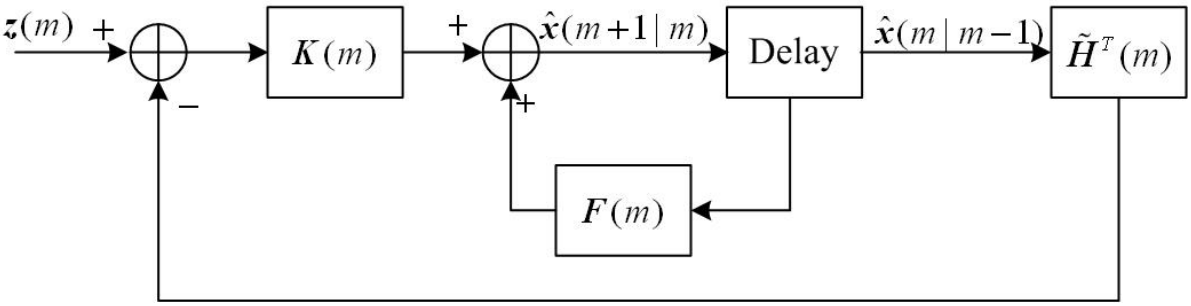

Fig. 2.8: Kalman Filter Structure

equations ([32], Chap. 3, eq.(1.9) and eq.(1.12)

$$\begin{aligned}
\boldsymbol{P}(m) &= \tilde{\boldsymbol{H}}^T(m)\boldsymbol{\Sigma}(m|m-1)\tilde{\boldsymbol{H}}(m) + \boldsymbol{V}(m) && (2.34)\\
\boldsymbol{K}(m) &= \boldsymbol{F}(m)\boldsymbol{\Sigma}(m|m-1)\tilde{\boldsymbol{H}}(m)\boldsymbol{P}^{-1}(m) && (2.35)\\
\hat{\boldsymbol{x}}(m|m) &= \hat{\boldsymbol{x}}(m|m-1) + \boldsymbol{K}(m)[\boldsymbol{z}(m) - \tilde{\boldsymbol{H}}^T(m)\hat{\boldsymbol{x}}(m|m-1)] && (2.36)\\
\boldsymbol{\Sigma}(m|m) &= \boldsymbol{\Sigma}(m|m-1) - \boldsymbol{\Sigma}(m|m-1)\boldsymbol{K}(m)\tilde{\boldsymbol{H}}(m) && (2.37)\\
\hat{\boldsymbol{x}}(m+1|m) &= \boldsymbol{F}(m)\hat{\boldsymbol{x}}(m|m) && (2.38)\\
\boldsymbol{\Sigma}(m+1|m) &= \boldsymbol{F}(m)\boldsymbol{\Sigma}(m|m)\boldsymbol{F}^T(m) + \boldsymbol{G}(m)\boldsymbol{W}(m)\boldsymbol{G}^T(m) && (2.39)
\end{aligned}$$

where $\boldsymbol{K}(m)$ is the Kalman gain; $\hat{\boldsymbol{x}}(m+1|m)$ and $\hat{\boldsymbol{x}}(m|m)$ are the predicted and updated state vector; and $\boldsymbol{\Sigma}(m+1|m)$ and $\boldsymbol{\Sigma}(m|m)$ are the predicted and updated error covariance matrices. With initialized value $\hat{\boldsymbol{x}}(0|-1)$ and $\boldsymbol{\Sigma}(0|-1)$, the KF recursively computes equations (2.34) through (2.39) and predict the MMSE estimate $\hat{\boldsymbol{x}}(m+1|m)$ for $\boldsymbol{x}(m+1)$. As the exact initial value of $\hat{\boldsymbol{x}}(0|-1)$ and $\boldsymbol{\Sigma}(0|-1)$ are unlikely known to the KF, the KF needs several periods to establish a track-on state before it can predict reliably. This initialization phase is done in communication system by sending known preambles to the receiver before data transmission.

Note that (2.34),(2.35),(2.37), and (2.39) are independent of the observation $\boldsymbol{z}(m)$, they can be calculated off-line. These equations are also known as Riccati equations. As $\boldsymbol{\Sigma}$ represents the MSE of the estimates, by solving those four equations recursively, a steady-state value of the MSE can be obtained. Especially for the one-dimensional case, the MSE has a closed-form expression as

$$\Sigma_\infty = \frac{VF^2 + G^2W\tilde{H}^2 - V + \sqrt{(V + VF^2 + G^2W\tilde{H}^2)^2 - 4V^2F^2}}{2\tilde{H}^2}. \qquad (2.40)$$

For KF more than one-dimensional, the MSE must be obtained by repeatedly computing the Riccati equations until a steady-state is reached. In Matlab, there is a **Riccati()** function in control toolbox to give readily the solution of Riccati equations.

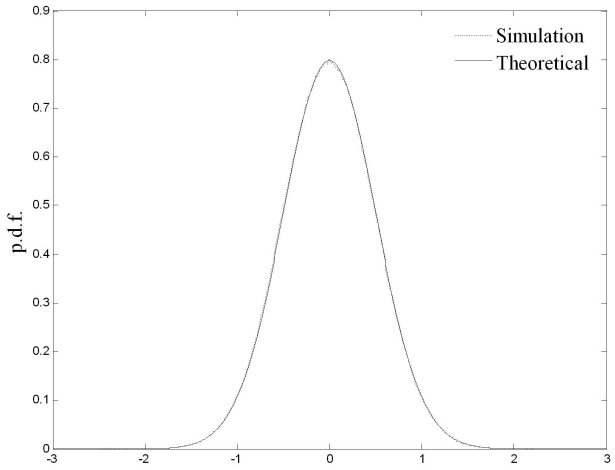

Fig. 2.9: Theoretical and simulated PDF's of the real part of the Jakes' simulator $\omega_d T_s = 0.1$ *and* $\sigma^2 = 0.25$. *The simulated PDF is obtained by averaging 1000 repeated trials*

2.2.3 Rayleigh Fading Channel with Jakes' PSD

The Jakes spectrum [33, 34] is commonly used to model the fading process for the land-mobile cellular channel. This Jakes power density spectrum is defined as

$$S(\omega) = \begin{cases} 2\sigma^2 \Big/ \omega_d \sqrt{1 - (\omega/\omega_d)^2} & |\omega| < \omega_d \\ 0 & |\omega| > \omega_d \end{cases}, \tag{2.41}$$

and its corresponding autocorrelation is given by

$$\mathcal{R}(\Delta m) = \mathrm{E}[x(m)x^T(m + \Delta m)] = \sigma^2 \, J_0(\Delta m \omega_d T_s), \tag{2.42}$$

where $J_0(\cdot)$ is the zero-th order Bessel function of the first kind.

Over the last three decades, there are quite a lot of different approaches to the simulation model of Jakes' model [34]. The most well-known mathematical reference model by Clarke [33] and its simplified simulation model by Jakes [34] have been widely accepted for Rayleigh fading channels for more than thirty years. However, the Jakes' simulator is a deterministic model, and the result is questionable when generating mul-

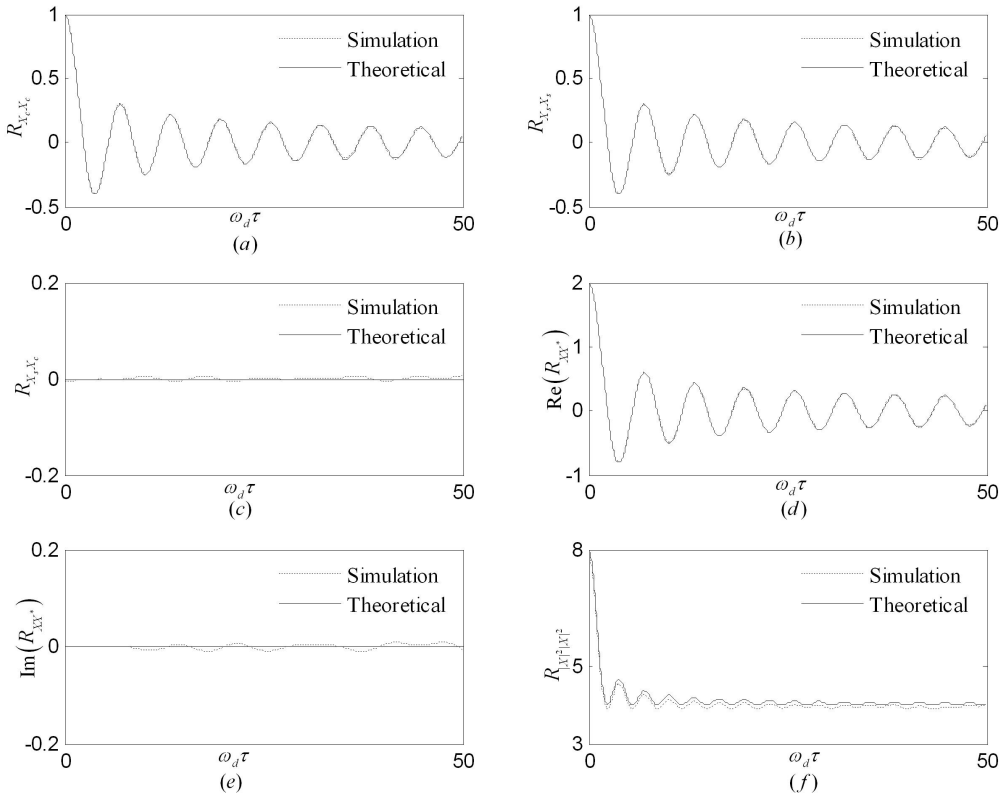

Fig. 2.10: *(a)Autocorrelation function of the real part;*
(b)Autocorrelation function of the imaginary part;
(c) Cross-correlation function between the real and imaginary part ;
(d)Real part of the autocorrelation function of the entire complex process;
(e)Imaginary part of the autocorrelation function of the entire complex process;
(f)Autocorrelation function of the output envelope;
of the Jakes' channel model with $\omega_d T_s = 0.01$ *and* $\sigma^2 = 0.25$. *The simulated results are obtained by averaging 1000 repeated trials*

tiple uncorrelated fading process for frequency selective fading channels and MIMO channels. Therefore, modifications of Jakes' simulator have been proposed [35–38]. Recently in [39], it was pointed out that the Jakes' model is wide-sense nonstationary when averaged across the physical ensemble of fading channels. An improved simulator

was also proposed in [39] to remove the stationarity problem by introducing random phase shifts in the low-frequency oscillators. However, it was addressed in [39] and later proved in [40] that the higher order statistics of this simulator do not match the desired ones. In [41], the authors propose a new sum-of-sinusoids model by re-introducing the randomness to Doppler frequency and initial phase of the sinusoids. This model was further improved in [42] by introducing path gain randomness to the model. This model has autocorrelations of quadrature components, the cross correlation of the quadrature components, and the autocorrelation of the complex envelope that match the desired ones exactly, even if the number of sinusoids used to generate the channel fading is as small as eight. Some higher order statistics are also proved to match the theoretical ones when the number of sinusoids approaches infinity, while good convergence can be reached even when the number of sinusoids is small. We choose to use this simulator [42] in this dissertation for Jakes' PSD.

The normalized low-pass fading process of the statistical sum-of-sinusoids simulation model is defined by

$$h(m) = x_c(m) + jx_s(m) \tag{2.43a}$$

$$x_c(m) = \frac{2}{\sqrt{N}} \sum_{n=1}^{N} \cos\psi_n \cdot \cos(m\omega_d T_s \cos\alpha_n + \phi) \tag{2.43b}$$

$$x_s(m) = \frac{2}{\sqrt{N}} \sum_{n=1}^{N} \sin\psi_n \cdot \cos(m\omega_d T_s \cos\alpha_n + \phi) \tag{2.43c}$$

where

$$\alpha_n = \frac{(2n-1)\pi + \theta}{4N}, \ n = 1, 2, ..., M. \tag{2.44}$$

The distribution p.d.f of the channel samples are plotted in Fig. 2.9, where simulated curve has a perfect match with theoretical one. The statistical property of the above

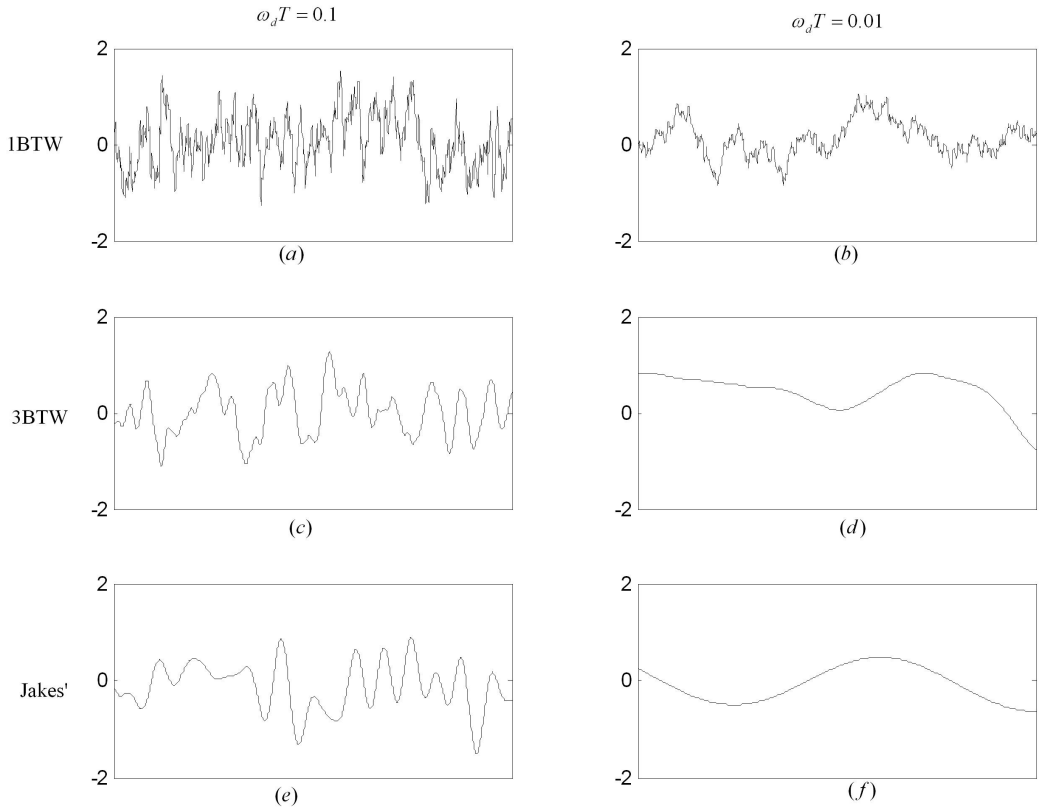

Fig. 2.11: Channel samples of size one thousand for different models

process is proven to be

$$\mathcal{R}_{x_c x_c}(\Delta m) = \mathcal{R}_{x_s x_s}(\Delta m) = J_0(\Delta m \omega_d T_s) \tag{2.45a}$$

$$\mathcal{R}_{x_c x_s}(\Delta m) = \mathcal{R}_{x_s x_c}(\Delta m) = 0 \tag{2.45b}$$

$$\mathcal{R}_{|x_c|^2|x_s|^2} = 4 + 4J_0^2(\Delta m \omega_d T_s) + \frac{4 + 2J_0(2\Delta m \omega_d T_s)}{N} \overset{N\to\infty}{=} 4 + 4J_0^2(\Delta m \omega_d T_s) \tag{2.45c}$$

Some statistics of the above simulator are presented in Fig. 2.10. The autocorrelations matches the theoretical ones perfectly. Even for envelope autocorrelation function $R_{|x_c|^2|x_s|^2}$, the improved simulator has a good match with the desired one.

The channel samples of the mentioned three channel models, namely, first-order

Butterworth channel, third-order Butterworth channel and Jakes' fading channel, are compared in Fig. 2.11. It is clear from Fig. 2.11 that with the same normalized fade rate $\omega_d T_s$, the first-order Butterworth channel fluctuates more rapidly than the third-order one. The 1BTW also has more small-scaled fluctuation. This can be explained from the PSD's of the Butterworth channel model. The 3BTW has a more compact frequency response than the 1BTW so that less high-frequency components are allowed to pass the 3BTW filter, thus making the output more smooth.

2.2.4 Wiener Filtering for Jakes' Model

In this dissertation, we use Wiener filter (WF) as estimator of fading channel with Jakes' model. The design criterion of WF is to minimize the mean square error between the desired filter output and the actual output. A commonly used WF model is depicted in Fig. 2.12, where the prediction output for current sample is a weighted summation of L_w previously received samples stored in vector $\tilde{\boldsymbol{y}}(m) = [y(m-1), y(m-2), \ldots, y(m-L_w)]^T$, where $y(m)$ is the noisy observation of $x_c(m)$ or $x_s(m)$. The tap-weight vector $\boldsymbol{w} = [w_1, w_2, \ldots, w_{L_w}]^T$ can be predetermined if the characteristic of Jakes' channel is known. This well-known MMSE estimator is described by the following equations

$$\hat{h}(m) = \boldsymbol{w}^T(m)\tilde{\boldsymbol{y}}(m) \tag{2.46}$$

$$\boldsymbol{w}(m) = \boldsymbol{\Xi}^{-1}\boldsymbol{p}(m) \tag{2.47}$$

$$\boldsymbol{\Xi} = \mathrm{E}[\tilde{y}_{il}(m)\tilde{y}_{il}^T(m)] \tag{2.48}$$

$$\boldsymbol{p}(m) = \mathrm{E}[h_{il}(m)\tilde{y}_{il}^T(m)] \tag{2.49}$$

The MSE of this WF is given by $\mathcal{R}(0) - \boldsymbol{p}^T(m)\boldsymbol{w}(m)$.

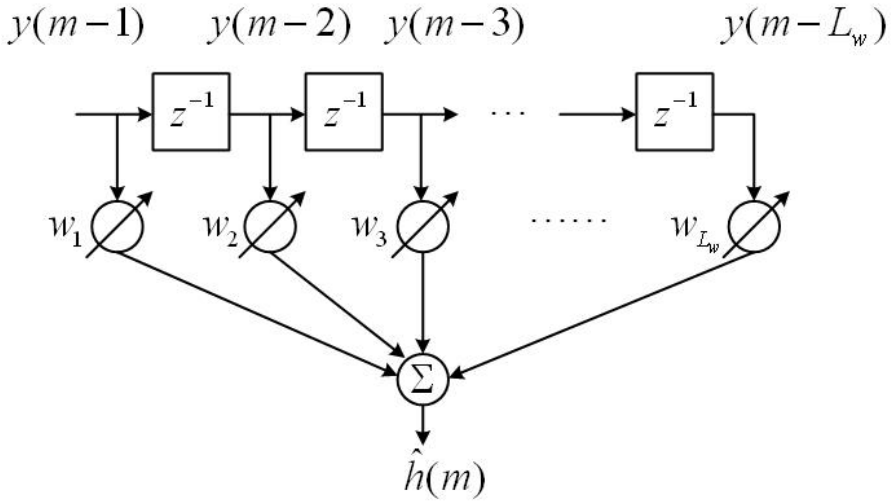

Fig. 2.12: Linear Wiener Filter Model

2.3 Phase-Shift Keying Modulation

The information is carried by the phase of the transmitted signal in phase-shift keying (PSK) modulation, so that the signaling has a constant envelope. Consider M-ary PSK modulation, where one symbol carries $log_2 M$ bits of information. The transmitted signal for $mT_s \leq t \leq (m+1)T_s$ is given by

$$s(t) = \sqrt{\frac{2E_s}{T_s}} \cos[\omega_c t - \phi(m)], \qquad mT_s \leq t \leq (m+1)T_s, \tag{2.50}$$

where E_s is the symbol energy, T_s is the symbol duration and $\phi(m)$ takes on one of the value from set $\{\phi_l | \phi_l = 2\pi l/M, l = 0, 1, ...M-1\}$ in the m-th symbol interval. Using the following set of orthonormal basis functions

$$\varphi_0(t) = \sqrt{\frac{2}{T_s}} \cos(\omega_c t), \ \varphi_1(t) = \sqrt{\frac{2}{T_s}} \sin(\omega_c t).$$

We can represent $s(t)$ in (2.50) in the m-th symbol interval in a complex discrete representation

$$s(m) = \sqrt{E_s} e^{j\phi(m)}. \tag{2.51}$$

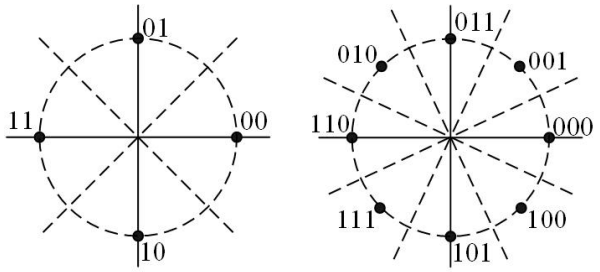

(a) QPSK (b) 8PSK

Fig. 2.13: Constellation maps of PSK signaling

The constellation maps of QPSK and 8PSK are illustrated in 2.13, where Gray coding is applied to minimize the BEP performance. Recall the signal model in 2.2, the received signal now can be expressed in a complex baseband representation

$$r(m) = \sqrt{E_s}\kappa(m)\angle[\phi(m) + \theta(m)] + n(m), \tag{2.52}$$

where $\kappa(m)$ and $\theta(m)$ denotes the magnitude and phase of the Rayleigh fading process $h(m)$, respectively; and $n(m)$ is AWGN process.

2.4 Summary

In this chapter, we analyzed the capacity of MIMO wireless communication systems from a perspective of information theory. The result clearly shows that the achievable capacity is significantly enhanced by deploying multiple antennas at the transmit side.

In communication, the mobile channel model plays a very important role from preliminary research to implementation phase. We assume the well-known Rayleigh fading channel model, which is non-frequency-selective and all the links are uncorrelated from one another. Butterworth and Jakes' channel models are in particular picked for the analysis works throughout this dissertation. We presented the detailed simulation algorithms for those selected channel models, as well as numerical verifications of those models.

Chapter 3

BEP Performance Analysis of Orthogonal Space-Time Block Codes

We present a symbol-by-symbol, channel estimation receiver for a space-time block coded system, and derive its analytical performance on a slow, nonselective, Rayleigh fading channel. Exact, closed-form expressions for its BEP performance for M -ary phase shift-keying modulations are obtained. These results are important because they enable us to theoretically predict the actual performance achievable under practical conditions with channel estimation error. Our BEP expressions show explicitly the dependence of BEP on the mean square error of the channel estimates, which in turn depend on the channel fading model and the channel estimator used. Tight upper bounds are presented that show more clearly the dependence of the BEP on various system parameters. Simulation results using various fading models are obtained to demonstrate the validity of the analysis.

3.1 Introduction

Over the years, various diversity techniques have been studied for reliable high-rate data transmission on wireless channels. Recently, it has been shown that the use of transmit diversity coupled with the use of space-time coding is an effective technique to improve the performance of wireless systems [6, 8, 15, 17, 43].

STBC [15, 17] in particular have been shown to have a simple decoder structure. A STBC with two transmit antennas was first introduced in [15], and it was later generalized to STBC's for an arbitrary number of transmit antennas in [17]. It was also pointed out in [17] that the full-rate complex orthogonal designs (COD) only exist for two transmit antennas [15], and COD for more than two transmit antennas must have a rate less than one. The existence theorems in [17] were later amended and improved in [44] and [45, 46]. Based on the generalized orthogonal code structure defined in [17], the designs of orthogonal STBC were extensively studied subsequently, and COD for more than two transmit antennas were presented in [47–51]. Achievable optimal rates of STBC were presented in [52]. Recently, a systematic COD algorithm has been proposed in [53]. The designs in [53] reach the optimal rate proposed in [52] for an arbitrary number of transmit antennas when the antenna number is less than eighteen. There are also non-orthogonal approaches for STBC, which can be found in [54–61],etc. The non-orthogonal structure involves the detection with interference from within the signal block, so that the performance would be worse than the equivalent orthogonal ones. However, we can achieve full-rate with those designs, meanwhile, there are more available non-orthogonal designs. Theoretically, equalization techniques or equivalent measures can also be taken to suppress the interferences from within the signal block.

The beauty of STBC is that its orthogonal structure allows detection of individual symbols to be performed independently using only linear processing. This was shown in [15] for the case of perfect CSI, i.e., when channel estimation is perfect. In practice, however, perfect channel estimates are not readily available, and one expects to perform

simultaneous data detection and channel estimation. The aim of this chapter is to develop a simple, symbol-by-symbol (SBS) , detection-estimation receiver for STBC. Following the approach in [62], we arrive at a receiver structure which is similar to that in [15], with the actual channel fading gains replaced by their MMSE estimates. The detector-estimator receiver structure shows that the symbol detection problem and the channel estimation problem are separate. While the detector structure is fixed, the optimum MMSE channel estimator structure depends on knowledge of the statistical model of the channel fading process and the additive channel noise. Having arrived at the receiver structure, we next obtain simple, exact, closed-form expressions for its BEP performance with PSK modulations, namely, BPSK, QPSK and 8-PSK. The BEP results show clearly the dependence of BEP on the MSE of the channel estimates, which in turn depends on the channel fading model, the additive channel noise level, and the estimator structure used. A tight upper bound is also presented to show more explicitly the dependence of the BEP on the various system parameters. Finally the theoretical results are validated with simulations.

To avoid the channel estimation problem, differential space-time modulation techniques with differential detection (DD) which requires no knowledge of the channel have been proposed in [18, 26, 29, 63, 64]. However, the performance of DD may degrade considerably when the channel fades rapidly. Joint channel estimation and data detection to approach coherent performance has thus been the preferred approach, and much previous work on this has appeared in the literature. In [65] and [66], an iterative space-time receiver based on the expectation-maximization (EM) algorithm has been proposed, and improved on later in [67] by using a symbol interleaver in the EM loop, and good performance has been obtained in fast fading at the expense of high computational complexity.

Most of the performance analysis for space-time coded systems is in terms of pairwise error probability (PEP) . For STBC systems, BEP is preferred over PEP. PEP is

more suitable for space-time trellis codes. Some BEP performance analysis results for STBC can be found in [68–73]. In [68], it was assumed that the receiver knows the CSI perfectly, and exact BEP expressions of BPSK and QPSK for Alamouti's code [15] with one receive antenna were presented for both coherent and differential detection. The coherent results in [68] can be shown to be a special case of ours in this dissertation when there is no channel estimation error. In [69], the author obtained a PEP expression based on perfect CSI knowledge using the moment generating function method, and the result is not in explicit form. Symbol error probability expressions for M -PSK and M -QAM constellations over the keyhole Nakagami- m channel were presented in [70] assuming perfect CSI at the receiver. More recently in [71], an accurate BEP upper bound is proposed for a symbol-by-symbol detector, but again, the result in [71] requires perfect CSI for decoding. Channel estimation error was taken into account in [72]. But, computation of the eigenvalues of a correlation matrix is necessary for the PEP analysis approach in [72]. Reference [73] used Alamouti's code [15] and pilot-symbol assisted modulation (PSAM) for channel estimation, but the BEP result is given in an unsolved integral form that must be evaluated by a numerical approach. In summary, the BEP results in [68–70, 72, 73] are either not explicit or assume perfect CSI at the receiver. In [74], a receiver for the Alamouti's STBC of [15] with two transmit and one receive antenna was proposed. This receiver uses decision-directed Kalman filtering for channel estimation, and considers a first-order Markov channel model. No BEP analysis is done, and BEP results are obtained only via simulations. It is well known that KF is applicable to a Markov model of any order [75]. Our work is more general than the work in the existing literature in that it builds on the theoretical foundation in [62] and presents exact, explicit, closed-form analytical BEP results. Simulation results are presented to verify the analysis. Reference [24] considers multiple-symbol DD which involves high computational complexity, and introduces decision-feedback DD as its low-complexity simplification. While the latter receiver is somewhat similar to our SBS receiver here,

the analysis in [24] does not lead to closed-form results for the BEP that show the error performance explicitly as a function of the system parameters as our results here do.

3.2 Receiver Structure for Orthogonal STBC

3.2.1 Definition of Orthogonal STBC

A generalized complex orthogonal STBC for a MIMO communication system with M_T transmit (Tx) and N_R receive antennas (Rx) is a $P \times M_T$ matrix $\boldsymbol{S}$. Each M_T -dimensional row vector of the code matrix $\boldsymbol{S}$ is transmitted through the M_T transmit antennas at one time, and the transmission of the matrix $\boldsymbol{S}$ is completed in P symbol periods. We consider in this dissertation linear COD of STBC. During the P symbol periods, the system transmits K symbols $s_k, k = 1, \ldots, K$, which are from a certain complex constellation. Each entry of $\boldsymbol{S}$ is a linear combination of $s_k, k = 1, \ldots, K$ and their conjugates s_k^*. The rate of the STBC is defined as K/P. In summary, a linear orthogonal STBC satisfies:

(i) Linearity: Each entry of $\boldsymbol{S}$ is a linear combination of K symbols $s_k, k = 1, \ldots, K$ and their conjugates s_k^*, i.e, $\boldsymbol{S}$ can be expressed as [47, 48]

$$\boldsymbol{S} = \sum_{k=1}^{K} (s_k \boldsymbol{A}_k + s_k^* \boldsymbol{B}_k), \tag{3.1}$$

where $\boldsymbol{A}_k, \boldsymbol{B}_k$ are $P \times M_T$ matrices with constant complex entries. Taking the Alamouti code in [15] as an example, one gets

$$\begin{gathered} \boldsymbol{S} = \begin{pmatrix} s_1 & s_2 \\ -s_2^* & s_1^* \end{pmatrix} \\ \boldsymbol{A}_1 = \begin{pmatrix} 1 & 0 \\ 0 & 0 \end{pmatrix}, \boldsymbol{A}_2 = \begin{pmatrix} 0 & 1 \\ 0 & 0 \end{pmatrix}, \boldsymbol{B}_1 = \begin{pmatrix} 0 & 0 \\ 0 & 1 \end{pmatrix}, \boldsymbol{B}_2 = \begin{pmatrix} 0 & 0 \\ -1 & 0 \end{pmatrix}. \end{gathered} \tag{3.2}$$

(ii) Orthogonality: The matrix $\boldsymbol{S}$ satisfies $\boldsymbol{S}^\dagger \boldsymbol{S} = \boldsymbol{D}$, where $\boldsymbol{S}^\dagger$ is the Hermitian

transpose of $\boldsymbol{S}$, and $\boldsymbol{D}$ is a diagonal matrix [17]. Using the STBC property in (i), we have

$$\begin{aligned}\boldsymbol{S}^{\dagger}\boldsymbol{S} &= \sum_{k=1}^{K}\sum_{k'=1}^{K}\left(s_k^* s_{k'}\boldsymbol{A}_k^{\dagger}\boldsymbol{A}_{k'} + s_k^* s_{k'}^*\boldsymbol{A}_k^{\dagger}\boldsymbol{B}_{k'} + s_k s_{k'}\boldsymbol{B}_k^{\dagger}\boldsymbol{A}_{k'} + s_k s_{k'}^*\boldsymbol{B}_k^{\dagger}\boldsymbol{B}_{k'}\right) \\ &= \text{diag}\left[\sum_{k=1}^{K}\lambda_{1,k}|s_k|^2, \ldots, \sum_{k=1}^{K}\lambda_{M_T,k}|s_k|^2\right] = \boldsymbol{D}\end{aligned} \tag{3.3}$$

where $\{\lambda_{i,k}\}_{i=1}^{M_T}$ are positive numbers. For arbitrary signal constellations to satisfy the orthogonality condition in (3.3), one requires that

$$\boldsymbol{A}_k^{\dagger}\boldsymbol{A}_{k'} + \boldsymbol{B}_{k'}^{\dagger}\boldsymbol{B}_k = \delta_{kk'}\text{diag}[\lambda_{1,k}, \ldots, \lambda_{M_T,k}] \qquad \text{and} \qquad \boldsymbol{A}_k^{\dagger}\boldsymbol{B}_{k'} + \boldsymbol{A}_{k'}^{\dagger}\boldsymbol{B}_k = \boldsymbol{0}, \tag{3.4}$$

where $\delta_{kk'}$ is the Kronecker delta.

3.2.2 Transmitter Structure

We assume M PSK modulation and constrain the average transmitted energy per bit to a constant E_b. Since there are K symbols with $\log_2 M$ bits per symbol to be transmitted in a $P \times M_T$ STBC, the total energy assigned to one block is $E_b K \log_2 M$. From the STBC definition in (3.3), it is clear that the total transmitted energy in a block is $\sum_{i=1}^{M_T}\sum_{k=1}^{K}\lambda_{i,k}|s_k|^2$. Thus, for each PSK symbol, the allocated energy is

$$E_s = |s_k|^2 = \frac{E_b K \log_2 M}{\sum_{i=1}^{M_T}\sum_{k=1}^{K}\lambda_{i,k}}. \tag{3.5}$$

The symbol is now defined as $s_k = \sqrt{E_s}e^{j\phi_k}$, where ϕ_k takes on a value in the set $\{2n\pi/M\}_{n=0}^{M-1}$.

3.2.3 Receiver Structure

Denoting the m - th transmitted signal block as $\boldsymbol{S}(m)$, the received signal matrix is

$$\boldsymbol{R}(m) = \boldsymbol{S}(m)\boldsymbol{H}(m) + \boldsymbol{N}(m). \tag{3.6}$$

Here $\boldsymbol{R}(m)$ is the $P \times N_R$ received matrix, where each entry $r_{pl}(m)$ is the received signal at the p - th symbol slot on the l - th receive antenna. $\boldsymbol{H}(m)$ is a $M_T \times N_R$ channel matrix, where each entry $h_{il}(m)$ is the fading gain on the il - th link, which is from the i - th transmit to l - th receive antenna, during the m - th block interval. The $h_{il}(m)$'s are spatially independent, identically distributed (i.i.d.) complex Gaussian processes from link to link. It is assumed in (3.6) that all the channels are block-wise constant, i.e., they remain constant for P symbol durations. Thus, for each link, $\{h_{il}(m)\}_{m=0}^{\infty}$ forms a sequence of zero-mean, complex, Gaussian random variables (r.v.'s) with autocorrelation function $\mathrm{E}[h_{il}(m)h_{il}^{*}(m')] = 2\mathcal{R}(m-m')$, where E is the expectation operator. The system model is shown in Fig. 3.1 and Fig. 3.2. It is assumed that the continuous-time fading process for which $\{h_{il}(m)\}_{m=0}^{\infty}$ is a piecewise-constant approximation has a power spectrum symmetric around the carrier so that the in-phase component $\{Re\,[h_{il}(m)]\}_{m=0}^{\infty}$ and the quadrature-phase component $\{Im\,[h_{i,l}(m)]\}_{m=0}^{\infty}$ are i.i.d. processes, each having correlation function $\mathcal{R}(m)$. $\boldsymbol{N}(m)$ is the $P \times N_R$ noise matrix, whose entries $n_{pl}(m)$'s are i.i.d., zero-mean, complex, Gaussian r.v.'s due to AWGN at the p - th symbol slot on the l - th receive antenna with $\mathrm{E}[n_{p'l'}^{*}(m')n_{pl}(m)] = \delta_{pp'}\delta_{ll'}\delta_{mm'}N_0$. $\boldsymbol{H}(m)$ and $\boldsymbol{N}(m)$ are independent of each other.

3.2.4 Channel Estimator Structure

We consider the DF and PSAM for channel estimation here. Figure 3.1 and Figure 3.2 illustrate the system structure.

In the DF scheme, the channel matrix $\boldsymbol{H}(m)$ over the m - th block interval is estimated based on all the previously received signals and decisions made, up till the $(m-1)$ - th block. Define the m - th decoded signal block as $\hat{\boldsymbol{S}}(m)$, and assume the SNR is sufficiently high and error probability sufficiently low so that all the past decisions can be assumed correct, i.e., $\hat{\boldsymbol{S}}(m') = \boldsymbol{S}(m'),\ 0 \le m' \le m-1$. The receiver performs modulation wipe-off on the past received signal blocks, and generates the signal samples

$$\boldsymbol{Y}(m') = [\hat{\boldsymbol{S}}^{\dagger}(m')\hat{\boldsymbol{S}}(m')]^{-1}\hat{\boldsymbol{S}}^{\dagger}(m')\boldsymbol{R}(m') = \boldsymbol{H}(m') + \tilde{N}(m'),\ 0 \leq m' \leq m-1. \quad (3.7)$$

$\boldsymbol{Y}(m')$ is a noisy observation on the channel matrix $\boldsymbol{H}(m')$, and each entry $y_{il}(m'), i = 1 \ldots M_T, l = 1 \ldots N_R$ of $\boldsymbol{Y}(m')$ can be expressed in the form $y_{il}(m') = h_{il}(m') + \tilde{n}_{il}(m')$, where $\{\tilde{n}_{il}(m')\}_{m'}$ is a set of i.i.d. zero mean complex Gaussian r.v.'s with variance $[\sum_{k=1}^{K} \lambda_{i,k}]^{-1} E_s^{-1} N_0$. Define $\Lambda(m) = \{\boldsymbol{Y}(m'),\ 0 \leq m' \leq m-1\}$ as the information set containing the channel measurements available to the receiver up to the beginning of m - th block.

After decoding the current block $\boldsymbol{S}(m)$, the measurement $\boldsymbol{Y}(m)$ on the current channel gain $\boldsymbol{H}(m)$ is obtained as in (3.7) from the received signal $\boldsymbol{R}(m)$ together with the present decoded block $\hat{\boldsymbol{S}}(m)$, and this channel information is fed back to update the channel estimator. Theoretically, the estimation filter stores all the acquired channel information $\Lambda(m)$ from the beginning of transmission up to the present, which is used to generate the channel estimate $\hat{\boldsymbol{S}}(m)$ for the next block. For such a filter working in DF mode, a known preamble must be sent in the beginning to allow the filter to first acquire accurate channel estimates before symbol decoding can begin. After that, the receiver uses the decoded symbols to extract the channel information from the received signals. A problem with such a scheme is that errors may accumulate in the stored channel information affecting the accuracy of the subsequent channel estimates. More errors then enter the filter due to the more frequent erroneous decisions, and this can cause a "runaway" in the receiver. To control the error propagation, pilot blocks must be periodically inserted into the transmission to update the filter with correct channel information.

PSAM was proposed in [76], and it avoids the error propagation problem in the DF scheme. For the STBC system using PSAM, one pilot block is inserted into the data stream every L_f blocks [76], and the estimation of the channel matrix $\boldsymbol{H}(m)$ is based

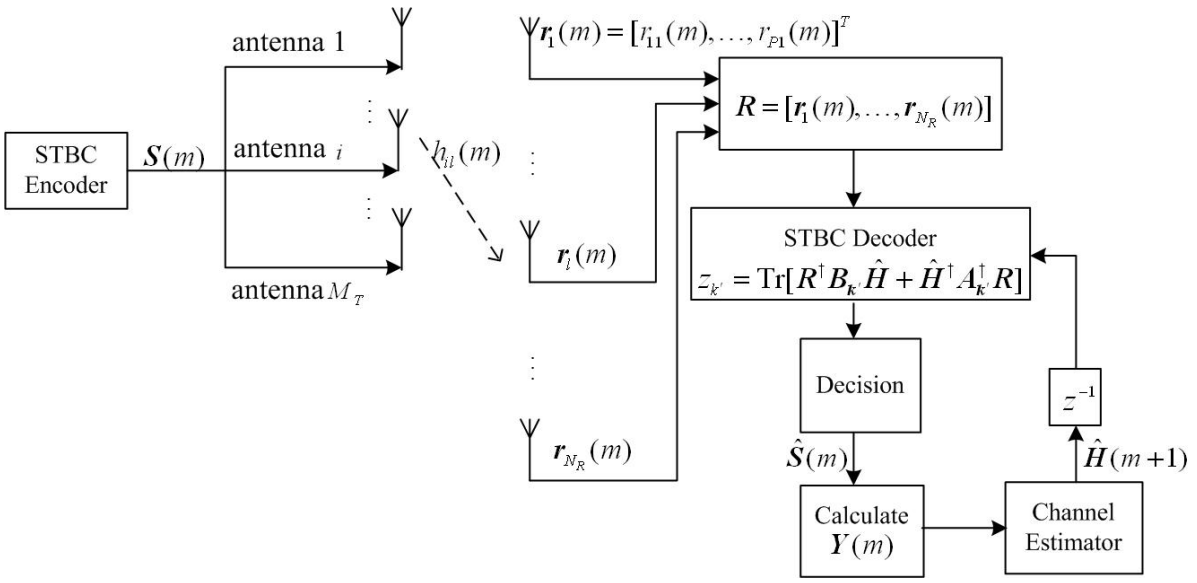

Fig. 3.1: Decision feedback channel estimation STBC system

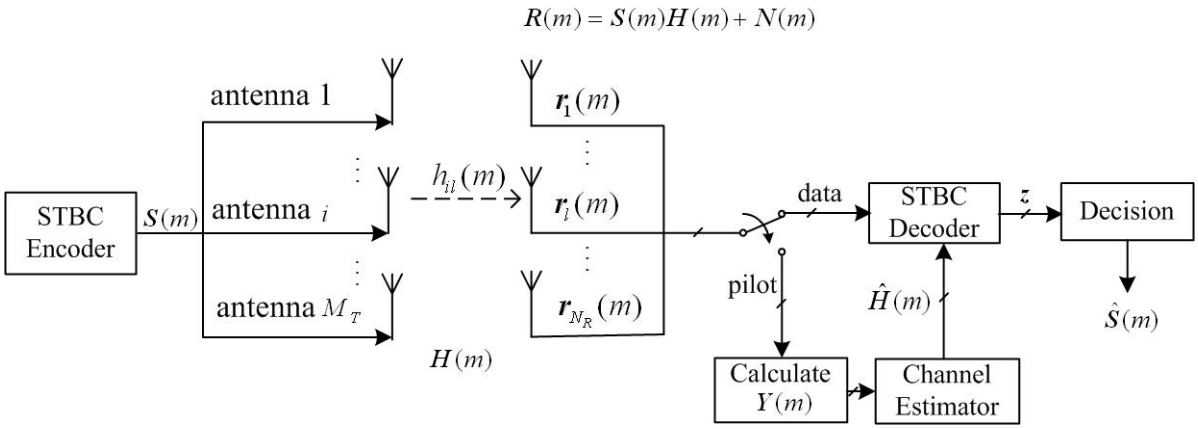

Fig. 3.2: PSAM channel estimation STBC system

on the $2L_p$ pilot blocks nearest to the m - th block. Thus, we define the information set

$$\Lambda(m) = \{\boldsymbol{Y}(m'),\ ([\![m/L_f]\!] - L_p + 1)L_f \leq m' \leq ([\![m/L_f]\!] + L_p)L_f\} \tag{3.8}$$

as the set of channel measurements for estimation of the channel matrix $\boldsymbol{H}(m)$, where $[\![\cdot]\!]$ denotes the floor function. There is no decision feedback involved, and no error

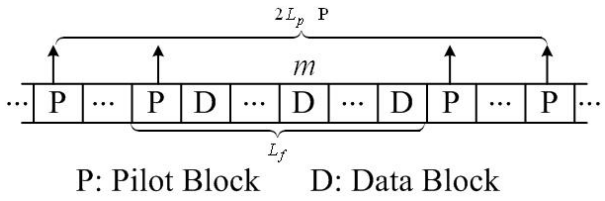

Fig. 3.3: PSAM frame structure

propagation due to past decision errors would occur in PSAM. Generally, however, decision delay is introduced in PSAM, as the receiver must wait until enough pilots are received before decoding. PSAM has been well accepted since it performs well for slow fading channels. However, it is expected that the DF scheme would outperform PSAM under fast fading conditions, because the DF scheme uses channel measurements from the immediately preceding symbol blocks on which symbol decisions have just been made, and these measurements are more strongly correlated with the current channel gain to be estimated. PSAM, on the other hand, uses the channel information from pilots located several blocks away in time.

The estimate $\hat{\boldsymbol{H}}(m)$ of $\boldsymbol{H}(m)$ is, from [62], the conditional mean or MMSE estimate of the channel gain matrix $\boldsymbol{H}(m)$ given $\Lambda(m)$, i.e., $\hat{\boldsymbol{H}}(m) = [\hat{h}_{ij}(m)]_{M_T \times N_R} = \mathrm{E}\left[\boldsymbol{H}(m)|\Lambda(m)\right]$, and can be generated linearly from the measurements in $\Lambda(m)$, since the r.v.'s concerned are all Gaussian and the observations are linear. Thus, given $\Lambda(m)$, each $h_{il}(m)$ is conditionally Gaussian with mean $\hat{h}_{il}(m)$, and variance $2\sigma_e^2(m)$, where

$$2\sigma_{e,i}^2(m) = \mathrm{E}[|h_{il}(m) - \hat{h}_{il}(m)|^2|\Lambda(m)] \tag{3.9}$$

is the MSE of the estimate $\hat{h}_{il}(m)$. Note that the MSE's $2\sigma_{e,i}^2(m)$ are identical for all $h_{il}(m), l = 1..N_R$ due to the identical channel assumption. According to (3.7), $2\sigma_{e,i}^2(m)$ would have a common value $2\sigma_{e,0}^2(m)$ for those STBC where the quantity $\sum_{k=1}^{K} \lambda_{i,k}$ is identical for all $i = 1..M_T$. The work in [62], [75] and [77] shows that the structure of the estimator for computing $\hat{\boldsymbol{H}}(m)$ and the associated MSE $2\sigma_{e,i}^2(m)$ depends on the

channel fading process spectral model.The detail of the MSE calculation can be found in Chapter 2.

3.2.5 Optimum Receiver Structure

Suppose a sequence of L signal blocks $\{\boldsymbol{S}(m')\}_{m'=0}^{L-1}$ is sent, and the sequence $\{\boldsymbol{R}(m')\}_{m'=0}^{L-1}$ of signals is received. The optimum receiver should make a decision on the entire sequence $\{\boldsymbol{S}(m')\}_{m'=0}^{L-1}$ based on $\{\boldsymbol{R}(m')\}_{m'=0}^{L-1}$ and the channel estimation information sets [30]. This receiver, of course, is too complex to implement. A simpler alternative is to detect the sequence $\{\boldsymbol{S}(m')\}_{m'=0}^{L-1}$ block-by-block. For most cases, especially when the number of transmit antennas and the constellation size are large, this block-by-block receiver would still be very complex. Thus, in what follows, we choose to use a suboptimum SBS receiver, whose complexity is manageable and error performance can be analytically determined.

In both the DF and the PSAM schemes, the block-by-block receiver detects the m - th signal block $\boldsymbol{S}(m)$ based on the m - th received signal block $\boldsymbol{R}(m)$ with the aid of the information set $\Lambda(m)$. For optimum maximum-likelihood (ML) decoding, the decoder computes the likelihood $p(\boldsymbol{R}(m), \Lambda(m)|\boldsymbol{S}(m))$ for each possible value of the signal block $\boldsymbol{S}(m)$, and decides on the signal block with the largest likelihood. However, we have

$$p(\boldsymbol{R}(m), \Lambda(m)|\boldsymbol{S}(m)) = p(\boldsymbol{R}(m)|\Lambda(m), \boldsymbol{S}(m))p(\Lambda(m)|\boldsymbol{S}(m)) \tag{3.10}$$

and since the information set $\Lambda(m)$ is independent of the current transmitted signal $\boldsymbol{S}(m)$, i.e., $p(\Lambda(m)|\boldsymbol{S}(m)) = p(\Lambda(m))$, the ML decoding rule simplifies to

$$\hat{\boldsymbol{S}}(m) = \arg\max_{\boldsymbol{S}(m)} p(\boldsymbol{R}(m)|\boldsymbol{S}(m), \Lambda(m)). \tag{3.11}$$

From (3.6), given $\boldsymbol{S}(m)$ and the set $\Lambda(m)$, $\boldsymbol{R}(m)$ is conditionally Gaussian with mean $\boldsymbol{S}(m)\hat{\boldsymbol{H}}(m)$. The column vectors of $\boldsymbol{R}(m)$ are independent to each other and each have

a covariance matrix as

$$\boldsymbol{C} = \boldsymbol{S}(m)\boldsymbol{V}(m)\boldsymbol{S}^{\dagger}(m) + N_0\boldsymbol{I}_{P\times P}, \tag{3.12}$$

where $\boldsymbol{V}(m) = \mathrm{diag}[\sigma^2_{e,i}(m)]_{i=1}^{M_T}$. The probability density function of the received signal is

$$\begin{aligned} p(\boldsymbol{R}(m)|\boldsymbol{S}(m),\Lambda(m)) =& \det{}^{-\mathrm{N_R}}(\pi \mathrm{C}) \\ & \cdot \exp\left(-\mathrm{Tr}\left[[\boldsymbol{R}(m) - \boldsymbol{S}(m)\hat{\boldsymbol{H}}(m)]^{\dagger}\boldsymbol{C}^{-1}[\boldsymbol{R}(m) - \boldsymbol{S}(m)\hat{\boldsymbol{H}}(m)]\right]\right). \end{aligned} \tag{3.13}$$

Thus, the ML block-by-block receiver (3.11) becomes

$$\hat{\boldsymbol{S}}(m) = \arg\min_{\boldsymbol{S}(m)}\left(N_R \ln\det(\boldsymbol{C}) + \mathrm{Tr}\left[[\boldsymbol{R}(m) - \boldsymbol{S}(m)\hat{\boldsymbol{H}}(m)]^{\dagger}\boldsymbol{C}^{-1}[\boldsymbol{R}(m) - \boldsymbol{S}(m)\hat{\boldsymbol{H}}(m))]\right]\right). \tag{3.14}$$

(3.11) indicates that the optimum receiver must test all possibilities of the signal matrix $\boldsymbol{S}(m)$ before it can make the decision. There are totally K^M combinations for the K signallings $\{s_k\}_{k=1}^{K}$, with each s_k chosen from a constellation set of size M. Thus K^M computation of (3.11) must be performed to decode one block. Such decoding is almost impossible if the values of K and M become relatively large, e.g., $K = 4$ and $M = 64$. In practice, we may prefer to choose some sub-optimal but computationally simple receiver structure. Similar work on optimal STBC receivers can also be found in [78].

3.2.6 A Symbol-by-Symbol Receiver Structure

The detector in the form (3.14) makes a simultaneous decision on all the symbols of the entire block $\boldsymbol{S}(m)$, instead of a decision on one symbol at a time, independently. This makes the decoder computationally complex, especially when the constellation size is large. Moreover, it has been found to be impossible to analyze the performance of the decoder (3.14). Thus, we choose to consider a simpler decoder which makes independent SBS decisions. Observe that with PSK modulation, if the STBC employed satisfies the

condition

$$\boldsymbol{S}^{\dagger}(m)\boldsymbol{S}(m) \propto \boldsymbol{I} \text{ and } \boldsymbol{S}(m)\boldsymbol{S}^{\dagger}(m) \propto \boldsymbol{I}, \tag{3.15}$$

then $\boldsymbol{C}$ becomes constant and proportional to an identity matrix, and (3.14) simplifies to

$$\hat{\boldsymbol{S}}(m) = \arg\min_{\boldsymbol{S}(m)} \|(\boldsymbol{R}(m) - \boldsymbol{S}(m)\hat{\boldsymbol{H}}(m))\|^2, \tag{3.16}$$

where $\|\cdot\|$ is the Frobenius norm. This receiver (3.16) can be further simplified to a SBS detector, given by

$$\hat{s}_k(m) = \arg\max_{s_{k'}} \max_{k'=1\ldots K} \mathrm{Re}[z_{k'}(m)s^*_{k'}(m)], \tag{3.17}$$

where $z_{k'}(m) = \mathrm{Tr}[\boldsymbol{R}^{\dagger}(m)\boldsymbol{B}_{\boldsymbol{k'}}\hat{\boldsymbol{H}}(m) + \hat{\boldsymbol{H}}^{\dagger}(m)\boldsymbol{A}^{\dagger}_{\boldsymbol{k'}}\boldsymbol{R}(m)]$. This detector (3.17) is computationally much simpler than the detector (3.14). For those STBC's that satisfy condition (3.15), it is clear that the detector (3.17) is the ML block-by-block detector. For such STBC's, the BEP performance analysis in section 3.3 would give the best performance achievable. For those STBC's that do not satisfy condition (3.15), we continue to use the SBS detector (3.17), which is then a mismatched receiver. The BEP analysis results in section 3.3 would then not represent the best performance achievable by such codes. For these latter codes, the optimum detector is the block-by-block detector in (3.14), whose performance analysis is left for future research. We note that in the special case of perfect CSI, we would have $\boldsymbol{V}(m) = \boldsymbol{0}$ and $\boldsymbol{C} = N_0\boldsymbol{I}$ in (3.12). The ML block-by-block receiver (3.11) would reduce immediately to (3.16), and hence to the symbol-by-symbol detector (3.17), as expected.

3.3 BEP Performance Analysis for OSTBC Systems

With PSK modulation, i.e., $s_k = \sqrt{E_s}e^{j\phi_k}$, the decoding rule (3.17) is equivalent to

$$\hat{s}_k(m) = \arg \max_{s_{k'}} \max_{k'=1...K} Re\left\{ z_{k'} e^{-j\phi_{k'}} \right\}, \tag{3.18}$$

where

$$z_{k'} = \mathrm{Tr}[\boldsymbol{R}^\dagger \boldsymbol{B}_{\boldsymbol{k'}} \hat{\boldsymbol{H}} + \hat{\boldsymbol{H}}^\dagger \boldsymbol{A}_{\boldsymbol{k'}}^\dagger \boldsymbol{R}] = x_{k'} + u_{k'} \tag{3.19a}$$

$$x_{k'} = \sum_{k=1}^{K} \left[s_k^* \mathrm{Tr}[\boldsymbol{H}^\dagger \boldsymbol{A}_k^\dagger \boldsymbol{B}_{\boldsymbol{k'}} \hat{\boldsymbol{H}} + \hat{\boldsymbol{H}}^\dagger \boldsymbol{A}_{\boldsymbol{k'}}^\dagger \boldsymbol{B}_k \boldsymbol{H}] + s_k \mathrm{Tr}[\hat{\boldsymbol{H}}^\dagger \boldsymbol{A}_{\boldsymbol{k'}}^\dagger \boldsymbol{A}_k \boldsymbol{H} + \boldsymbol{H}^\dagger \boldsymbol{B}_k^\dagger \boldsymbol{B}_{\boldsymbol{k'}} \hat{\boldsymbol{H}}] \right] \tag{3.19b}$$

$$u_{k'} = \mathrm{Tr}[\boldsymbol{N}^\dagger \boldsymbol{B}_{\boldsymbol{k'}} \hat{\boldsymbol{H}} + \hat{\boldsymbol{H}}^\dagger \boldsymbol{A}_{\boldsymbol{k'}}^\dagger \boldsymbol{N}] \tag{3.19c}$$

Hereafter, we drop the block index m for simplicity. For equally likely symbols, the main quantity of interest is the probability $P\left(\mathrm{Re}[z_{k'}e^{-j\alpha}] < 0 \,\middle|\, s_{k'} = \sqrt{E_s}\right)$ [13], where α is some angle. By conditioning on having the information set Λ, we first evaluate the conditional probability $P\left(\mathrm{Re}[z_{k'}e^{-j\alpha}] < 0 \,\middle|\, s_{k'} = \sqrt{E_s}\,, \Lambda\right)$.

Proposition 3.1 *The quantity $z_{k'}$ defined in (3.19a) is a Gaussian random variable conditioning on the information set Λ.*

Proof:

Investigate the first component $x_{k'}$ of $z_{k'}$. We first rewrite the STBC construction matrices $\boldsymbol{A}_k, \boldsymbol{B}_k$ as

$$\boldsymbol{A}_k = [\boldsymbol{a}_k^1, \boldsymbol{a}_k^2, ..., \boldsymbol{a}_k^{M_T}], \boldsymbol{B}_k = [\boldsymbol{b}_k^1, \boldsymbol{b}_k^2, ..., \boldsymbol{b}_k^{M_T}], \tag{3.20}$$

where $\{\boldsymbol{a}_k^i, \boldsymbol{b}_k^i\}_{i=1}^{M_T}$ are $P \times 1$ column vectors of $\boldsymbol{A}_k, \boldsymbol{B}_k$. Now the orthogonal properties in (3.4) can be re-defined as

$$\boldsymbol{a}_k^{i\dagger}\boldsymbol{a}_{k'}^j + \boldsymbol{b}_{k'}^{i\dagger}\boldsymbol{b}_k^j = \lambda_{i,k}\delta_{ij}\delta_{kk'} \text{ and } \boldsymbol{a}_k^{i\dagger}\boldsymbol{b}_{k'}^j + \boldsymbol{a}_{k'}^{i\dagger}\boldsymbol{b}_k^j = 0. \tag{3.21}$$

Using the linear property of the trace function, the definition of $x_{k'}$ can be expanded into four terms as

$$x_{k'} = \sum_{k=1}^{K} \left[\begin{array}{l} s_k^*\mathrm{Tr}[\boldsymbol{H}^\dagger \boldsymbol{A}_k^\dagger \boldsymbol{B}_{\boldsymbol{k'}} \hat{\boldsymbol{H}}] + s_k^*\mathrm{Tr}[\hat{\boldsymbol{H}}^\dagger \boldsymbol{A}_{\boldsymbol{k'}}^\dagger \boldsymbol{B}_k \boldsymbol{H}] + \\ s_k\mathrm{Tr}[\hat{\boldsymbol{H}}^\dagger \boldsymbol{A}_{\boldsymbol{k'}}^\dagger \boldsymbol{A}_k \boldsymbol{H}] + s_k\mathrm{Tr}[\boldsymbol{H}^\dagger \boldsymbol{B}_k^\dagger \boldsymbol{B}_{\boldsymbol{k'}} \hat{\boldsymbol{H}}] \end{array} \right]. \tag{3.22}$$

Take the matrix $\boldsymbol{H}^\dagger \boldsymbol{A}_k^\dagger \boldsymbol{B}_{\boldsymbol{k'}} \hat{\boldsymbol{H}}$ in the first term for example

$$\begin{aligned} \boldsymbol{H}^\dagger \boldsymbol{A}_k^\dagger \boldsymbol{B}_{k'} \hat{\boldsymbol{H}} &= \boldsymbol{H}^\dagger \begin{pmatrix} \boldsymbol{a}_k^{1\dagger} \\ \vdots \\ \boldsymbol{a}_k^{M_T\dagger} \end{pmatrix} \begin{pmatrix} \boldsymbol{b}_{k'}^1 & \cdots & \boldsymbol{b}_{k'}^{M_T} \end{pmatrix} \hat{\boldsymbol{H}} \\ &= \begin{pmatrix} h_{11}^* & \cdots & h_{M_T 1}^* \\ \vdots & \ddots & \vdots \\ h_{1N_R}^* & \cdots & h_{M_T N_R}^* \end{pmatrix} \begin{pmatrix} \boldsymbol{a}_k^{1\dagger}\boldsymbol{b}_{k'}^1 & \cdots & \boldsymbol{a}_k^{1\dagger}\boldsymbol{b}_{k'}^{M_T} \\ \vdots & \ddots & \vdots \\ \boldsymbol{a}_k^{M_T\dagger}\boldsymbol{b}_{k'}^1 & \cdots & \boldsymbol{a}_k^{M_T\dagger}\boldsymbol{b}_{k'}^{M_T} \end{pmatrix} \begin{pmatrix} \hat{h}_{11} & \cdots & \hat{h}_{1N_R} \\ \vdots & \ddots & \vdots \\ \hat{h}_{M_T 1} & \cdots & \hat{h}_{M_T N_R} \end{pmatrix}, \\ &= \begin{pmatrix} \sum_{j=1}^{M_T}\sum_{i=1}^{M_T} h_{j1}^* \boldsymbol{a}_k^{j\dagger}\boldsymbol{b}_{k'}^i \hat{h}_{i1} & \cdots & \sum_{j=1}^{M_T}\sum_{i=1}^{M_T} h_{j1}^* \boldsymbol{a}_k^{j\dagger}\boldsymbol{b}_{k'}^i \hat{h}_{iN_R} \\ \vdots & \ddots & \vdots \\ \sum_{j=1}^{M_T}\sum_{i=1}^{M_T} h_{jN_R}^* \boldsymbol{a}_k^{j\dagger}\boldsymbol{b}_{k'}^i \hat{h}_{i1} & \cdots & \sum_{j=1}^{M_T}\sum_{i=1}^{M_T} h_{jN_R}^* \boldsymbol{a}_k^{j\dagger}\boldsymbol{b}_{k'}^i \hat{h}_{iN_R} \end{pmatrix} \end{aligned} \tag{3.23}$$

taking the trace of which gives

$$\mathrm{Tr}[\boldsymbol{H}^\dagger \boldsymbol{A}_k^\dagger \boldsymbol{B}_{k'} \hat{\boldsymbol{H}}] = \sum_{l=1}^{N_R}\sum_{j=1}^{M_T}\sum_{i=1}^{M_T} h_{jl}^* \boldsymbol{a}_k^{j\dagger}\boldsymbol{b}_{k'}^i \hat{h}_{il}. \tag{3.24}$$

Similarly, we have

$$\begin{aligned} x_{k'} &= \sum_{k=1}^{K}\Big[s_k^*\mathrm{Tr}[\boldsymbol{H}^\dagger\boldsymbol{A}_k^\dagger\boldsymbol{B}_{k'}\hat{\boldsymbol{H}}+\hat{\boldsymbol{H}}^\dagger\boldsymbol{A}_{k'}^\dagger\boldsymbol{B}_k\boldsymbol{H}]+s_k\mathrm{Tr}[\hat{\boldsymbol{H}}^\dagger\boldsymbol{A}_{k'}^\dagger\boldsymbol{A}_k\boldsymbol{H}+\boldsymbol{H}^\dagger\boldsymbol{B}_k^\dagger\boldsymbol{B}_{k'}\hat{\boldsymbol{H}}]\Big] \\ &= \sum_{k=1}^{K}\sum_{l=1}^{N_R}\sum_{j=1}^{M_T}\sum_{i=1}^{M_T}\Big[s_k^*(h_{jl}^*\boldsymbol{a}_k^{j\dagger}\boldsymbol{b}_{k'}^i\hat{h}_{il}+\hat{h}_{jl}^*\boldsymbol{a}_{k'}^{j\dagger}\boldsymbol{b}_k^i h_{il})+s_k(\hat{h}_{jl}^*\boldsymbol{a}_{k'}^{j\dagger}\boldsymbol{a}_k^i h_{il}+h_{jl}^*\boldsymbol{b}_k^{j\dagger}\boldsymbol{b}_{k'}^i\hat{h}_{il})\Big]. \end{aligned} \tag{3.25}$$

It is clear from the expression above that $x_{k'}$ is a linear summation of the complex Gaussian r.v.'s h_{il} and h_{jl}^*, so that $x_{k'}$ must be a Gaussian r.v. itself. Now let's investigate its mean and variance with the fact that $h_{il}\sim N(\hat{h}_{il},2\sigma_{e,i}^2)$. The mean of $x_{k'}$ is

$$\begin{aligned} \mathrm{E}[x_{k'}] &= \sum_{k=1}^{K}\sum_{l=1}^{N_R}\sum_{j=1}^{M_T}\sum_{i=1}^{M_T}\Big[s_k^*(\hat{h}_{jl}^*\boldsymbol{a}_k^{j\dagger}\boldsymbol{b}_{k'}^i\hat{h}_{il}+\hat{h}_{jl}^*\boldsymbol{a}_{k'}^{j\dagger}\boldsymbol{b}_k^i\hat{h}_{il})+s_k(\hat{h}_{jl}^*\boldsymbol{a}_{k'}^{j\dagger}\boldsymbol{a}_k^i\hat{h}_{il}+\hat{h}_{jl}^*\boldsymbol{b}_k^{j\dagger}\boldsymbol{b}_{k'}^i\hat{h}_{il})\Big] \\ &= \sum_{l=1}^{N_R}\sum_{j=1}^{M_T}\sum_{i=1}^{M_T}\left(\hat{h}_{jl}^*\hat{h}_{il}\sum_{k=1}^{K}\Big[s_k^*(\boldsymbol{a}_k^{j\dagger}\boldsymbol{b}_{k'}^i+\boldsymbol{a}_{k'}^{j\dagger}\boldsymbol{b}_k^i)+s_k(\boldsymbol{a}_{k'}^{j\dagger}\boldsymbol{a}_k^i+\boldsymbol{b}_k^{j\dagger}\boldsymbol{b}_{k'}^i)\Big]\right) \\ &= \sum_{l=1}^{N_R}\sum_{j=1}^{M_T}\sum_{i=1}^{M_T}\left(\hat{h}_{jl}^*\hat{h}_{il}s_{k'}\lambda_{j,k'}\delta_{ij}\right)=s_{k'}\sum_{l=1}^{N_R}\sum_{i=1}^{M_T}\lambda_{i,k'}\left|\hat{h}_{il}\right|^2 \end{aligned} \tag{3.26}$$

and the variance is

$$\begin{aligned} &\mathrm{var}[x_{k'}] \\ &= E_s\mathrm{var}\left[\sum_{k=1}^{K}\sum_{l=1}^{N_R}\sum_{j=1}^{M_T}\sum_{i=1}^{M_T}\Big[(h_{jl}^*\boldsymbol{a}_k^{j\dagger}\boldsymbol{b}_{k'}^i\hat{h}_{il}+\hat{h}_{jl}^*\boldsymbol{a}_{k'}^{j\dagger}\boldsymbol{b}_k^i h_{il})+(\hat{h}_{jl}^*\boldsymbol{a}_{k'}^{j\dagger}\boldsymbol{a}_k^i h_{il}+h_{jl}^*\boldsymbol{b}_k^{j\dagger}\boldsymbol{b}_{k'}^i\hat{h}_{il})\Big]\right] \\ &= 2E_s\sum_{k=1}^{K}\sum_{l=1}^{N_R}\sum_{j=1}^{M_T}\sum_{i=1}^{M_T}\left[\sigma_{e,j}^2\left|\hat{h}_{il}\right|^2\left(\left|\boldsymbol{a}_k^{j\dagger}\boldsymbol{b}_{k'}^i\right|^2+\left|\boldsymbol{b}_k^{j\dagger}\boldsymbol{b}_{k'}^i\right|^2\right)+\sigma_{e,i}^2\left|\hat{h}_{jl}\right|^2\left(\left|\boldsymbol{a}_{k'}^{j\dagger}\boldsymbol{b}_k^i\right|^2+\left|\boldsymbol{a}_{k'}^{j\dagger}\boldsymbol{a}_k^i\right|^2\right)\right] \\ &= 2E_s\sum_{k=1}^{K}\sum_{l=1}^{N_R}\sum_{j=1}^{M_T}\sum_{i=1}^{M_T}\sigma_{e,j}^2\left|\hat{h}_{il}\right|^2\left[\left|\boldsymbol{a}_k^{j\dagger}\boldsymbol{b}_{k'}^i\right|^2+\left|\boldsymbol{b}_k^{j\dagger}\boldsymbol{b}_{k'}^i\right|^2+\left|\boldsymbol{a}_{k'}^{i\dagger}\boldsymbol{b}_k^j\right|^2+\left|\boldsymbol{a}_{k'}^{i\dagger}\boldsymbol{a}_k^j\right|^2\right] \\ &= 2E_s\sum_{l=1}^{N_R}\sum_{j=1}^{M_T}\sum_{i=1}^{M_T}\sigma_{e,j}^2\left|\hat{h}_{il}\right|^2\xi_{j,i,k'}, \end{aligned} \tag{3.27}$$

where

$$\xi_{j,i,k'}=\sum_{k=1}^{K}\Big[|\boldsymbol{a}_k^{j\dagger}\boldsymbol{b}_{k'}^i|^2+|\boldsymbol{b}_k^{j\dagger}\boldsymbol{b}_{k'}^i|^2+|\boldsymbol{a}_{k'}^{i\dagger}\boldsymbol{b}_k^j|^2+|\boldsymbol{a}_{k'}^{i\dagger}\boldsymbol{a}_k^j|^2\Big]. \tag{3.28}$$

So that $x_{k'}$ is a Gaussian r.v. defined as

$$(x_{k'}|s_{k'},\Lambda) \sim N\left(s_{k'}\sum_{l=1}^{N_R}\sum_{i=1}^{M_T}\lambda_{i,k'}\left|\hat{h}_{il}\right|^2, 2E_s\sum_{l=1}^{N_R}\sum_{j=1}^{M_T}\sum_{i=1}^{M_T}\sigma_{e,j}^2\left|\hat{h}_{il}\right|^2\xi_{j,i,k'}\right). \tag{3.29}$$

Similarly, for the second noise term $u_{k'}$ of $z_{k'}$, it is easy to show that $u_{k'}$ is also a conditional Gaussian r.v. with mean zero and variance $N_0\sum_{l=1}^{N_R}\sum_{i=1}^{M_T}\lambda_{i,k'}\left|\hat{h}_{il}\right|^2$. In conclusion, $z_{k'}$ is a conditional complex Gaussian r.v. given by

$$(z_{k'}|s_{k'},\Lambda) \sim N(s_{k'}\sum_{i=1}^{M_T}\sum_{l=1}^{N_R}\lambda_{i,k'}|\hat{h}_{il}|^2, 2E_s\sum_{i=1}^{M_T}\sum_{l=1}^{N_R}\sum_{j=1}^{M_T}\xi_{j,i,k'}\sigma_{e,j}^2|\hat{h}_{il}|^2+N_0\sum_{i=1}^{M_T}\sum_{l=1}^{N_R}\lambda_{i,k'}|\hat{h}_{il}|^2). \tag{3.30}$$

□

The quantity $Re\{z_{k'}e^{-j\alpha}\}$ in the detector (3.18) is a conditionally Gaussian variable with mean $\sqrt{E_s}\cos(\phi_{k'}-\alpha)\sum_{i=1}^{M_T}\sum_{l=1}^{N_R}\lambda_{i,k'}|\hat{h}_{il}|^2$ and variance $E_s\sum_{i=1}^{M_T}\sum_{l=1}^{N_R}\sum_{j=1}^{M_T}\xi_{j,i,k'}\sigma_{e,i}^2|\hat{h}_{il}|^2+\frac{N_0}{2}\sum_{i=1}^{M_T}\sum_{l=1}^{N_R}\lambda_{i,k'}|\hat{h}_{il}|^2$, and the conditional probability $P(Re\{z_{k'}e^{-j\alpha}\}<0|s_{k'},\Lambda)$ can now be evaluated as

$$P(Re\left\{z_{k'}e^{-j\alpha}\right\}<0|s_{k'},\Lambda) = Q\left(\sqrt{\frac{E_s\cos^2(\phi_{k'}-\alpha)\left(\sum_{i=1}^{M_T}\sum_{l=1}^{N_R}\lambda_{i,k'}|\hat{h}_{il}|^2\right)^2}{E_s\sum_{i=1}^{M_T}\sum_{l=1}^{N_R}\sum_{j=1}^{M_T}\xi_{j,i,k'}\sigma_{e,j}^2|\hat{h}_{il}|^2+\frac{N_0}{2}\sum_{i=1}^{M_T}\sum_{l=1}^{N_R}\lambda_{i,k'}|\hat{h}_{il}|^2}}\right). \tag{3.31}$$

Next, we have to average over the random variables in the information set Λ, or equivalently, over the estimates $\hat{h}_{il}(m)$ in (3.31) to obtain the average error probability $P(Re\{z_{k'}e^{-j\alpha}\}<0|s_{k'}=\sqrt{E_s})$. To make the averaging tractable, we make use of the monotonic property of the Q -function. Defining

$$\omega_{i,k'} = \sum\nolimits_{j=1}^{M_T}\xi_{j,i,k'}, \quad \rho_{i,k'} = \omega_{i,k'}/\lambda_{i,k'},$$

$$\sigma_{\max}^2 = \max_{i=1\ldots M_T}\left\{\sigma_{e,i}^2\right\}, \quad \sigma_{\min}^2 = \min_{i=1\ldots M_T}\left\{\sigma_{e,i}^2\right\},$$

$$\begin{aligned}\rho_{\max,k'} &= \max_{i=1\ldots M_T}\left\{\rho_{i,k'}\right\},\ \rho_{\min,k'} = \min_{i=1\ldots M_T}\left\{\rho_{i,k'}\right\},\\ \lambda_{\max,k'} &= \max_{i=1\ldots M_T}\left\{\lambda_{i,k'}\right\},\quad \lambda_{\min,k'} = \min_{i=1\ldots M_T}\left\{\lambda_{i,k'}\right\}.\end{aligned} \tag{3.32}$$

The probability in (3.31) can be bounded as

$$\begin{aligned}Q\left(\sqrt{\frac{\lambda_{\max,k'}E_s\cos^2\alpha\sum_{i=1}^{M_T}\sum_{l=1}^{N_R}|\hat{h}_{il}|^2}{\rho_{\min,k'}E_s\sigma^2_{\min}+\frac{N_0}{2}}}\right) &\le P(Re\left\{z_{k'}e^{-j\alpha}\right\}<0|s_{k'}=\sqrt{E_s},\Lambda)\\ &\le Q\left(\sqrt{\frac{\lambda_{\min,k'}E_s\cos^2\alpha\sum_{i=1}^{M_T}\sum_{l=1}^{N_R}|\hat{h}_{il}|^2}{\rho_{\max,k'}E_s\sigma^2_{\max}+\frac{N_0}{2}}}\right)\end{aligned} \tag{3.33}$$

The equality signs hold in (3.33) when

$$\lambda_{i,k'} = \lambda_{k'},\ \omega_{i,k'} = \omega_{k'},\ \text{for all } i = 1\ldots M_T, \tag{3.34}$$

and the $\rho_{i,k'}$'s will then have a common value $\rho_{k'} = \omega_{k'}/\lambda_{k'}$, for all $i = 1\ldots M_T$. Note that (3.34) includes the condition that $2\sigma^2_{e,i}(m) = 2\sigma^2_{e,0}(m)$ for all $i = 1...M_T$. Since the estimates $\hat{h}_{il}(m)$'s are generated linearly from the elements of set Λ, they are themselves complex Gaussian r.v.'s, each with mean zero and variance $2[\mathcal{R}(0)-\sigma^2_{e,i}(m)]$ [13, 31]. Therefore, the quantity $d^2(m) = \sum_{i=1}^{M_T}\sum_{l=1}^{N_R}|\hat{h}_{il}(m)|^2$ in the argument of the Q (.) function in (3.33) has a chi-square pdf with $2M_TN_R$ degrees of freedom [79]. Using this pdf to average the upper and lower bounds in (3.33) over the quantity $d^2(m)$ gives the result [79]

$$\begin{aligned}F(\alpha,\mu(\rho_{\min,k'},\lambda_{\max,k'},\sigma^2_{\min})) &\le P(Re\left\{z_{k'}e^{-j\alpha}\right\}<0|s_{k'}=\sqrt{E_s})\\ &\le F(\alpha,\mu(\rho_{\max,k'},\lambda_{\min,k'},\sigma^2_{\max}))\end{aligned} \tag{3.35}$$

Here, the function $F(\alpha, \mu)$ is given by

$$F(\alpha,\mu) = \left[\frac{1-\mu}{2}\right]^{M_T N_R} \sum_{k=0}^{M_T N_R - 1} \begin{pmatrix} M_T N_R - 1 + k \\ k \end{pmatrix} \left[\frac{1+\mu}{2}\right]^{k} \tag{3.36}$$

where

$$\mu(\rho,\lambda,\sigma_e^2) = \left(1 + \frac{N_R + \rho\gamma_s(1-\eta)}{\lambda\gamma_s\eta\cos^2\alpha}\right)^{-1/2}, \gamma_s = N_R\frac{2\mathcal{R}(0)E_s}{N_0}, \quad \text{and} \quad \eta = 1 - \frac{\sigma_e^2}{\mathcal{R}(0)}. \tag{3.37}$$

The bounds in (3.35) describe the error performance of a single signal symbol $s_{k'}$. As there are K symbols in one block, the average BEP is obtained from the average probability $\Gamma(\alpha)$ given by

$$\Gamma(\alpha) = \frac{1}{K}\sum_{k'=1}^{K} P(Re\left\{z_{k'}e^{-j\alpha}\right\} < 0 | s_{k'} = \sqrt{E_s}). \tag{3.38}$$

Now, for BPSK, it is clear that the BEP is given by

$$P_b^B = \Gamma(\alpha = 0). \tag{3.39}$$

For QPSK with Gray coding, following the argument in [62], the BEP is given by

$$P_b^Q = \Gamma(\alpha = \pi/4). \tag{3.40}$$

Finally, for 8PSK with Gray coding, the argument in [80] gives a very good approximation

$$P_b^{(8)} \approx \frac{2}{3}\Gamma(\alpha = 3\pi/8)[1 + \Gamma(\alpha = \pi/8)]. \tag{3.41}$$

In addition to these two tight upper and lower bounds in (3.35), $\Gamma(\alpha)$ also admits the Chernoff upper bound. Applying the bound $Q(x) < 0.5e^{-x^2/2}$ to the upper bound in (3.33) before averaging over the estimates $\hat{h}_{il}(m)$ gives

$$\Gamma(\alpha) < \frac{1}{2K}\sum_{k'=1}^{K}\left(1 + \frac{\lambda_{\min,k'}\gamma_s\eta\cos^2\alpha}{N_R + \rho_{\max,k'}\gamma_s(1-\eta)}\right)^{-M_T N_R}. \tag{3.42}$$

The Chernoff bound in (3.42) shows clearly that the BEP decays exponentially with the product $M_T N_R$ of the number of transmit and receive antennas.

From (3.38-3.41), it is clear that the BEP depends on the total mean received signal-to-noise ratio per symbol, γ_s, and the MSE, $\sigma_e^2(m)$, which in turn depends on the channel model and the estimator used. Our receiver and BEP results here reduce to those of Alamouti [15] and Tarohk [17] if the CSI were perfect, i.e., $\sigma_e^2(m) = 0$. The block-wise constant channel assumption plays a key role in obtaining the results. It leads to the conditional mean and variance of $z_{k'}$ in (3.19a) being a function only of $\sum_{i=1}^{M_T}\sum_{l=1}^{N_R}\lambda_{i,k'}|\hat{h}_{il}(m)|^2$, independent of the cross-terms in the channel estimates. We now apply the analytical results above to the existing orthogonal STBC designs. When condition (3.34) is satisfied, the upper and lower bounds in (3.33) and hence those in (3.35) coincide with each other. The BEP expression in (3.38) is now given by

$$\Gamma(\alpha) = \frac{1}{K}\sum_{k'=1}^{K} F(\alpha, \mu(\rho_{k'}, \lambda_{k'})). \tag{3.43}$$

The STBC's that satisfy (3.34) include the Alamouti's design [15], the full rate real designs for two to eight transmit antennas [17], the systematic half-rate complex designs [17], the 4×4 rate-3/4 STBC in [17] and [47], and the 30×6 rate-2/3 design in [53]. For those square designs which satisfy $\boldsymbol{S}^\dagger\boldsymbol{S} = \boldsymbol{S}\boldsymbol{S}^\dagger = \sum_{k=1}^{K}|s_k|^2\boldsymbol{I}$, e.g., Alamouti's design [15], the 4×4 and 8×8 real designs [17], and the the 4×4 rate-3/4 STBC in [47], it can be shown that $\omega_{i,k'} = K$ from (3.28). The BEP expression is then given in (3.43) with $\rho_{k'} = K, \lambda_{k'} = 1,$ for all k'. A summary of those known STBC's having the exact BEP expression (3.43) is given in Table 3.1.

When condition (3.34) cannot be met, it is impossible to average (3.31) over all channel estimates analytically. Only the upper and lower bounds in (3.33) can be obtained in general. It will be shown in section 3.4 that these two bounds are very close to each other for most codes, and, thus they provide a very good approximation to the BEP performance for PSK modulations. Those orthogonal STBC's known so far that

	STBC proposed in	Size($P \times M_T$)	Rate	$\lambda_{k'}$	$\rho_{k'}$
Real Orthogonal Designs	[5]	2×2	1	1	2
		$4\times4,3$	1	1	4,3
		$8\times8,7,6,5$	1	1	8,7,6,5
Complex Orthogonal Designs	[13] (1Tx case)	1×1	1	1	1
	[4] (Alamouti)	2×2	1	1	2
	[5] [6]	4×4	3/4	1	3
	[12]	30×6	2/3	1	4
	[5] (systematically constructed half-rate STBC's)	4×2	1/2	2	2
		$8\times4,3$		2	4,3
		$16\times8,7,6,5$		2	8,7,6,5

Table 3.1: Parameters list for exact BEP evaluation

STBC proposed in	Size ($P \times M_T$)	Rate	$[\lambda_{\min,k'}, \rho_{\max,k'}]$ for upper bound	$[\lambda_{\max,k'}, \rho_{\min,k'}]$ for lower bound
[5][6]	4×3	3/4	[1 ,3]	[1,2]
[8]	7×4	4/7	[1,4]	[1,2]
[8]	11×5	5/8	[1,4]	$[2,3]_{k'=1,2,3}$ $[1,3]_{k'=4,5,6,7}$
[9] [10]	15×5	2/3	[1,4]	[1,3]
[8]	30×6	3/5	$[1,5]_{k'=1\ldots11,18}$ $[1,3]_{k'=11\ldots14}$	$[2,4]_{k'=1,2,3}$ $[2,3.5]_{k'=4\ldots11}$ $[1,4]_{k'=12\ldots17}$ $[1,3]_{k'=18}$
[12]	56×7	5/8	[1,5]	[1,4]

Table 3.2: Parameters list for lower and upper bound of BEP evaluation

do not satisfy (3.34) are summarized in Table 3.2.

3.4 Numerical Results and Discussion

In simulation, 20 preamble blocks are firstly sent to train the estimator. The parameters are chosen by default as, 1 pilot block is periodically inserted into the transmission after every 9 data blocks were sent. This incurs 10% loss of bandwidth efficiency. For Jakes' channel model, a decision feedback Wiener filter with 10 taps is used, and the estimator for PSAM uses the 10 nearest pilot block for generating the estimation. Using

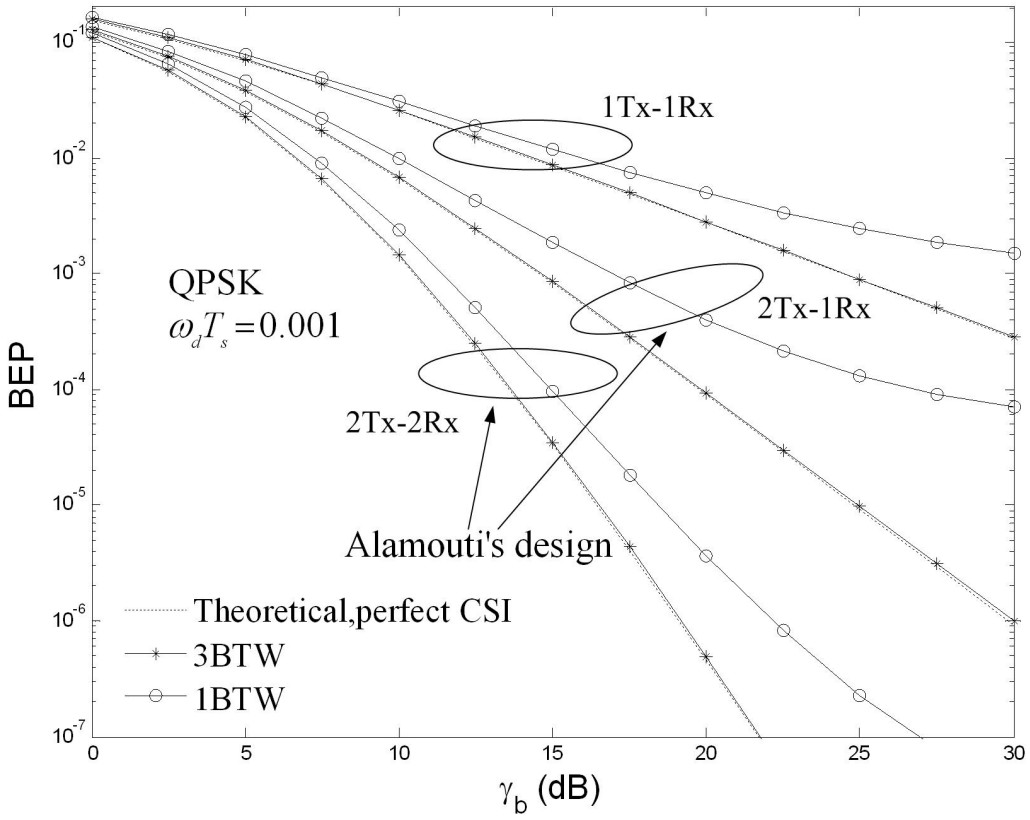

Fig. 3.4: Theoretical BEP performance of Alamouti's STBC under BTW channel

the above results, the BEP's of M PSK are computed and plotted against the total mean received SNR per bit given by $\gamma_b = \frac{10}{9}\gamma_s \sum_{i=1}^{M_T}\sum_{k=1}^{K}\lambda_{i,k}/K\log_2 M$. These BEP results represent the actual performance achievable by our receiver, under a block-wise constant channel model. BEP performances of Alamouti's scheme under Butterworth channel models are demonstrated in Fig.3.4 and Fig.3.5. Also plotted in Fig.3.4 are the BEP with perfect CSI at the receiver, i.e., perfect channel estimation with $\sigma_e^2(m) = 0$, as well as the conventional one-transmit antenna result obtained from [62] to show the diversity gains. As mentioned in section 3.2, the performance calculation is based on the assumption of block-wise constant channel and, thus, uses the block normalized fade rate $\omega_d T_B$, instead

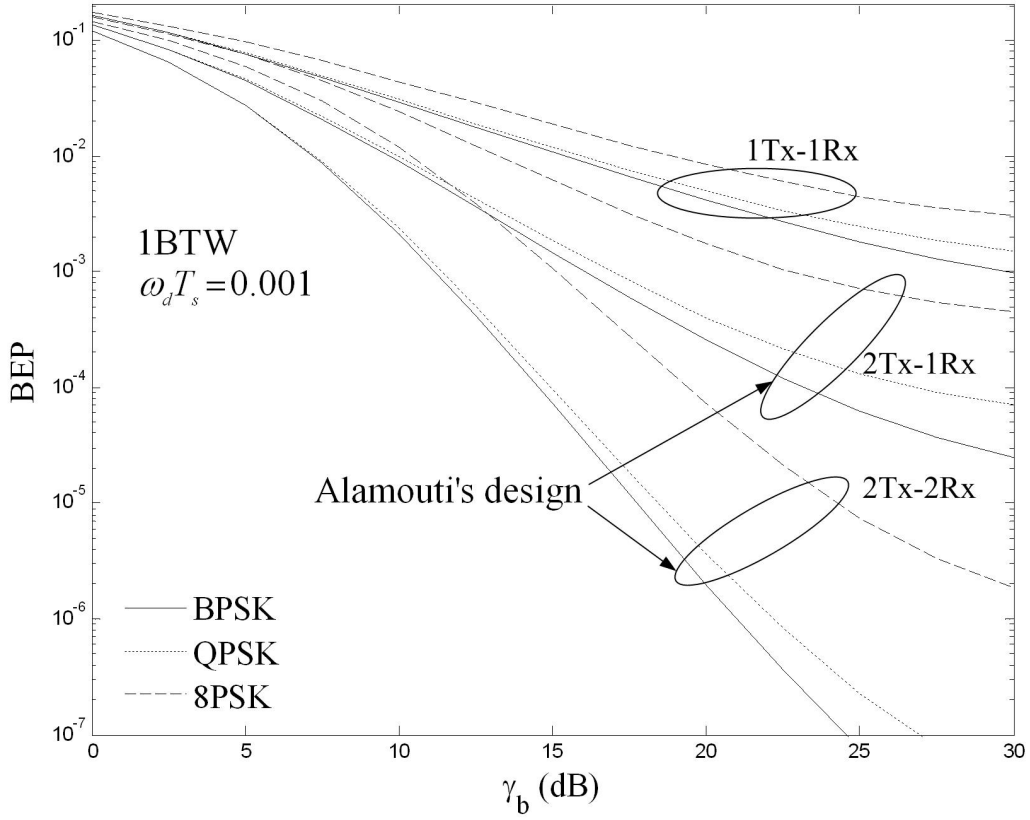

Fig. 3.5: Theoretical BEP performance of Alamouti's STBC under 1BTW channel

of the symbol normalized one $\omega_d T_s$, i.e., we actually use $\omega_d T_B = 0.002$ for the BEP computation of the Alamouti's STBC with the normalized fade-rate of $\omega_d T_s = 0.001$. This idea is used throughout this dissertation unless otherwise stated. For this low fade rate, the performance under the 3BTW channel is almost the same as that of the receiver with perfect CSI. However, performance under the 1BTW channel is worse than that under the 3BTW channel. This is because for the same fade-rate, the 3BTW channel fluctuates more slowly than the 1BTW channel does, making it easier to track. The fade rate, of course, determines the accuracy with which the channel can be tracked, and a higher fade rate in general tends to lead to a larger channel estimation MSE. It is

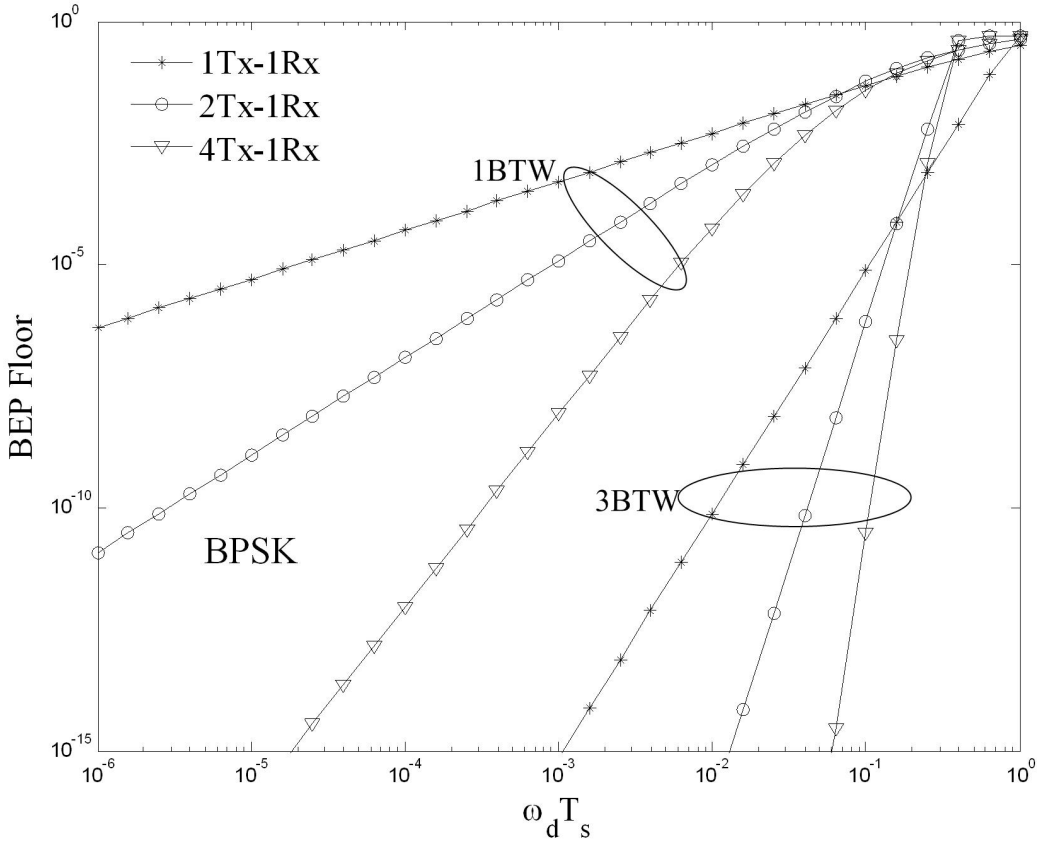

Fig. 3.6: Theoretical BEP floor under BTW channel

shown in Fig.3.5 that the 8PSK modulation is much worse than the BPSK and QPSK even under a slow fade rate, which indicates 8PSK is not an efficient modulation for STBC.We focus on the performances of BPSK and QPSK afterwards. Also in Fig.3.5, it is obvious that the BEP's tend to reach a floor as SNR increases. The BEP curve of our receiver asymptotically reaches an irreducible floor as the SNR approaches infinity. This is as expected, because the estimated channel gain matrix $\hat{\boldsymbol{H}}(m)$ is a predicted estimate, and for any nonzero channel fade rate $\omega_d T_s$ there is an irreducible, nonzero error variance in the prediction, even as the SNR becomes very large. This irreducible prediction error variance leads to the error floor. For the 1BTW channel model, for instance,

this BEP floor can be obtained analytically. Setting E_s/N_0 to infinity in (2.40), the steady-state MSE $\sigma^2_{e,\infty}$ of the channel estimates can be shown to be $\mathcal{R}(0)(1-e^{-2\omega_d T_B})$, which is purely a function of the fade rate $\omega_d T_s$. Using this value of $\sigma^2_{e,\infty}$ as the value for $\sigma^2_e(m)$ in (3.37) gives a limiting value of $\eta_\infty = e^{-2\omega_d T_B}$. This limiting value of η gives the irreducible BEP for M PSK. Fig.3.6 demonstrated this ultimate floor value for BTW channel against the normalized fade rate, where the 4×4 real orthogonal design [17] is used for 4-Tx case. As the fade rate becomes larger than some thresholds, the BEP floor of STBC's with more transmit antennas become even worse than that of those with less. As the size of STBC increase, it also requires longer coherent time to satisfy the block-wise constant channel assumption. As the fade rate increases, the performance of large-size STBC's surely degrade much earlier than the small ones. We use Alamouti's design[15] and the 4-by4 rate-3/4 designs in [47, 48] in Fig.3.7, and as can be seen, for a faster channel with a normalized fade rate of $\omega_d T_s = 0.1$, the performance curves with channel estimation deviate more from those with perfect CSI, with the deviation being greater for the QPSK than for the BPSK modulation. Since we use a block fade-rate $\omega_d T_B$ for performance analysis, the block length P is critical to the performance. In Fig.3.8, we compare the performance of 2×2, 4×4, 8×8 full-rate real designs together with the systematically constructed 4×2, 8×4, 16×8 half-rate COD proposed in [17], respectively. The half-rate codes use QPSK for fair comparison. According to the result in Table 3.1, they have identical performance when CSI is perfectly known. Under a 1BTW channel of $\omega_d T_s = 0.001$, it is shown that the full-rate designs with shorter block length P outperform their corresponding half-rate ones, and the performance gap between them becomes larger as P increases. This loss is only due to the increased block fade rate $\omega_d T_B$. One can expect that when the channel is fast enough to be considered symbol-wise constant, there will be more loss due to a longer block length P. This indicates that in designing a practical STBC, one should keep the P as small as possible while gaining from the space-time diversity. When P is too large, the resulting perfor-

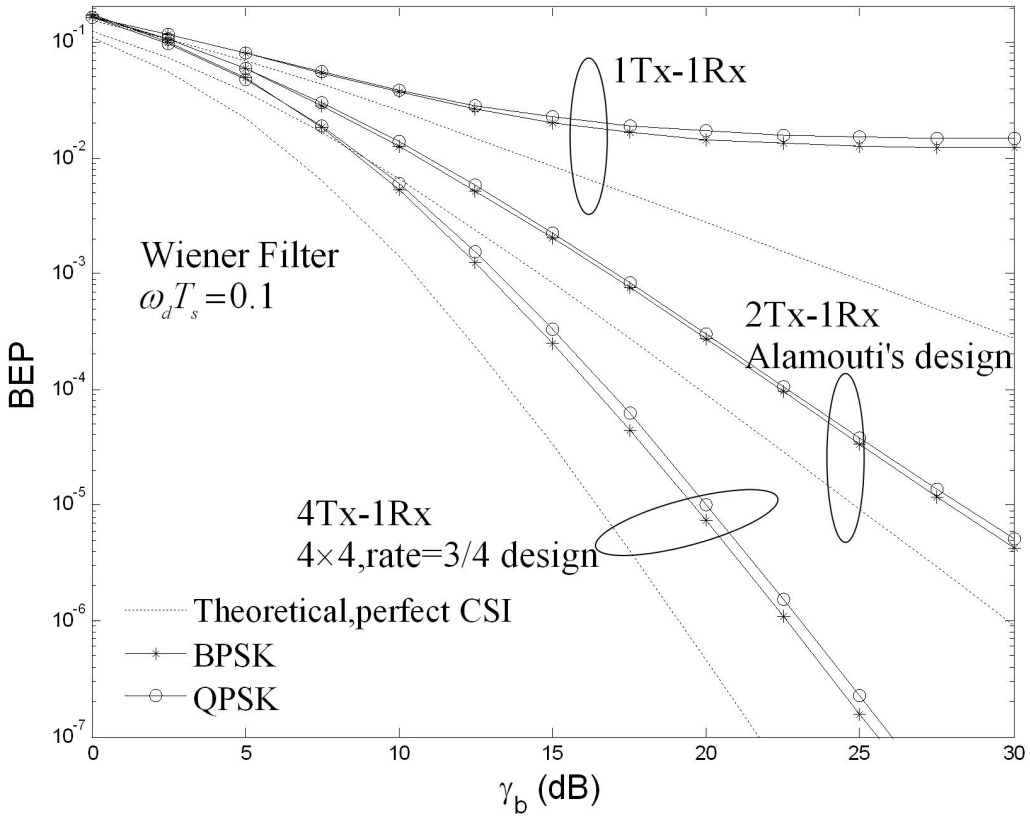

Fig. 3.7: Theoretical BEP performance comparison with different numbers of transmit antennas under Jakes' channel model using DF WF estimator

mance loss so caused might be greater than the diversity gain, making the performance even worse. As discussed in Section 3.3, an exact BEP expression cannot be obtained for those STBC's which do not satisfy condition (3.34). In Fig.3.9, the upper bound and lower bound of several such STBC's in Table 3.2 are plotted. It can be seen that under Jakes' channel model with $\omega_d T_s = 0.01$ and PSAM, these two bounds are very close to each other, the difference being even negligible for the STBC with a small P ($P = 4$). The bounds thus provide a very good approximation to the actual BEP. Recall that the receiver and its theoretical BEP performance were obtained under the assumption that the channel is constant over a block. Thus, it would be of interest to know how

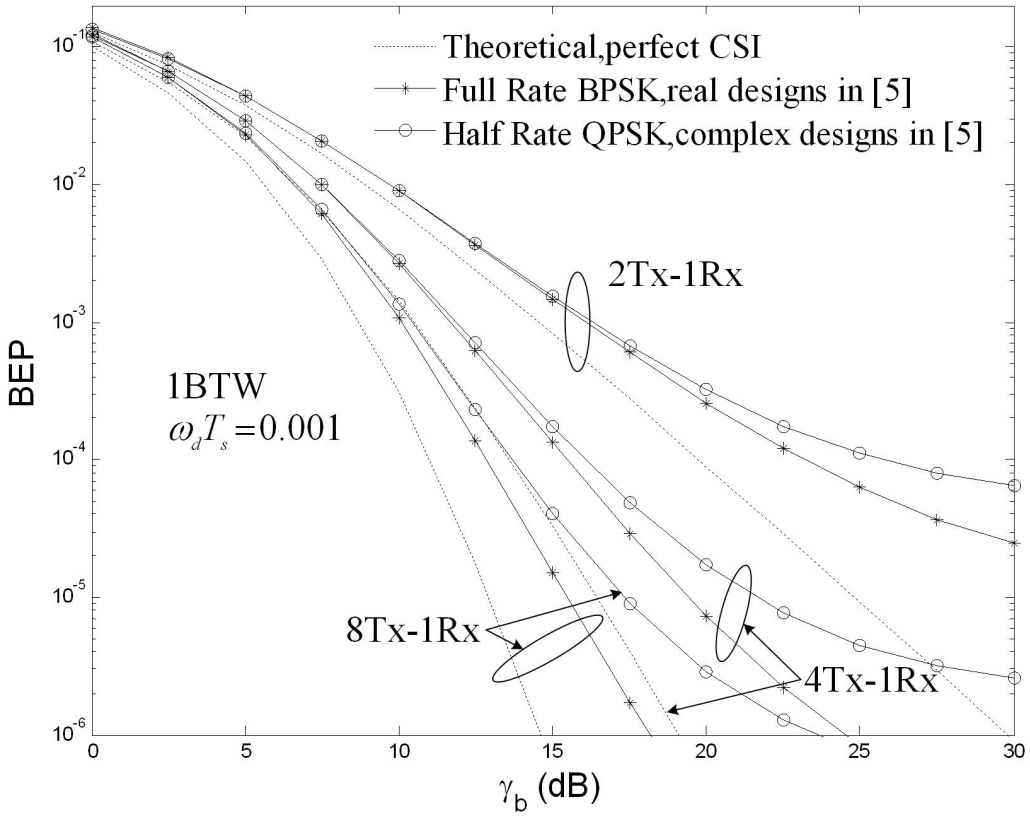

Fig. 3.8: Theoretical BEP performance comparison between full- and half- rate STBC's under Jakes' channel model using PSAM

accurately our theoretical BEP results predict the actual performance of our receiver when the latter is operating under a symbol-wise channel where the channel fading gain is constant only over a symbol period and fluctuates from one symbol period to the next. Fig. 3.10 shows the BPSK performance under Jakes' fading channel with Alamouti's scheme for single receive antenna. The gap caused by the error of the imperfect channel estimation between the theoretical performance and the one with perfect CSI is within 1dB. The Chernoff bound is about 2-3dB higher from the theoretical performance. The simulation is conducted under a symbol-wise constant channel,i.e., it fluctuates from symbol period to symbol period, while the theoretical BEP performances were obtained

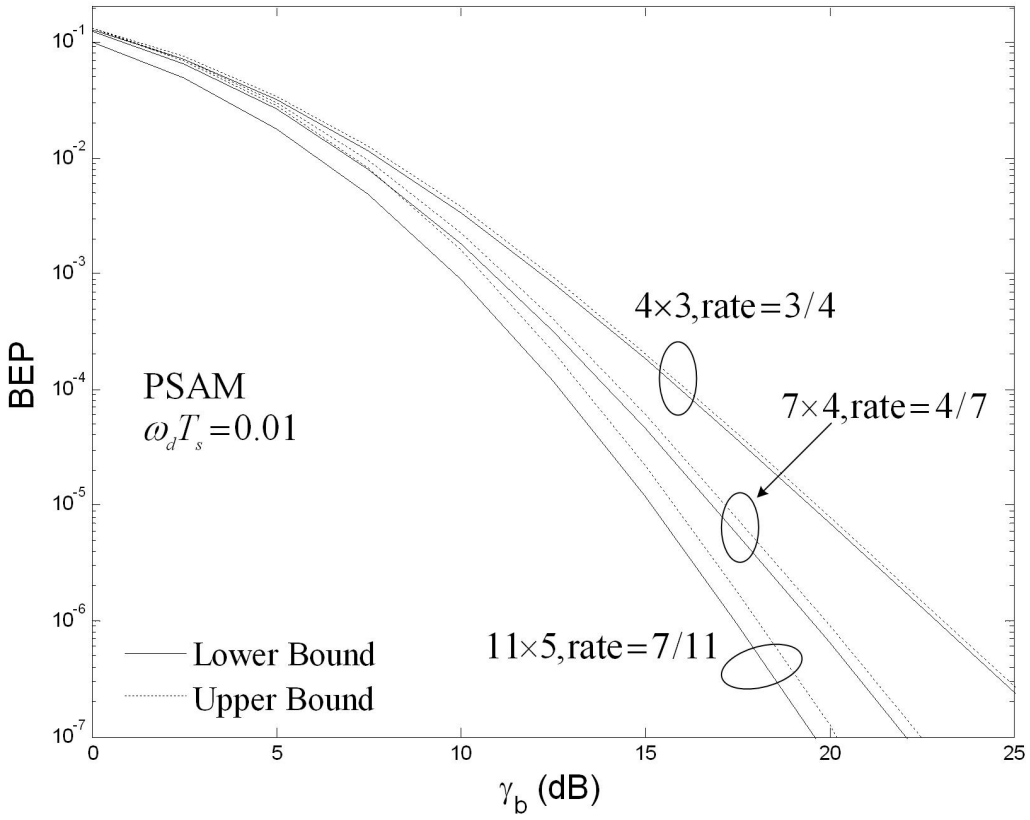

Fig. 3.9: Theoretical bounds of BEP performance for different STBC's under Jakes' channel model using PSAM

under the quasi-static assumption. It can be seen in Fig. 3.10 that the simulation result is close to the theoretical performance, with around 1dB difference. To show the cause of this gap, we also simulated the case with ideal decision feedback (IDF) . In IDF mode, different from the actual decision feedback (ADF) mode, the estimator uses $\boldsymbol{S}(m)$ instead of $\hat{\boldsymbol{S}}(m)$ when computing (3.7), i.e., the estimator knows the transmitted symbols perfectly, and thus can remove the errors due to erroneous decision-feedback. Using the IDF results as a benchmark, we see that decision errors lead to a performance degradation of about 2 dB. The IDF result matches the theoretical calculation perfectly, which means a realistic fading channel with $\omega_d T_s = 0.001$ is slow enough to validate

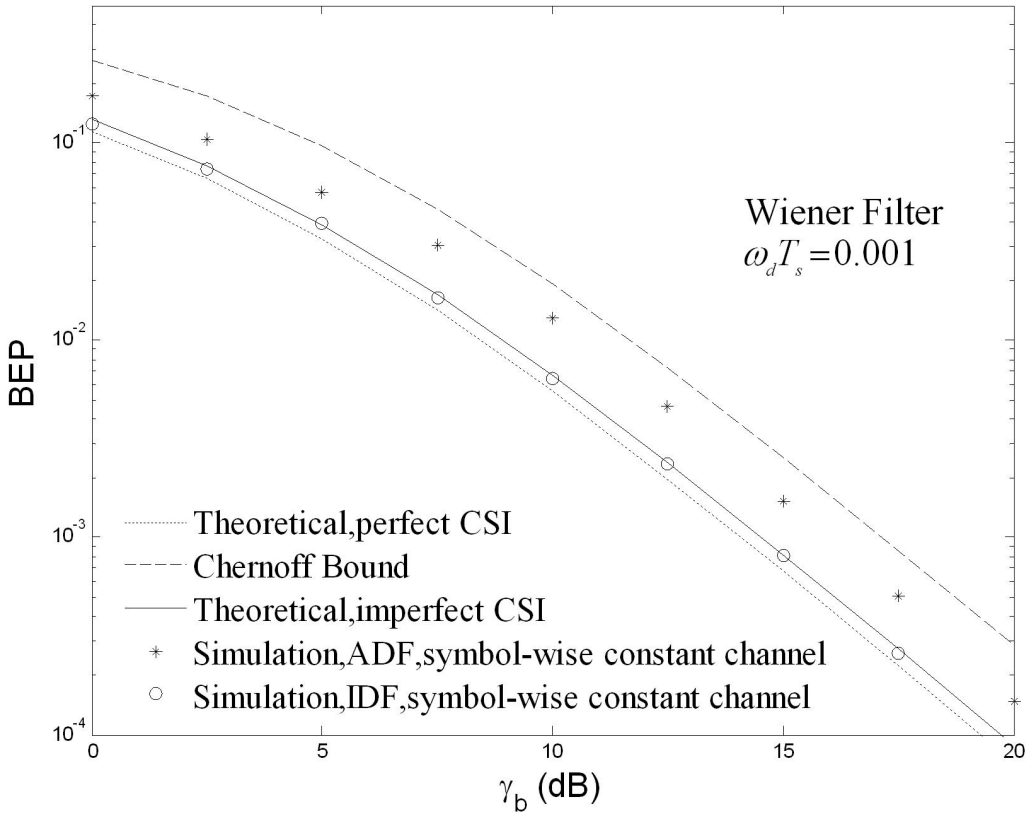

Fig. 3.10: BEP of BPSK with Alamouti's STBC with one receive antenna under Jakes' channel model

the quasi-static assumption and it is sound for us to make such an assumption in our derivations. In Fig.3.11, we adopt the 4×4 rate-3/4 STBC proposed in [47] under a 3BTW channel. Besides the IDF condition, we also generate a block-wise constant channel for simulation. The curves in the figure clearly show the factors that influence the STBC performance. The simulation results with block-wise constant channel and IDF match the theoretical predication perfectly, thus validating our analysis. The performance difference between symbol-wise constant channel case and block-wise constant channel case is due to the channel fluctuations that disturb the orthogonality of the STBC. Similar to Fig.3.12, the error propagation caused by the errors in decision feed-

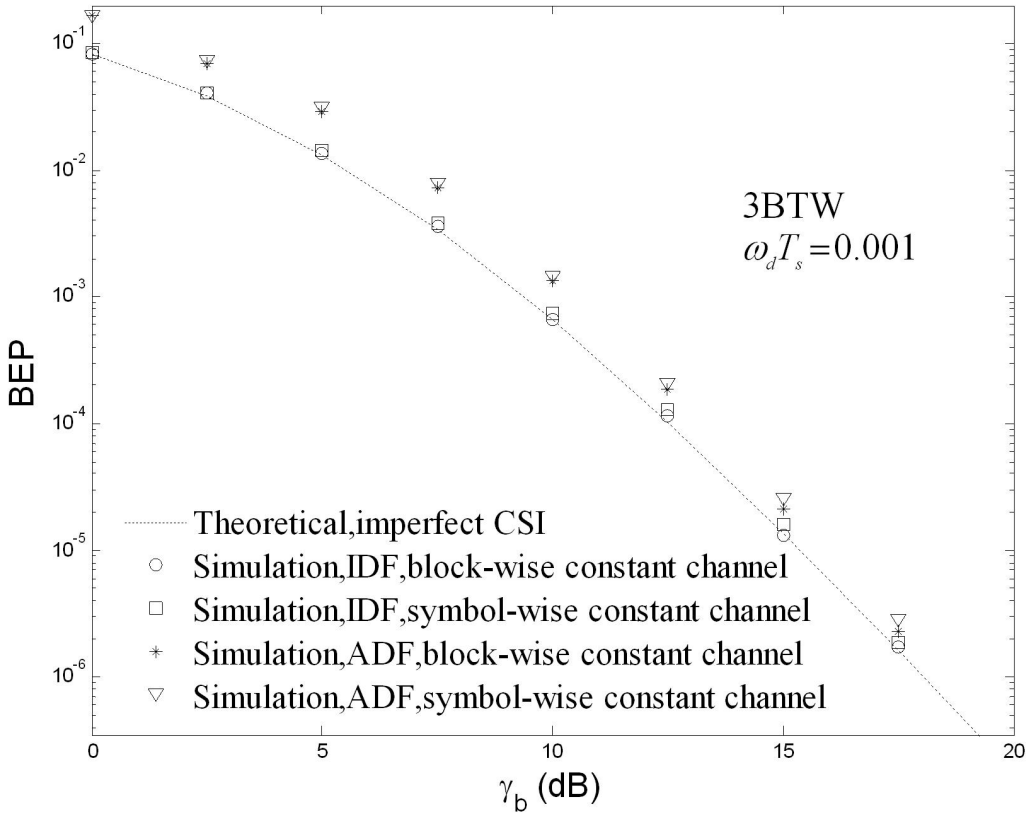

Fig. 3.11: BEP Performance of 4×4 *rate-3/4 STBC with QPSK under 3BTW Channel*

back is still the main reason for the performance degradation in an actual STBC system. We use PSAM in Fig. 3.12 to remedy this problem. The simulation is carried out under a fast fading Jakes' channel with $\omega_d T_B = 0.2$. Again, the simulation under a block-wise constant channel matches the theoretical performance perfectly, and the loss caused by the symbol-to-symbol fluctuation of the channel is within 1dB even under high SNR. PSAM is still more preferable than a DF system for STBC when the block length is not very large.

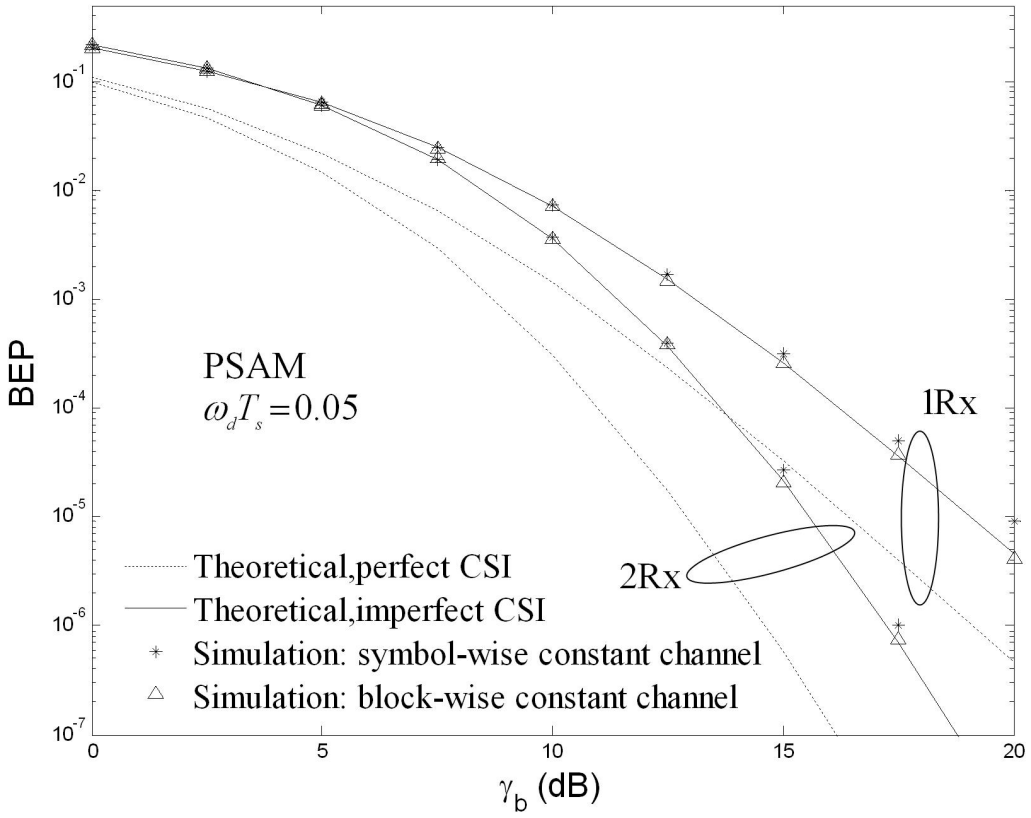

Fig. 3.12: BEP performance of 4×4 *rate-3/4 STBC with QPSK under Jakes' channel model using PSAM*

3.5 Summary

We presented a SBS channel estimation receiver for space-time block coded systems. A simple, closed-form expression for its BEP is obtained, showing clearly the dependence of the BEP on the channel estimation MSE. We simulated the receiver under the more realistic assumption that the channel is constant over only a symbol period, and fluctuates from one symbol period to the next. The simulations validate the theoretical performance prediction, and verify that the accuracy of the latter prediction depends on the fade rate $\omega_d T_s$.

Chapter 4

STBC Communication System with Receive Antenna Selection

In this chapter, we present receive antenna selection combining schemes for wireless communication systems with STBC. As channel estimation is compulsory at the receiver for coherent detection of STBC systems, we make use of the estimated SNR as the selection criteria for receive antenna selection. Based on this estimated SNR criterion, we propose STBC systems with selection combining at the receiver, which choose one or several branches with the maximum or the maximum several estimated SNR's. We analyze the performance and develop closed-form BEP expressions with PSK modulation for such systems. Comparing to those results in the literature, both space-time block coding and channel estimation are considered, and the results are explicit in that they show direct BEP dependence on the MSE of estimator and the system parameters chosen. We also show that the selection combining with STBC achieves full diversity provided by both transmit and receive multiple antennas. With the calculated BEP performances, it is found that the proposed selection combining schemes are efficient means to maintain a simple receiver structure with tolerable performance loss from MRC.

4.1 Introduction

Diversity reception techniques are well known for enhancing the performance of wireless communication systems [81, 82]. The commonly used linear diversity combining techniques include selection combining, maximum ratio combining , equal gain combining , etc. Selection combining, which chooses one branch according to certain criteria, named single selection combining (SSC) , is the simplest realization at the receiver. It avoids high power consumption. A commonly used criterion for selection combining is the SNR. Generalized selection combining (GSC) schemes, which combine several branches with most significant SNR, was proposed to bridge the performance gap between the SSC and MRC/EGC [83–87]. In [83], the authors present a GSC scheme that chooses the best two and three branches according to the SNR criteria and analyze the performance for binary signaling over i.i.d. Rayleigh fading channels. In [84], the mean output SNR for GSC over Rayleigh fading channels is obtained in a closed form. The authors also extended their work in [85] for non-i.i.d. channels. A unified approach for GSC is proposed in [86], where both moment generating function (MGF) and p.d.f. of the SNR are obtained in exact closed-form for performance evaluation. Another GSC scheme that selects those links whose SNR exceeds a preset threshold is proposed in [87]. The performance analysis of selection combining schemes over independent or correlated Nakagami- m channels can be found in [88–91]. All these literatures assume perfect SNR knowledge at the receiver. In [92], the performance of binary DPSK with selection combining is analyzed over Rayleigh fading channels, where the CSI is unknown at the receiver. Recently in [93], the authors use a channel estimation receiver, and obtain an estimation-error-dependent closed-form symbol error probability expression for 2-D constellation with selection combining.

To the best of authors' knowledge, not much work has been done on selection combining for STBC systems. In [94], SSC is proposed for Alamouti's STBC and the BEP is presented in an unsolvable integral form. In [95], an upper bound for the BEP

of STBC with GSC is presented by releasing the integral limits in [94] for the ordered statistics. The performance analysis in [95] gives an exact closed-form expression for Alamouti's STBC. However, perfect CSI is assumed at the receiver in both [94] and [95].

In our previous works in Chapter 3, we developed a symbol-by-symbol channel estimation receiver structure for STBC systems, and obtained its BEP expressions with PSK modulations for MRC under non-selective Rayleigh fading channels. The results clearly show the dependence of BEP on the mean-square error (MSE) of the estimator. In this chapter, we extend our receiver structure to selection combining. In this receiver, by knowing the channel estimates, the receiver chooses one or several branches with the largest amplitudes of channel estimate for selection combining. We investigate the selection combining schemes for the case of conventional single-input-multi-output (SIMO) system, Alamouti's STBC system, and generalized STBC systems. Particularly, closed-form BEP expressions are obtained for SSC and GSC for SIMO system, SSC and dual selection combining (DSC) for Alamouti's STBC system, and SSC for generalized STBC with two receive antennas. The results explicitly show that the BEP performances depend on the MSE of estimator and the system parameters chosen.

4.2 System Model and Receiver Structure

Consider a MIMO communication system with M_T-Tx and N_R-Rx, in which, the received signals from N_C antennas with the most significant estimated SNR are selected and combined for decoding. The system employs a $P \times M_T$ generalized complex orthogonal STBC $\boldsymbol{S}$. The definition of orthogonal STBC follows that in section 3.2. Similar to that in Chapter 3, the $M_T \times N_R$ channel matrix is denoted as $\boldsymbol{H}(m)$ for the m - th block interval. In order to coherently detect the transmitted symbols, estimation of channel matrix, $\hat{H}(m)$, must be made before the decoding. Let $\hat{h}_{il}(m)$ be the channel estimate

of $h_{il}(m)$ available at the receiver and

$$\hat{\gamma}_l = E_s \sum\nolimits_{i=1}^{M_T} |\hat{h}_{il}(m)|^2 / N_0 \tag{4.1}$$

be the instantaneous estimated output SNR at the l - th receive antenna, where $E_s = E_0/M_T$ is the energy per symbol. For the sake of simplicity and clarity of the analysis, we assume $E_s = E_0/M_T$ instead of (3.5) in this chapter and hereafter. Arranging $\{\hat{\gamma}_l\}_{l=1}^{N_R}$ in a decreasing order as

$$\hat{\gamma}_{1:N_R} \geq \hat{\gamma}_{2:N_R} \geq \cdots \geq \hat{\gamma}_{N_R:N_R} \geq 0, \tag{4.2}$$

the receiver then selects and combines those branches with $\{\hat{\gamma}_{l:N_R}\}_{l=1}^{N_C}$ for decoding. As only N_C out of N_R receive antennas are actually used for decoding, define $\boldsymbol{H}_T(m)$ of size $M_T \times N_C$ as the effective transmission channel matrix that consists of CSI from transmit antennas to those selected N_C receive antennas. Denoting the m - th ($m = 0, 1, 2...$) transmitted signal block as $\boldsymbol{S}(m)$, the effective received signal can be written in matrix form as

$$\boldsymbol{R}(m) = \boldsymbol{S}(m)\boldsymbol{H}_T(m) + \boldsymbol{N}(m). \tag{4.3}$$

Each entry $r_{pl}(m)$ of the $P \times N_C$ received matrix $\boldsymbol{R}(m)$ is the received signal on the l - th selected receive antenna at the p - th symbol slot of the m - th block, and $\boldsymbol{N}(m)$ is the $P \times N_C$ noise matrix, whose entries $n_{pl}(m)$ are i.i.d., zero-mean, complex, Gaussian random variables due to AWGN at the p - th symbol slot on the l - th receive antenna with $\mathrm{E}[n^*_{p'l'}(m')n_{pl}(m)] = \delta_{pp'}\delta_{ll'}\delta_{mm'}N_0$.

In order to make combining decision from the ordered statistics (4.2), CSI of all links contained in $\boldsymbol{H}(m)$ must be estimated. We use PSAM [76] for channel estimation. A PSAM frame contains one pilot block and $(L_f - 1)$ STBC data blocks. With the time index m starting from zero, the $(m = qL_f)$- th block is a pilot block, where $q = 0, 1, 2....$ We choose the q-th pilot block as an $M_T \times M_T$ diagonal matrix $\tilde{S}_P(qL_f)$ that lasts for

M_T symbol durations, i.e., each transmit antenna sends known PSK symbols in turn to sound the channels while the remaining ones keep silent during the pilot time. Assume each diagonal entry of $\tilde{S}_P$ is a PSK signal with energy E_P. After receiving the pilot block, the receiver removes the known signal $\tilde{S}_P$ from the received signal $\tilde{R}_P$ by calculating

$$\boldsymbol{Y}_q = [\tilde{S}_P^{\dagger}(qL_f)\tilde{S}_P(qL_f)]^{-1}\tilde{S}_P(qL_f)\tilde{R}_P(qL_f) = \boldsymbol{H}(qL_f) + \tilde{N}. \tag{4.4}$$

By assuming $P \simeq M_T$, it can be shown that $\boldsymbol{Y}_q$ is a noisy observation of the channel matrix $\boldsymbol{H}(qL_f)$, and each entry $y_{il,q}, i = 1 \ldots M_T, l = 1 \ldots N_R$ of $\boldsymbol{Y}_q$ can be expressed in the form $y_{il,q} = h_{il}(qL_f) + \tilde{n}_{il,q}$, where $\{\tilde{n}_{il,q}\}_q$ is a set of i.i.d. zero mean complex Gaussian random variables with variance $E_P^{-1}N_0$. Define $\tilde{\boldsymbol{y}}_{il}(m) = [y_{il,q}]_{q=\llbracket m/L_f \rrbracket - L_p + 1}^{\llbracket m/L_f \rrbracket + L_p}$ as the array storing the $2L_p$ nearest pilot information of the m - th block, where $\llbracket \cdot \rrbracket$ denotes the floor operation. The channel estimate $\hat{h}_{il}(m)$ is then given by

$$\hat{h}_{il}(m) = \boldsymbol{w}^{\dagger}(m)\tilde{\boldsymbol{y}}_{il}(m),\ i = 1...M_T, l = 1...N_R, \tag{4.5}$$

where $\boldsymbol{w}(m) = \boldsymbol{\Xi}^{-1}\boldsymbol{p}(m)$, $\boldsymbol{\Xi} = \mathrm{E}[\tilde{\boldsymbol{y}}_{il}(m)\tilde{\boldsymbol{y}}_{il}^{\dagger}(m)]$ and $\boldsymbol{p}(m) = \mathrm{E}[h_{il}(m)\tilde{\boldsymbol{y}}_{il}^{\dagger}(m)]$. Note that the (l_1, l_2) - th entry of $\boldsymbol{\Xi}$ is

$$\Xi(l_1, l_2) = \begin{cases} \mathcal{R}(0) + E_P^{-1}N_0/2,\ l_1 = l_2 \\ \mathcal{R}(l_1 - l_2),\ l_1 \neq l_2 \end{cases},\ l_1, l_2 = 1...2L_p \tag{4.6}$$

while the l_1 - th entry of vector $\boldsymbol{p}(m)$ is

$$p(m, l_1) = \mathcal{R}([\llbracket m/L_f \rrbracket + L_p - l_1 + 1]L_f - m). \tag{4.7}$$

With MMSE channel estimation, each $h_{il}(m)$ is a Gaussian random variable with mean $\hat{h}_{il}(m)$, and variance $2\sigma_e^2(m)$, conditioned on channel measurements available at the receiver. Note that the MSE's $2\sigma_e^2(m)$ defined as

$$2\sigma_e^2(m) = \mathrm{E}[|h_{il}(m) - \hat{h}_{il}(m)|^2] = \mathcal{R}(0) - \boldsymbol{p}^T(m)\boldsymbol{w}(m) \tag{4.8}$$

are identical for all channels due to the i.i.d. channel assumption.

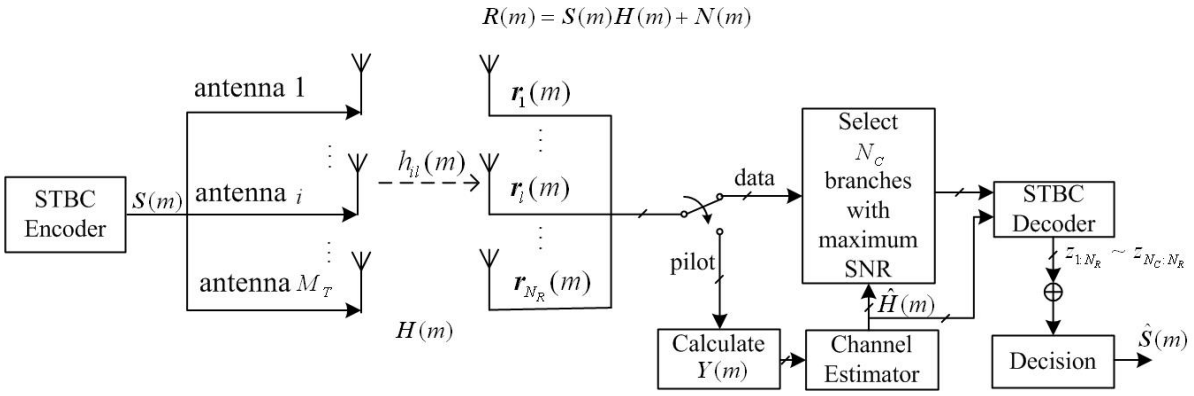

Fig. 4.1: System model of STBC with selection combining

After the channel estimation process described above, a channel estimation matrix $\hat{\boldsymbol{H}}(m)$ on $\boldsymbol{H}(m)$ is now known to the receiver. The receiver now decides a $M_T \times N_C$ sub-matrix $\hat{\boldsymbol{H}}_T(m)$ of $\hat{\boldsymbol{H}}(m)$ that maximize the Frobenius norm $||\hat{\boldsymbol{H}}_T(m)||^2$. The effective received signal in (4.3) is then sent to a symbol-by-symbol decoder defined by

$$\hat{s}_k(m) = \arg \max_{s_k} \max_{k=1\ldots K} Re[z_k(m) s_k^*(m)], \tag{4.9}$$

where $z_k(m) = \mathrm{Tr}[\boldsymbol{R}^\dagger(m)\boldsymbol{B_k}\hat{\boldsymbol{H}}_T(m) + \hat{\boldsymbol{H}}_T^\dagger(m)\boldsymbol{A_k^\dagger}\boldsymbol{R}(m)]$. This detector is not optimum with imperfect channel estimation but computationally the simplest for implementation. The system model for STBC with selection combining with PSAM channel estimation and the receiver structure are illustrated in Fig. 4.1.

4.3 Performance Analysis of STBC with Selection Combining

The BEP depends on the quantity $P(Re\{z_k e^{-j\alpha}\} < 0 | s_k = \sqrt{E_s}, \Lambda)$, where $\Lambda = \{\tilde{y}_{il}(m)\}_{i,l=1}^{M_T,N_R}$ is the set containing the channel information from the pilot sequence, and α is some angle. Hereafter we drop the time index m for simplicity. It has been shown

in Chapter 3 that

$$P(Re\left\{z_k e^{-j\alpha}\right\} < 0 | s_k = \sqrt{E_s}, \Lambda) = or \cong Q\left(\sqrt{\frac{\lambda_k E_s \cos^2\alpha \sum_{i=1}^{M_T}\sum_{l=1}^{N_C} |\hat{h}_{il}|^2}{\rho_k E_s \sigma_e^2 + \frac{N_0}{2}}}\right), \quad (4.10)$$

where ρ_k and λ_k are constants determined by the STBC used. The equal sign holds for those STBC designs where $\boldsymbol{S}^\dagger \boldsymbol{S}$ is proportional to an identity matrix. Otherwise, (4.10) still gives a very good approximation to the BEP evaluation though not exact. For simplicity, we use equal sign hereafter. However, it should be noted that not all STBC's have exact BEP expressions as mentioned. The values of ρ_k and λ_k for different STBC designs can be found in Table 3.1 and Table 3.2. Now rewrite (4.10) in a simple form as

$$P(Re\left\{z_k e^{-j\alpha}\right\} < 0 | s_k = \sqrt{E_s}, \Lambda) = Q\left(\sqrt{\beta_k \sum_{l=1}^{N_C} \hat{\gamma}_{l:N_R}}\right), \quad (4.11)$$

where $\beta_k = 2\lambda_k \cos^2\alpha/[\rho_k(1-\eta)\bar{\gamma}_s + 1]$, $\eta = 1 - \sigma_e^2/\mathcal{R}(0)$ and $\bar{\gamma}_s = 2E_s\mathcal{R}(0)/N_0$ is the mean SNR per symbol per receive antenna. The equivalent estimated output SNR per symbol at the output of the selection combiner, $\hat{\gamma}_{s,\text{out}} = 2E_s||\boldsymbol{H}_T||^2/N_0$ is the summation of the first N_C quantities from the order statistics (4.2), i.e.,

$$\hat{\gamma}_{s,\text{out}} = \sum_{l=1}^{N_C} \hat{\gamma}_{l:N_R}. \quad (4.12)$$

To evaluate the BEP , we average the quantity in (4.11) over the estimated SNR as

$$F_k(\alpha) = \int_0^\infty Q\left(\sqrt{\beta_k \gamma}\right) f_{\hat{\gamma}_{s,\text{out}}}(\gamma) d\gamma. \quad (4.13)$$

The probability in (4.13) only provides the BEP evaluation for a single symbol s_k. Hence, it must be averaged over all K transmitted symbols. Given that all symbols are equally

likely, define the BEP function $\mathrm{P}(\alpha)$ as

$$\mathrm{P}(\alpha) = \frac{1}{K}\sum_{k=1}^{K} F_k(\alpha). \tag{4.14}$$

And the BEP for PSK signaling is given as in (3.39-3.41). As discussed in Chapter 3, $h_{il}(m)$ is a Gaussian random variable with mean $\hat{h}_{il}(m)$, and variance $2\sigma_e^2(m)$, conditioned on channel measurements available at the receiver. Furthermore, $\hat{h}_{il}(m)$ is itself a Gaussian random variable with mean zero and variance $[\mathcal{R}(0) - \sigma_e^2]$ [62]. The instantaneous estimated SNR at the l - th receiver $\hat{\gamma}_l$ defined in (4.1) thus has a χ^2 -distribution with $2M_T$ degrees of freedom with mean

$$\bar{\gamma} = E[\hat{\gamma}_l] = E_s \cdot 2M_T(\mathcal{R}(0) - \sigma_e^2)/N_0 = \eta M_T \bar{\gamma}_s = \eta\bar{\gamma}_0. \tag{4.15}$$

The p.d.f. and c.d.f of $\hat{\gamma}_l$ are respectively given by [79]

$$f_{\hat{\gamma}_l}(\gamma) = \frac{M_T^{M_T}}{\bar{\gamma}^{M_T}(M_T-1)!}\gamma^{M_T-1}e^{-M_T\gamma/\bar{\gamma}} \tag{4.16}$$

and

$$F_{\hat{\gamma}_l}(\gamma) = 1 - e^{-\frac{M_T\gamma}{\bar{\gamma}}}\sum_{n=0}^{M_T-1}\frac{1}{n!}\left(\frac{M_T\gamma}{\bar{\gamma}}\right)^n. \tag{4.17}$$

Consequently, the joint p.d.f of the maximum N_C estimated SNR $\{\hat{\gamma}_{l:N_R}\}_{l=1}^{N_R}$ is [86]

$$\begin{aligned} &f_{\hat{\gamma}_{1:N_R},\hat{\gamma}_{2:N_R},\cdots,\hat{\gamma}_{N_C:N_R}}(\hat{\gamma}_{1:N_R},\hat{\gamma}_{2:N_R},\cdots,\hat{\gamma}_{N_C:N_R}) \\ &\qquad = N_C!\binom{N_R}{N_C}\left[F_{\hat{\gamma}_l}(\hat{\gamma}_{N_C:N_R})\right]^{N_R-N_C}\prod_{l=1}^{N_C} f_{\hat{\gamma}_l}(\hat{\gamma}_{1:N_R}) \end{aligned} \tag{4.18}$$

where $\hat{\gamma}_{1:N_R} \geq \hat{\gamma}_{2:N_R} \geq \cdots \geq \hat{\gamma}_{N_R:N_R}$.

The MGF of the total combined SNR $\sum_{l=1}^{N_C} \hat{\gamma}_{l:N_R}$ is given by

$$M(s) = \int_0^\infty \int_{\gamma_{N_C:N_R}}^\infty \cdots \int_{\gamma_{2:N_R}}^\infty e^{s\sum_{l=1}^{N_C} \gamma_{l:N_R}} f_{\gamma_{1:N_R},\gamma_{2:N_R},\cdots,\gamma_{N_C:N_R}}(\hat{\gamma}_{1:N_R}, \hat{\gamma}_{2:N_R}, \cdots, \hat{\gamma}_{N_C:N_R}) \\ d\hat{\gamma}_{1:N_R} d\hat{\gamma}_{2:N_R} \cdots d\hat{\gamma}_{N_C:N_R}. \tag{4.19}$$

With this MGF, the BEP function P(α) in (4.14) can be obtained as

$$F_k(\alpha) = \int_0^{\pi/2} M(\frac{\beta\gamma}{2\sin^2\theta}) d\theta. \tag{4.20}$$

The closed form solution for the N_C - fold integral in (4.19) cannot be obtained, as there are $\hat{\gamma}_{l:N_R}$'s in the lower limit of the integral interval. Numerical approaches must be taken for the BEP calculations. In [95], the authors obtained a performance upper bound by replacing all the $\hat{\gamma}_{l:N_R}$ in the integral limits in (4.19) by zeros. Here we consider special cases where the equation (4.20) has an exact closed-form expression.

4.3.1 Single selection combining

In single selection combining, the receiver selects the branch with maximum estimated SNR for decoding. By substituting $N_C = 1$ in (4.18), the p.d.f. of the maximum SNR, $\hat{\gamma}_{1:N_R}$ can be written as

$$f_{\hat{\gamma}_{1:N_R}}(\gamma) = N_R \left[F_{\hat{\gamma}_l}(\gamma)\right]^{N_R-1} f_{\hat{\gamma}_l}(\gamma). \tag{4.21}$$

4.3.1.1 One Transmit Antenna($M_T = 1$)

As we mentioned earlier, the conventional 1Tx system is a special case of STBC with $\boldsymbol{S} = [s_1]$. In a SIMO system, each $\hat{\gamma}_l$ is Rayleigh distributed. The distribution of

maximum estimated SNR, $\hat{\gamma}_{1:N_R}$ is

$$f_{\gamma_{1:N_R}}(\gamma) = \frac{N_R}{\bar{\gamma}} \sum_{n=0}^{N_R-1} \binom{N_R-1}{n} (-1)^n e^{-\frac{(n+1)\gamma}{\bar{\gamma}}}. \tag{4.22}$$

For 1-Tx case, $\rho_k = \lambda_k = 1$, thus $\beta_k = \beta = 2\cos^2\alpha/[(1-\eta)\bar{\gamma}_s + 1]$ for all $k = 1...K$ in (4.11). The MGF of p.d.f. in (4.22) is readily evaluated as

$$M_{f_{\gamma_{1:N_R}}}(s) = \sum_{n=0}^{N_R-1} \binom{N_R-1}{n} \frac{(-1)^n N_R}{1+n-s\bar{\gamma}}. \tag{4.23}$$

Substituting (4.23) in (4.20), we have

$$\mathrm{P}(\alpha) = N_R \sum_{n=0}^{N_R-1} \binom{N_R-1}{n} \frac{(-1)^n}{n+1} G_1(\frac{\beta\bar{\gamma}}{2n+2}), \tag{4.24}$$

where the function $G_n(\cdot)$ is defined as [96]

$$G_n(c) = \frac{1}{\pi} \int_0^{\pi/2} \left(1 + \frac{c}{\sin^2\theta}\right)^{-n} d\theta = \frac{1}{2}\left[1 - \mu(c) \sum_{k=0}^{n-1} \binom{2k}{k} \left(\frac{1-\mu^2(c)}{4}\right)^k\right] \tag{4.25}$$

and

$$\mu(c) = \sqrt{\frac{c}{1+c}}. \tag{4.26}$$

For $\bar{\gamma} \gg 1$, (4.24) can be approximated as

$$\mathrm{P}(\alpha) \simeq \frac{(2N_R-1)!!}{2} \left(\frac{1}{\beta\bar{\gamma}}\right)^{N_R}, \tag{4.27}$$

which is obtained by expanding (4.24) using Taylor's series. The expression in (4.27) indicates that the system achieves the full diversity provided by the N_R receive antennas though only one branch is selected for decoding.

4.3.1.2 Alamouti's STBC ($M_T = 2$)

Consider a 2-Tx and N_R - Rx communication system with Alamouti's STBC scheme, where $\rho_k = 2, \lambda_k = 1$ for all $k = 1...K$, then $\beta_k = \beta = 2\cos^2\alpha/[2(1-\eta)\bar{\gamma}_s + 1]$

in (4.11). With $M_T = 2$, each $\hat{\gamma}_l$ is a χ^2 -distributed random variable with four degrees of freedom. The distribution of maximum estimated SNR is

$$f_{\hat{\gamma}_{1:N_R}}(\gamma) = N_R \left[1 - e^{-\frac{2\gamma}{\bar{\gamma}}} \left(1 + \frac{2\gamma}{\bar{\gamma}}\right)\right]^{N_R-1} \left[\frac{4\gamma}{\bar{\gamma}^2} e^{-\frac{2\gamma}{\bar{\gamma}}}\right]. \tag{4.28}$$

The MGF of (4.28) is

$$\begin{aligned} M_{\hat{\gamma}_{1:N_R}}(s) &= \int_0^\infty e^{s\gamma} f_{\hat{\gamma}_{1:N_R}}(\gamma) d\gamma \\ &= N_R \sum_{n_1=0}^{N_R-1} \sum_{n_2=0}^{n_1} \binom{N_R-1}{n_1} \binom{n_1}{n_2} (-1)^{n_1} (n_2+1)! \left(\frac{1}{n_1+1-0.5\bar{\gamma}s}\right)^{n_2+2}. \end{aligned} \tag{4.29}$$

The mean output of the maximum estimated SNR can then be evaluated from the MGF as

$$\begin{aligned} \bar{\gamma}_{out} &= \frac{d}{ds} M_{\hat{\gamma}_{1:N_R}}(s)|_{s=0} \\ &= \frac{N_R\bar{\gamma}}{2} \sum_{n_1=0}^{N_R-1} \sum_{n_2=0}^{n_1} \binom{N_R-1}{n_1} \binom{n_1}{n_2} (-1)^{n_1} (n_2+2)! \left(\frac{1}{n_1+1}\right)^{n_2+3}. \end{aligned} \tag{4.30}$$

By substituting (4.28) in (4.13), the BEP function can be obtained in a closed-form as

$$\mathrm{P}(\alpha) = N_R \sum_{n_1=0}^{N_R-1} \sum_{n_2=0}^{n_1} \binom{N_R-1}{n_1} \binom{n_1}{n_2} (-1)^{n_1} (n_2+1)! (n_1+1)^{-n_2-2} G_{n_2+2}\left(\frac{\beta\bar{\gamma}}{4n_1+4}\right), \tag{4.31}$$

where $G_n(\cdot)$ is as defined in (4.25). Under high SNR condition $\bar{\gamma} \gg 1$, (4.31) can be approximated by

$$\mathrm{P}(\alpha) \simeq 2^{N_R-1} \prod_{n=1}^{2N_R} (2n-1) \cdot \left(\frac{1}{\beta\bar{\gamma}}\right)^{2N_R}. \tag{4.32}$$

Similar to (4.27), (4.32) shows that full diversity can asymptotically be achieved for SSC system with Alamouti's STBC.

4.3.1.3 Generalized STBC with Dual Receive Diversity ($N_R = 2$)

For a generalized STBC of size $P \times M_T$, M_T transmit antennas are deployed at the transmitter. The estimated SNR $\hat{\gamma}_l$ is a χ^2 -distributed random variable with $2M_T$ degrees of freedom as defined in (4.16). By substituting (4.16) and (4.17) in (4.21), the p.d.f. of the maximum $\hat{\gamma}_l$ is

$$f_{\hat{\gamma}_{1:N_R}}(\gamma) = \frac{M_T N_R}{(M_T-1)!\bar{\gamma}} e^{-\frac{M_T\gamma}{\bar{\gamma}}} \left(\frac{M_T\gamma}{\bar{\gamma}}\right)^{M_T-1} \left[1 - e^{-\frac{M_T\gamma}{\bar{\gamma}}} \sum_{n=0}^{M_T-1} \frac{1}{n!}\left(\frac{M_T\gamma}{\bar{\gamma}}\right)^n\right]^{N_R-1}. \tag{4.33}$$

This p.d.f. expression is too complex to get a closed-form MGF expression. Numerical calculation must be performed for BEP evaluation. To obtain a closed form solution for the generalized STBC with SSC, we consider the case where there are only two receive antennas, which is later shown to be the case having comparable performance to MRC schemes. With $N_R = 2$, the MGF of the p.d.f. in (4.33) is

$$M_{\hat{\gamma}_{1:N_R}}(s) = 2\left[\left(1 - \frac{s\bar{\gamma}}{M_T}\right)^{-M_T} - \sum_{n=0}^{M_T-1} \binom{M_T+n-1}{n} \frac{1}{2^{M_T+n}} \left(1 - \frac{s\bar{\gamma}}{2M_T}\right)^{-M_T-n}\right]. \tag{4.34}$$

The mean estimated output SNR is

$$\bar{\gamma}_{out} = 2\bar{\gamma}\left[1 - \sum_{n=0}^{M_T-1} \binom{M_T+n-1}{n} \frac{1}{2^{M_T+n+1}} \left(1 + \frac{n}{M_T}\right)\right]. \tag{4.35}$$

The closed form expression for the BEP is

$$F_k(\alpha) = 2G_{M_T}(\frac{\beta_k\bar{\gamma}}{2M_T}) - \sum_{n=0}^{M_T-1} \binom{M_T+n-1}{n} 2^{-M_T-n+1} G_{M_T+n}(\frac{\beta_k\bar{\gamma}}{4M_T}). \tag{4.36}$$

When $\bar{\gamma} \gg 1$, this BEP expression can be approximated as

$$F_k(\alpha) \simeq \frac{M_T^{2M_T-1} \prod_{n=1}^{2M_T} (2n-1)}{2M_T!(M_T-1)!} \left(\frac{1}{\beta_k\bar{\gamma}}\right)^{2M_T}, \tag{4.37}$$

which again shows that the diversity order achievable is determined by the total number of transmit and receive antennas for SSC with generalized STBC.

4.3.2 Generalized Selection Combining

In GSC, the combiner selects N_C receive antennas with most significant estimated SNR out of N_R receive antennas. The general solution is given in (4.18) and (4.19). Here, we illustrate the following 1-Tx and 2-Tx cases where closed-form expressions can be obtained.

4.3.2.1 One Transmit Antenna ($M_T = 1$)

According to (4.15), the estimated mean SNR of the proposed MMSE channel estimation receiver degrades from actual SNR proportionally to the coefficient η. For this case, the MGF of combined SNR in (4.19) reduces to [86]

$$\begin{aligned} M_{\hat{\gamma}_{GSC}}(s) &= (1-s\bar{\gamma})^{-N_C+1} \prod_{n=N_C}^{N_R} \left(1 - \frac{s\bar{\gamma}N_C}{n}\right)^{-1} \\ &= (1-s\bar{\gamma})^{-N_C+1} \sum_{n=0}^{N_R-N_C} \frac{(-1)^n \binom{N_R}{N_C}\binom{N_R-N_C}{n}}{1+\frac{n}{N_C}-s\bar{\gamma}}. \end{aligned} \tag{4.38}$$

The mean estimated output SNR has a simple expression as [84, 86]

$$\bar{\gamma}_{out} = E[\hat{\gamma}_{GSC}] = N_C\bar{\gamma}\left(1 + \sum_{n=N_C+1}^{N_R} \frac{1}{n}\right). \tag{4.39}$$

By taking the inverse Laplace transformation of (4.38), the p.d.f of combined SNR is

$$\begin{aligned} f_{\gamma_{GSC}}(\gamma) = \binom{N_R}{N_C}\Bigg[\frac{\gamma^{N_C-1}e^{-\gamma/\bar{\gamma}}}{\bar{\gamma}^{N_C}(N_C-1)!} + \frac{1}{\bar{\gamma}} \sum_{n_1=1}^{N_R-N_C} \Bigg((-1)^{N_C+n_1-1}\binom{N_R-N_C}{n_1}\left(\frac{N_C}{n_1}\right)^{N_C-1} \\ \cdot e^{-(\gamma/\bar{\gamma})}\left[e^{-(n_1\gamma/N_C\bar{\gamma})} - \sum_{n_2=0}^{N_C-2}\frac{1}{n_2!}\left(\frac{-n_1\gamma}{N_C\bar{\gamma}}\right)^{n_2}\right]\Bigg)\Bigg]. \end{aligned} \tag{4.40}$$

Substituting (4.40) in (4.20), the BEP can be written as [86]

$$\mathrm{P}(\alpha) = \binom{N_R}{N_C}\Big[G_{N_C}(c_1) + \sum_{n_1=1}^{N_R-N_C}(-1)^{N_C+n_1-1}\binom{N_R-N_C}{n_1}\left(\frac{N_C}{n_1}\right)^{N_C-1} \cdot\left(\frac{N_C}{n_1+N_C}G_1(c_2) - \sum_{n_2=0}^{N_C-2}\left(\frac{-n_1}{N_C}\right)^{n_2}G_{n_2+1}(c_1)\right)\Big], \tag{4.41}$$

where $c_1 = \beta\bar{\gamma}/2, c_2 = \beta N_C\bar{\gamma}/[2(n_1+N_C)]$. Similarly, we have a high-SNR approximation for (4.41) as

$$\mathrm{P}(\alpha) \simeq \frac{(2N_R-1)!!}{2N_C^{N_R-M_T}N_C!}\left(\frac{1}{\beta\bar{\gamma}}\right)^{N_R}. \tag{4.42}$$

4.3.2.2 Alamouti's STBC with Dual Selection Combining ($M_T = N_C = 2$)

For Alamouti's STBC, the p.d.f. of the combination of the N_C branches with maximum estimated SNR is not readily available in closed form. By observing the fact that the χ^2 distribution with four degrees of freedom is the same as the Nakagami-2 distribution, one can refer to [88–91] for an MGF of the combined $\hat{\gamma}_{GSC}$. However, the MGF expression therein is still too complex for BEP evaluation. The results in [86] indicate that with fixed number of total receive antennas, increasing N_C from one to two gives the maximum gain from single selection combining. Here in this dissertation, we investigate the performance for this dual selection combining, i.e., $N_C = 2$. By substituting $M_T = N_C = 2$ in (4.16) and (4.18), the p.d.f. of $\hat{\gamma}_{GSC}$ for Alamouti's STBC is

$$f_{\gamma_{DSC}}(\gamma) = \frac{2N_R(N_R-1)}{\bar{\gamma}^2}e^{-\frac{2\gamma}{\bar{\gamma}}}\left(\frac{2\gamma^3}{3\bar{\gamma}^2} + \sum_{n_1=1}^{N_R-2}\sum_{n_2=0}^{n_1}\binom{N_R-2}{n_1}\binom{n_1}{n_2}\frac{(-1)^{n_1}(n_2+1)!}{n_1^{n_2+3}} \left[(2n_1\gamma - (n_2+2)\bar{\gamma}) + e^{-\frac{n_1\gamma}{\bar{\gamma}}}\left((n_2+2)\bar{\gamma} + \sum_{n_3=0}^{n_2+1}\frac{(n_1\gamma)^{n_3+1}}{\bar{\gamma}^{n_3}(n_3+1)!}[n_2-2n_3]\right)\right]\right). \tag{4.43}$$

The mean output of the combined estimated SNR is

$$\bar{\gamma}_{out} = \bar{\gamma} N_R (N_R - 1) \left(1 + \sum_{n_1=1}^{N_R-2} \sum_{n_2=0}^{n_1} \binom{N_R - 2}{n_1} \binom{n_1}{n_2} (-1)^{n_1} \frac{(n_2+1)!}{n_1^{n_2+3}} \left[n_1 - \frac{n_2+2}{2} + \frac{2(n_2+2)}{(n_1+2)^2} + \sum_{n_3=0}^{n_2+1} \frac{2n_1^{n_3+1}(n_3+2)(n_2-2n_3)}{(n_1+2)^{n_3+3}} \right] \right) \tag{4.44}$$

.

With the available p.d.f. in (4.43), the BEP can be expressed as

$$\mathrm{P}(\alpha) = \frac{N_R(N_R-1)}{2} \left(G_4(\frac{\beta\bar{\gamma}}{4}) + \sum_{n_1=1}^{N_R-2} \sum_{n_2=0}^{n_1} \binom{N_R-2}{n_1} \binom{n_1}{n_2} (-1)^{n_1} \frac{(n_2+1)!}{n_1^{n_2+3}} \left[\begin{array}{l} 2n_1 G_2(\frac{\beta\bar{\gamma}}{4}) - 2(n_2+2) G_1(\frac{\beta\bar{\gamma}}{4}) + 4(\frac{n_2+2}{n_1+2}) G_1(\frac{\beta\bar{\gamma}}{2n_1+4}) + \\ \sum_{n_3=0}^{n_2+1} \frac{4n_1^{n_3+1}(n_2-2n_3)}{(n_1+2)^{n_3+2}} G_{n_3+2}(\frac{\beta\bar{\gamma}}{2n_1+4}) \end{array} \right] \right) \tag{4.45}$$

.

The BEP function in (4.45) still has an approximation when $\bar{\gamma} \gg 1$

$$\mathrm{P}(\alpha) \simeq B \cdot \left(\frac{1}{\beta\bar{\gamma}} \right)^{M_T N_R}, \tag{4.46}$$

where B is a constant which depends on the system parameters. In general, (4.46) indicates that the selection combining with STBC can achieve the full diversity order $M_T N_R$ asymptotically. This achievable full diversity is only determined by the number of transmit antennas M_T and the number of receive antennas N_R. It is independent from the number of antennas chosen for combining N_C.

4.4 Numerical Results and Discussion

We choose $L_f = 10$ and $L_p = 5$ for PSAM . With $E_P = E_0$ and $P \simeq M_T$, as one pilot block is inserted into the data stream for every ten blocks, there is a 10% loss

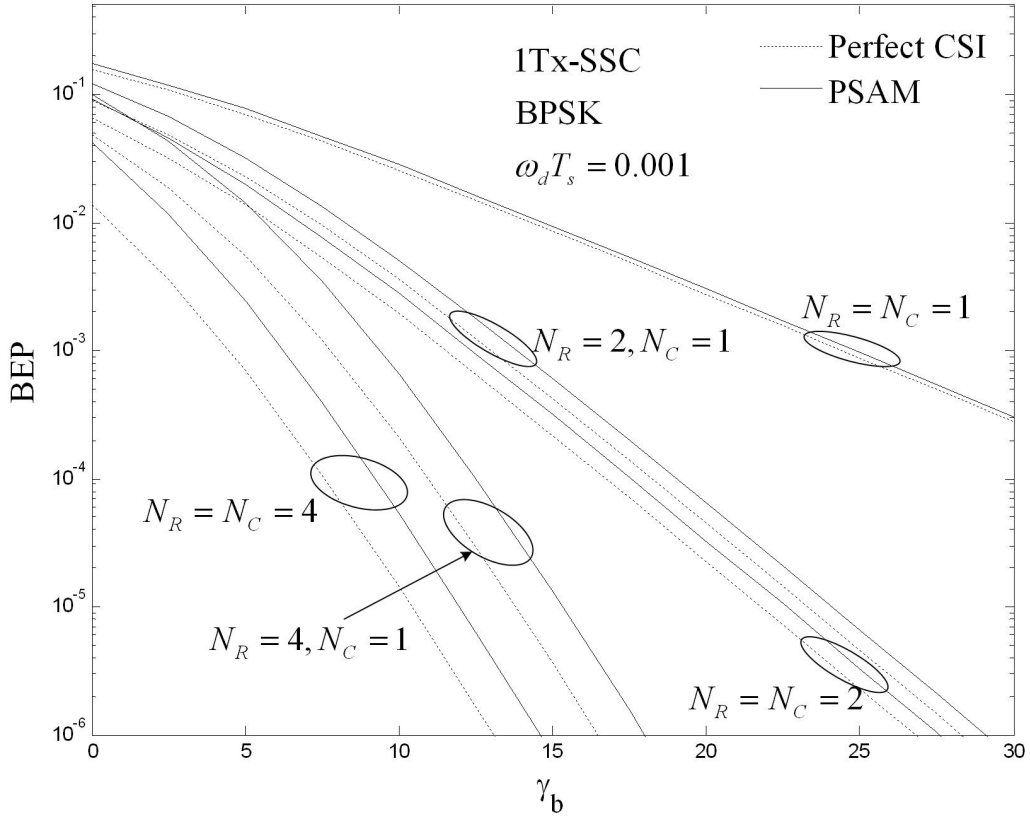

Fig. 4.2: BEP Performance of 1-Tx system with single selection combining

in bandwidth efficiency. The BEP is thus plotted against $\gamma_b = (11/10)\bar{\gamma}_0/\log_2 M$ for compensation. BEP performances with perfect CSI are also plotted for comparison by setting all channel estimation MSE to zero.

4.4.1 Single Selection Combining

Fig. 4.2 shows the BEP performance of SIMO system with SSC. This figure shows that the performance gap between the systems with imperfect and perfect CSI increases proportionally with the number of receive antennas N_R. When $N_R = 2$, this gap is less than 1dB, while the performance loss of SSC from MRC is within 2dB, which indicates

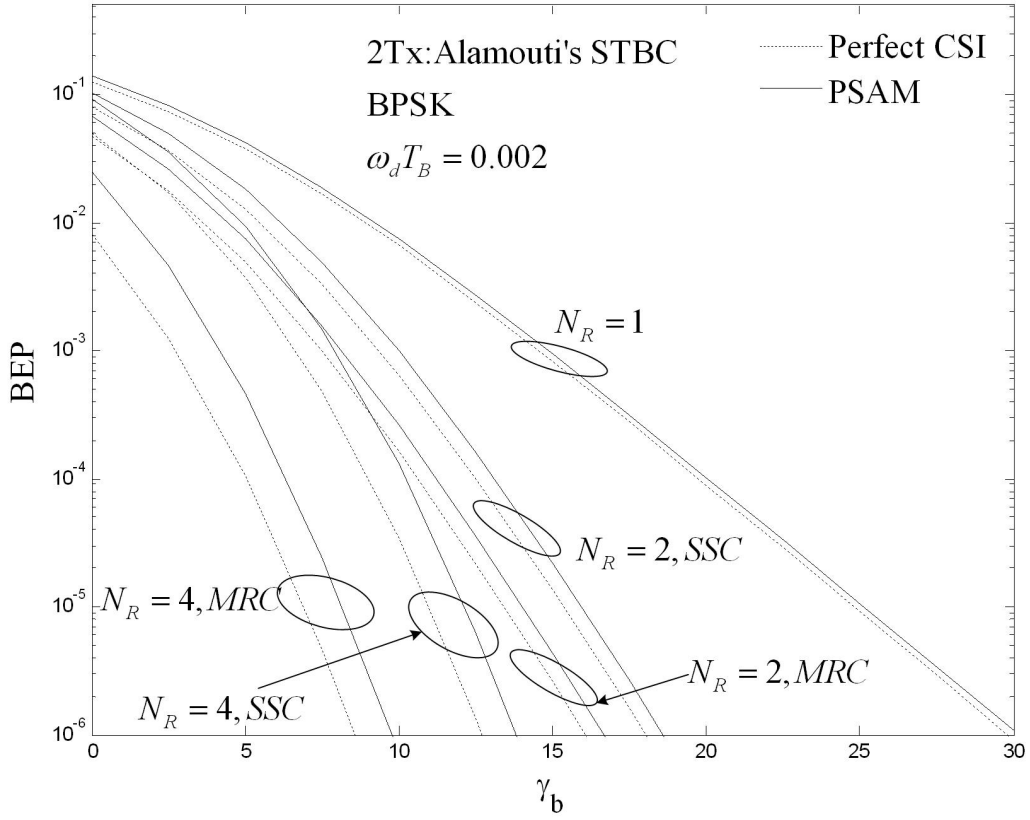

Fig. 4.3: Performance comparison between MRC and SSC systems for Alamouti's STBC with BPSK

that SSC is an efficient way for decoding with simple receiver structure.

Fig. 4.3 shows the BEP performance of SSC for Alamouti's STBC under Jakes' fading channel with normalized block fade rate $\omega_d T_B = 0.002$. Similar to the results in Fig. 4.2, the performance gap between the systems with imperfect and perfect CSI increases with the number of receive antennas. From Fig. 4.2 and Fig. 4.3, one can observe that the performance improvement is significant when the number of receive antennas is increased from one to two. However, further increase, from two to four, gives relatively small gain. Therefore, we can come to a conclusion that the dual diversity ($N_R = 2$) is the most efficient scheme for SSC, because, it provides limited loss from

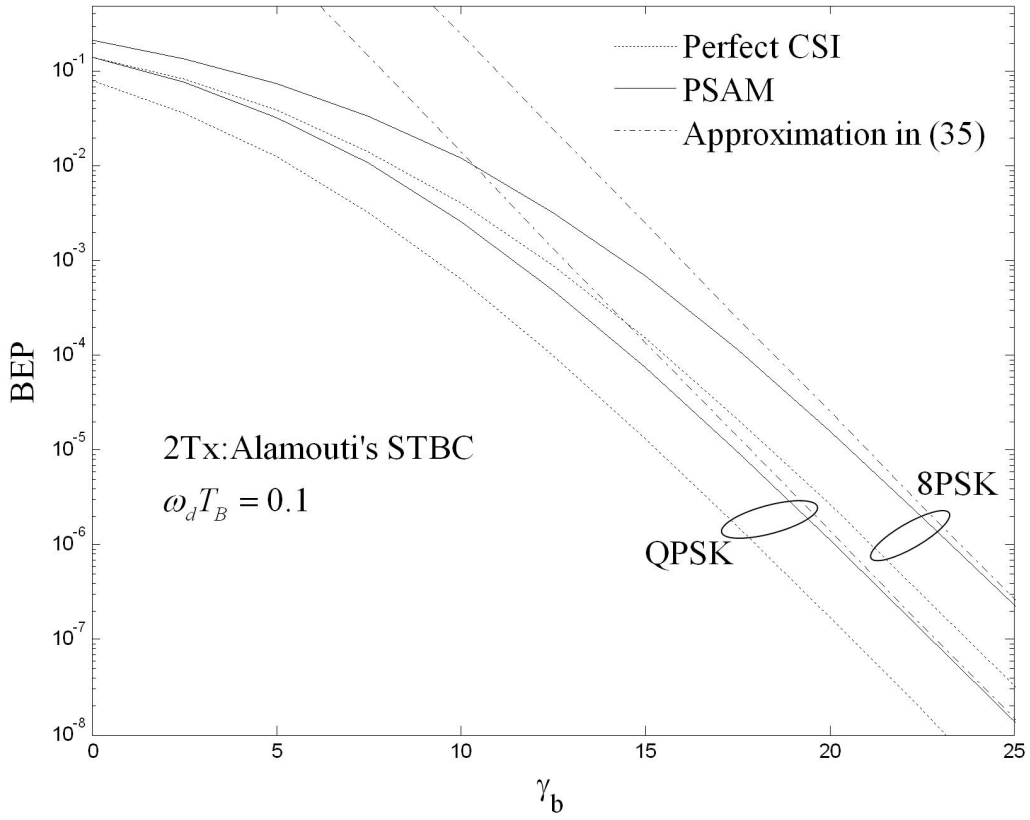

Fig. 4.4: Performances QPSK and 8PSK modulation with SSC and Alamouti's STBC

MRC, while having a simple receiver structure.

Fig. 4.4 shows the BEP performance of SSC for Alamouti's STBC with QPSK and 8PSK under fast fading channel ($\omega_d T_B = 0.1$). As the channel estimator does not track the channel when it fades fast, the resulting greater MSE of estimation increases the performance gap between the systems with imperfect and perfect CSI. The approximations under high SNR for Alamouti's STBC with SSC in (4.32) are also plotted for comparison. Under high SNR, the BEP performance is dominated by the term $(\beta\bar{\gamma})^{-M_T N_R}$ as indicated in (4.46). Those approximations in (4.27), (4.32), (4.37), and (4.42) give the asymptotic BEP limits achievable by the selection combining systems.

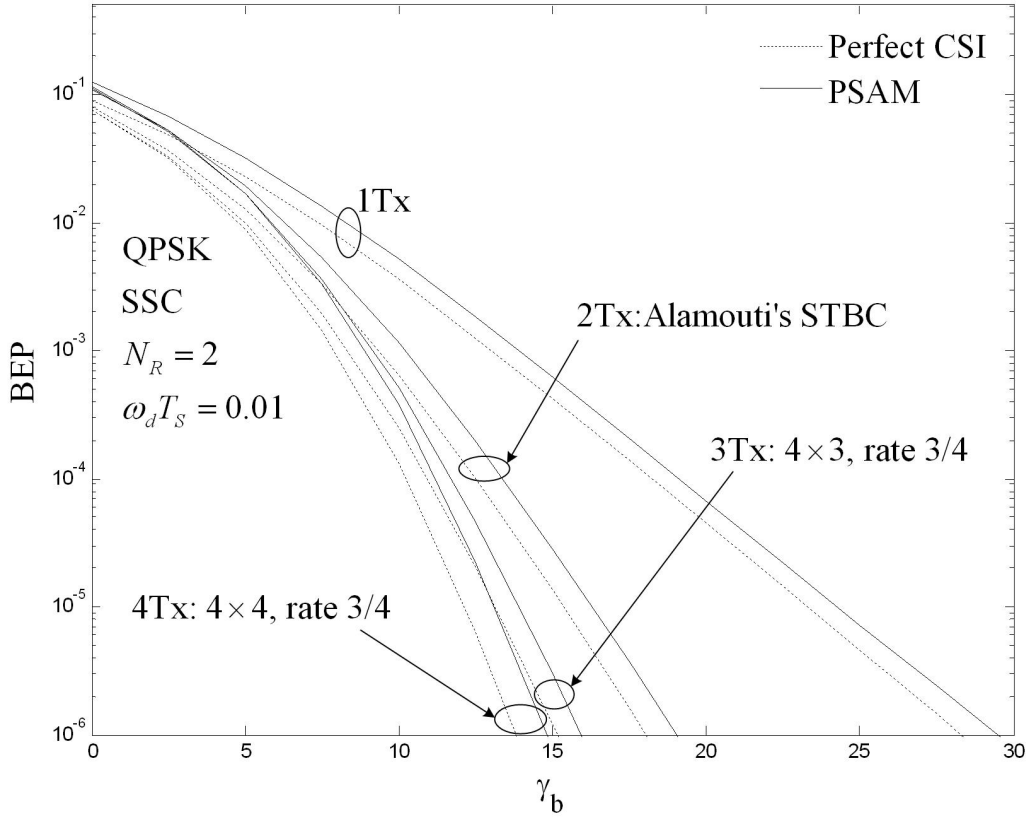

Fig. 4.5: Performance comparison among different STBC's with two receive antennas and SSC

Fig. 4.5 shows the BER performance of SSC for generalized STBC with two receive antennas under relatively fast fading channel ($\omega_d T_B = 0.01$). The 4×3 and 4×4 STBC with rate 3/4 are used for 3Tx and 4Tx respectively. The parameters for the 4×4 STBC are $\rho_k = 3, \lambda_k = 1$, and $\rho_k = 2.5, \lambda_k = 1$ for the 4×3 STBC, for all $k = 1...K$. For the 4×3 rate-3/4 STBC, the computed BEP performance is an approximation but very close to the actual one, as shown in Chapter 3. As different STBC requires different coherent time to satisfy the block-wise constant channel assumption, the BEP's are plotted according to the normalized fade rate $\omega_d T_S$ to make fair comparisons. For a M_T -Tx system with $P \times M_T$ STBC, the performance plotted is actually under a block-wise

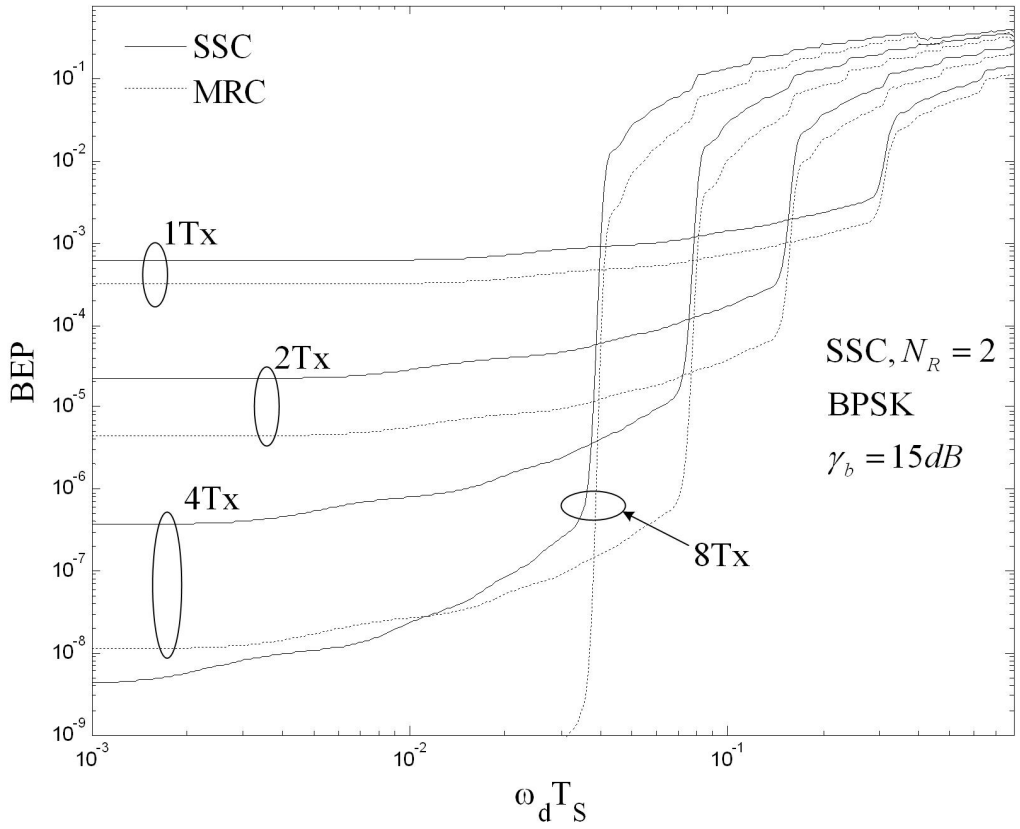

Fig. 4.6: Performance comparison of different STBC's against channel fade rate

constant fading channel with $\omega_d T_B = P\omega_d T_S$. When the number of receive antennas are fixed, increasing the number of transmit antennas from one to two gives the largest gain, while increasing from three to four gives limited gain. However, in all cases, the performance gap between the imperfect and perfect CSI is same.

Fig. 4.6 compares the performance of SSC for different STBC schemes with two receiver antennas against the channel fade rate. Real designs with four and eight antennas proposed in [17] are used, where $\rho_k = 4, \lambda_k = 1$ for 4-Tx and $\rho_k = 8, \lambda_k = 1$ for 8-Tx case, respectively. Although STBC with larger size has better performance under slow fading since it employs more transmit antennas, the performance degrades rapidly

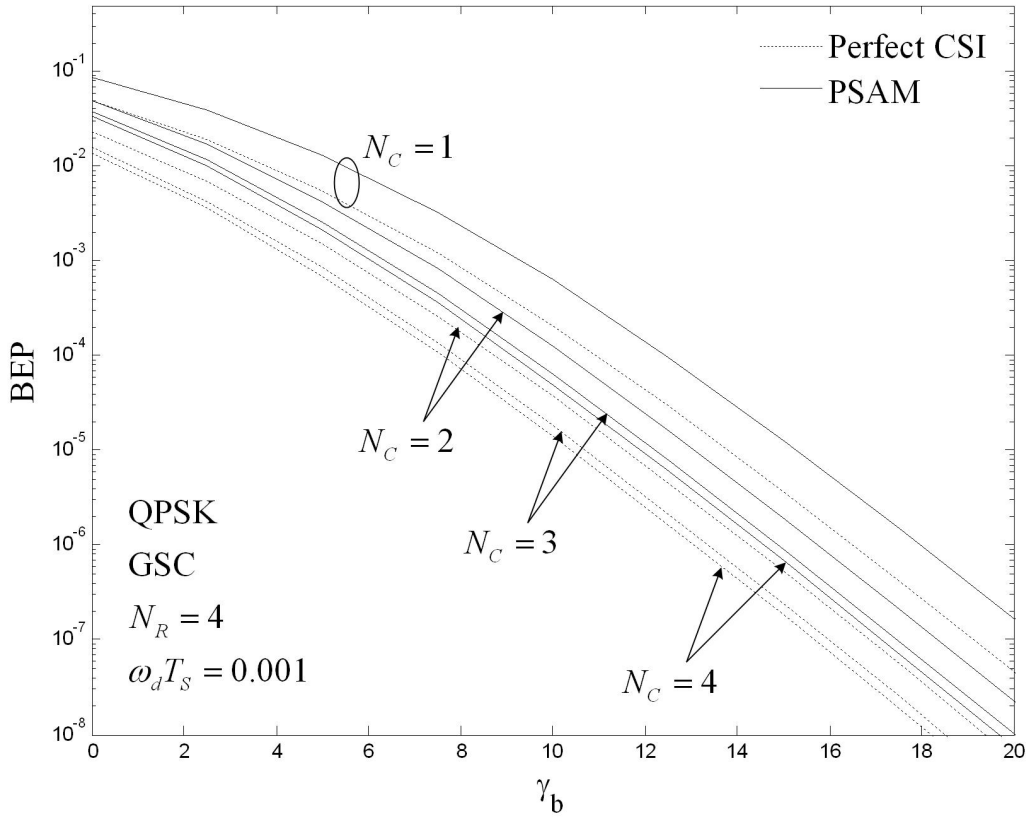

Fig. 4.7: Performance of GSC with 1-Tx and 4-Rx

after some threshold and becomes worse than those with less transmit antennas. Under fast-fading, the less be the STBC size, the better the performance would be. One can expect that such thresholds would appear earlier as the $\omega_d T_S$ increase under a realistic system where channel fluctuates from symbol to symbol.

4.4.2 Generalized selection combining

Fig. 4.7 shows the BER performance of GSC for the SIMO system with 1Tx and 4Rx. With the total number of receive antennas fixed, the improvement in BEP performance is significant when N_C is increased from one to two. However, the increase of N_C

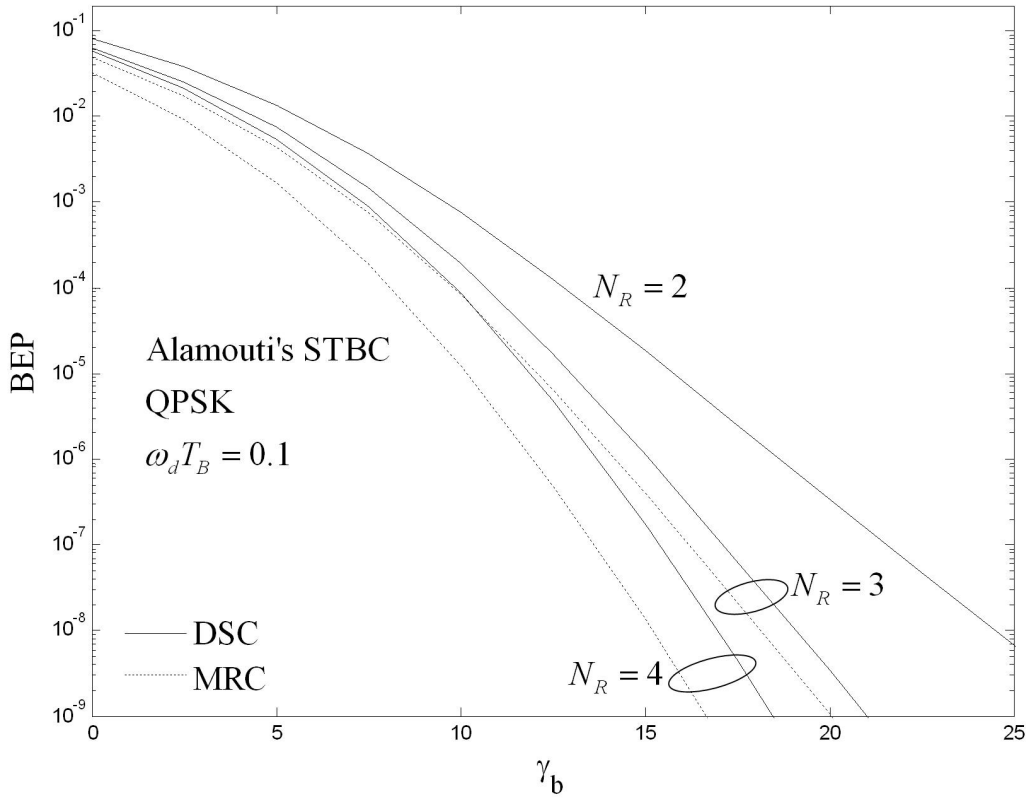

Fig. 4.8: Performance of Alamouti's STBC with dual selection combining

from $N_R - 1$ to N_R (MRC) gives a very limited gain.

Fig. 4.8 shows the BEP performances of Alamouti's STBC when N_C is fixed to two. Increasing the number of receive antennas from two to three gives significant gain. This verifies the conclusion that with N_C fixed, increasing the total number of receive antennas from N_C to N_C+1 gives the best gain per additional branch. It is also exhibited in Fig. 4.8 that the performance loss of DSC from MRC increases as N_R increases.

The mean output estimated SNR's for single and dual selection combining against the total number of receive antenna N_R are shown in Fig. 4.9. The real designs with four antennas [17] is used for 4Tx and its results are obtained by numerical approaches, while

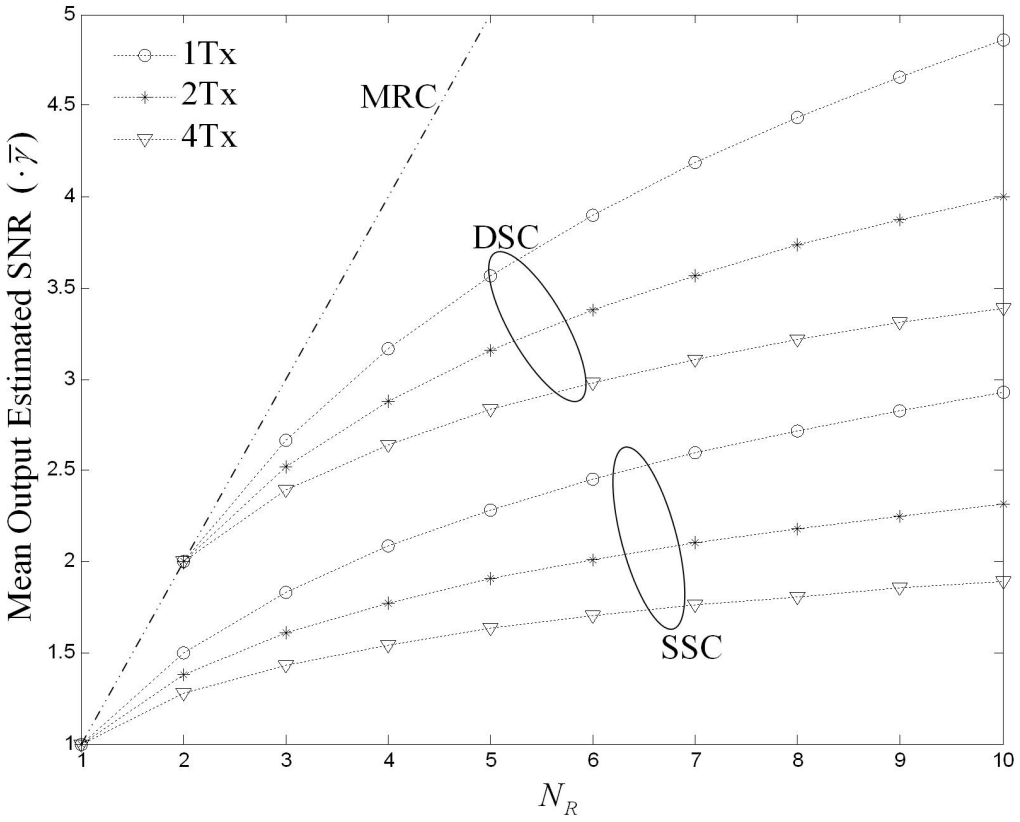

Fig. 4.9: Mean output of the estimated SNR with single and dual selection combining

others are calculated from their exact expressions in (4.30), (4.35), (4.39) and (4.44). It is interesting to find that the more the transmit antennas are used, the less the estimated output SNR would be. This suggests that introducing STBC into a selection combining system can reduce the power consumption in decoding considerably while the performance is improved by the transmit diversity gain.

4.5 Summary

In this chapter, we presented the performance analysis of STBC communication systems with selection combining and imperfect channel estimation. The selection criterion

is based on the estimated SNR obtained from channel estimation. As the channel estimation is imperfect, the BEP results depend on both SNR and estimation MSE. Exact closed-form BEP expressions are derived for (a) general selection combining with single transmit antenna (b) single and dual selection combining for Alamouti's STBC (c) single selection combining for generalized STBC with more than two transmit antennas. The approximations of BEP under high SNR show that the selection combining schemes can achieve full diversity provided by the total available number of receive antennas, while maintaining simple receiver structures. The numerical results show that receive selection combining exhibits limited performance loss compared with MRC schemes.

Chapter 5

STBC Communication System with Transmit Antenna Selection

In this Chapter, we present transmit antenna selection scheme for wireless communication systems with STBC. We make transmit antenna selection based on knowledge of estimated channel state information. The transmitter chooses the one or several antennas for STBC transmission by knowing the estimated SNR. We analyze the performance and obtain an upper bound for TAS system with PSK modulation. Specifically, an exact closed-form BEP expression is developed for single receiver antenna systems. With the analytical performance results, it is found that the achievable diversity of the proposed TAS system is determined by the total number of transmit and receive antennas, while independent of the number of antennas selected.

5.1 Introduction

Independent of space-time coding, transmit antenna selection has long been known as an efficient way to exploit diversity at the transmitter side. With multiple antennas available at the transmitter, the performance can be improved by injecting more transmit

energy into the channels with better channel gains. The discussion in [97] concludes the optimal weight assignment problem over Rayleigh fading channels, where all antennas transmit the same symbol. The power allocation discussion in [97] simplifies to transmit antenna selection (TAS) when all the channels have identical estimation error, i.e., all the transmission power is assigned to the one channel that has the maximum channel gain. TAS with Alamouti's STBC is proposed in [98], where the antennas are so chosen such that the channel Frobenius-norm is maximized. However, the performance analysis in [98] is not in an explicit form. In [99], the authors investigate the TAS for Alamouti's STBC with perfect CSI and obtain an exact BEP expression for binary signaling. TAS schemes with space-time trellis codes are reported in [100] and [101].

In our previous work in Chapter 3, we have set up a symbol-by-symbol channel estimation STBC receiver structure, and obtained its BEP expressions with PSK modulations under non-selective Rayleigh fading channels. Based on the results therein, we extend the above system by introducing TAS at the transmitter in this chapter. We first propose a TAS system based on estimated SNR for STBC over a MIMO channel model. In such a system, the receiver indicates to the transmitter which antennas are to be chosen for STBC transmission according to the estimated SNR. Exact closed-form BEP expressions are presented for multi-input-single-output (MISO) systems as well as dual-input-multi-output (DIMO). Comparing to those results in the literature, our results here take account of both space-time block coding and channel estimation. The results explicitly show that the BEP performance depends on the MSE of estimator and the system parameters chosen.

5.2 System Model

Consider a MIMO communication system with M_X -Tx and N_R -Rx illustrated in 5.1. A generalized complex orthogonal STBC $\boldsymbol{S}$ of size $P \times M_T$ is employed, where

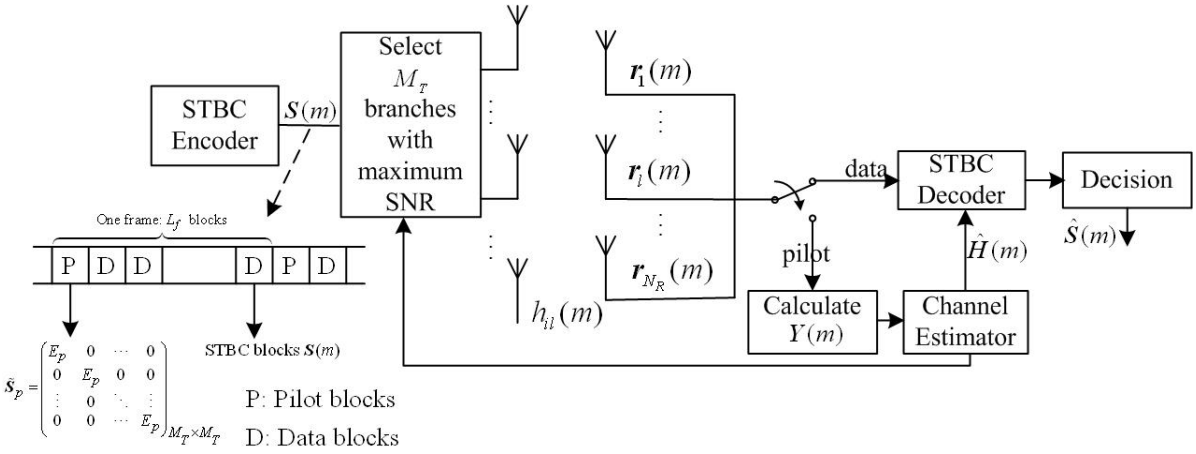

Fig. 5.1: STBC system with transmit selection and imperfect channel estimation using PSAM

$M_X \geq M_T$. Prior to the transmission of each data block, the transmitter is indicated by the receiver to choose M_T out of the total of M_X available transmit antennas with best estimated channel gain for transmission. Denote $h_{il}(m)$ as the fading gain from the i-th transmit to l-th receive antenna, during the m-th block interval. All the links are spatially independent from one another but with identical distribution. Each $h_{il}(m)$ has an autocorrelation function as in (2.42)

$$\mathcal{R}(\Delta m) = \mathrm{E}[x(m)x^T(m+\Delta m)] = \sigma^2\, J_0(\Delta m \omega_d T_s),$$

As the transmitter actually choose M_T antennas for transmission, we define the active channel matrix of size $M_T \times N_R$ as $\boldsymbol{H}_T$, which is a sub-matrix containing M_T rows of the complete channel matrix $\boldsymbol{H}_X = \{h_{il}\}_{i,l=1}^{M_X,N_R}$. Now the received signal matrix of the m-th$(m = 0, 1, 2...)$ transmitted signal block $\boldsymbol{S}(m)$ is

$$\boldsymbol{R}(m) = \boldsymbol{S}(m)\boldsymbol{H}_X(m) + \boldsymbol{N}(m). \tag{5.1}$$

Each entry $r_{pl}(m)$ of the $P \times N_R$ received matrix $\boldsymbol{R}(m)$ is the received signal on the l - th receive antenna at the p - th symbol slot of the m - th block. $\boldsymbol{N}(m)$ is the $P \times N_R$ noise matrix, whose entries $n_{pl}(m)$'s are i.i.d., zero-mean, complex, Gaussian r.v.'s due to

AWGN at the p - th symbol slot on the l - th receive antenna with $\mathrm{E}[n^*_{p'l'}(m')n_{pl}(m)] = \delta_{pp'}\delta_{ll'}\delta_{mm'}N_0$.

The system adopts PSAM for channel estimation. The basic PSAM setups are the same as that introduced in section 4.2. After the channel estimate matrix $\hat{\boldsymbol{H}}$ is acquired, the received signal is then sent to a decoder defined in (4.9) with $z_k(m) = \mathrm{Tr}[\boldsymbol{R}^\dagger(m)\boldsymbol{B_k}\hat{\boldsymbol{H}}_T(m) + \hat{\boldsymbol{H}}^\dagger_T(m)\boldsymbol{A}^\dagger_{\boldsymbol{k}}\boldsymbol{R}(m)]$. With PSK modulation, the BEP is dependent on the quantity $P(Re\{z_k e^{-j\alpha}\} < 0|s_k = \sqrt{E_0/M_T}, \hat{\boldsymbol{H}}_T)$, which has been shown in Chapter 3 to be equal or closely approximated by

$$P(Re\left\{z_k e^{-j\alpha}\right\} < 0|s_k = \sqrt{E_0/M_T}, \hat{\boldsymbol{H}}_T) = Q\left(\sqrt{\beta_k \hat{\gamma}_{TAS}/M_T}\right), \tag{5.2}$$

where $\beta_k = 2\lambda_k \cos^2\alpha/[\rho_k(1-\eta)\bar{\gamma}_0/M_T + 1]$, $\eta = 1 - \sigma_e^2/\mathcal{R}(0)$, $\bar{\gamma}_0 = 2E_0\mathcal{R}(0)/N_0$ is the mean SNR per symbol per receive antenna, and $\hat{\gamma}_{TAS} = E_0||\hat{\boldsymbol{H}}_T||^2/N_0$ is the equivalent estimated output SNR per symbol at the receiver. To evaluate the BEP performance, one must average the quantity in (5.2) over the estimated SNR as

$$F_k(\alpha) = \int_0^\infty Q\left(\sqrt{\beta_k\gamma}\right) f_{\hat{\gamma}_{TAS}}(\gamma)d\gamma. \tag{5.3}$$

Similarly, we define the BEP function $\mathrm{P}(\alpha)$ as in 4.14 and the BEP for PSK signaling is given as in (3.39-3.41).

If perfect CSI is available at the transmitter, $\boldsymbol{H}_T$ is chosen to consist of the maximum M_T rows of $\boldsymbol{H}_X$ according to the quantity $\sum_{l=1}^{N_R}|h_{il}|^2,\ i = 1...M_X$. In the implementation of this transmit selection scheme, the selection decision of transmit antennas must be sent to the transmitter before data transmission. Thus the channel estimation based on which the receiver decides the antenna selection can only be made with previously received pilots. Another channel estimation $\hat{h}'_{il}(m)$ based on only those L_p pilots previously received, i.e., $\tilde{\boldsymbol{y}}'_{il}(m) = \{y_{il,q}|[\![m/L_f]\!] - L_p + 1 \le q \le [\![m/L_f]\!]\}$, must be made right after the receipt of the $(m-1)$ - th data block. Therefore the receiver actually makes channel estimation twice, one for antenna selection based only on previously received pilots, one

for STBC decoding after receiving the data blocks and necessary pilot blocks. Similarly, conditioned on $\tilde{\boldsymbol{y}}'_{il}(m)$, $h_{il}(m)$ is a Gaussian random variable with mean $\hat{h}'_{il}(m)$ and variance $2\sigma'^2_e(m)$. Theoretically, we have $\sigma'^2_e > \sigma^2_e$ for a continuously changing channel so that the TAS decisions are less reliable compared to the case if PSAM estimation is available for TAS. However in this dissertation, we assume that the TAS decision based on $\hat{h}'_{il}(m)$ is the same as if the PSAM estimation is known, for the sake of analytical simplicity.

5.3 Performance Analysis of STBC with TAS

In the system model defined above, once acquainted with the channel estimation, the receiver indicates to the transmitter which M_T antennas to choose based on the estimated SNR, through a delay-less, error-free reverse link. We define the estimated SNR contributed by the i - th transmit antenna as $\hat{\gamma}_i = \sum_{l=1}^{N_R} E_0|\hat{h}_{il}|^2/M_T N_0,\ i = 1...M_X$, which is a χ^2 -distributed random variable with $2N_R$ degrees of freedom with p.d.f

$$f_{\hat{\gamma}_i}(\gamma) = \frac{N_R^{N_R}}{\bar{\gamma}^{N_R}(N_R-1)!}\gamma^{N_R-1}e^{-N_R\gamma/\bar{\gamma}}, \tag{5.4}$$

where

$$\bar{\gamma} = \mathrm{E}[\hat{\gamma}_i] = N_R E_0[R(0) - \sigma_e^2]/M_T N_0 = N_R\eta\bar{\gamma}_0/M_T,\ i = 1...M_X. \tag{5.5}$$

The $\hat{\gamma}_i$ has a c.d.f. given by

$$F_{\hat{\gamma}_l}(\gamma) = 1 - e^{-\frac{M_T\gamma}{\bar{\gamma}}}\sum_{n=0}^{M_T-1}\frac{1}{n!}\left(\frac{M_T\gamma}{\bar{\gamma}}\right)^n. \tag{5.6}$$

The transmitter then chooses the first M_T antennas from the ordered statistics $\hat{\gamma}_{1:M_X} \geq \hat{\gamma}_{2:M_X} \geq \cdots \geq \hat{\gamma}_{M_X:M_X}$ of $\{\hat{\gamma}_i\}_{i=1}^{M_X}$ for STBC transmission. The joint p.d.f of the

maximum M_T estimated SNR $\{\hat{\gamma}_{i:M_X}\}_{i=1}^{M_X}$ is [86]

$$f_{\hat{\gamma}_{1:M_X},\hat{\gamma}_{2:M_X},\cdots,\hat{\gamma}_{M_T:M_X}}(\hat{\gamma}_{1:M_X},\hat{\gamma}_{2:M_X},\cdots,\hat{\gamma}_{M_T:M_X})$$
$$= M_T!\binom{M_X}{M_T}\left[F_{\hat{\gamma}_l}(\hat{\gamma}_{M_T:M_X})\right]^{M_X-M_T}\prod_{l=1}^{M_T} f_{\hat{\gamma}_l}(\hat{\gamma}_{1:M_X}) \tag{5.7}$$
$$\text{where } \hat{\gamma}_{1:M_X} \geq \hat{\gamma}_{2:M_X} \geq \cdots \geq \hat{\gamma}_{M_T:M_X}.$$

The BEP function $\mathrm{P}(\alpha)$ can be calculated with

$$F_k(\alpha) = \int_0^{\infty}\int_{\gamma_{M_T:M_X}}^{\infty}\cdots\int_{\gamma_{2:M_X}}^{\infty}\int_0^{\pi/2} e^{\frac{\beta_k\gamma}{2\sin^2\theta}\sum_{l=1}^{M_T}\hat{\gamma}_{l:M_X}}\cdot \tag{5.8}$$
$$f_{\gamma_{1:M_X},\gamma_{2:M_X},\cdots,\gamma_{M_T:M_X}}(\hat{\gamma}_{1:M_X},\hat{\gamma}_{2:M_X},\cdots,\hat{\gamma}_{M_T:M_X})d\theta d\hat{\gamma}_{1:M_X}d\hat{\gamma}_{2:M_X}\cdots d\hat{\gamma}_{M_T:M_X},$$

or alternatively, using the MGF,

$$F_k(\alpha) = \int_0^{\pi/2} M(\frac{\beta\gamma}{2\sin^2\theta})d\theta. \tag{5.9}$$

We first derive a closed-form upper bound for (5.3), and then solve (5.8). We obtain closed-form solutions for the special cases when $N_R = 1$ or $M_T = 1$.

5.3.1 An Upper Bound for BEP

As the quantity $\sum_{i=1}^{M_T}\hat{\gamma}_{i:M_X}$ denotes the summation of the most significant M_T out of the set $\{\hat{\gamma}_{i:M_X}\}_{i=1}^{M_X}$ of size M_X, the following inequality always holds

$$\sum_{i=1}^{M_T}\hat{\gamma}_{i:M_X} \geq \frac{M_T}{M_X}\sum_{i=1}^{M_X}\hat{\gamma}_{i:M_X}. \tag{5.10}$$

Substituting (5.10) into (5.2), we have

$$P(Re\left\{z_k e^{-j\alpha}\right\} < 0 | s_k = \sqrt{E_0/M_T}, \Lambda) \leq Q\left(\sqrt{\beta_k||\hat{\boldsymbol{H}}_X||^2/M_X}\right). \tag{5.11}$$

Then following the argument in Chapter 3, an upper bound can be obtained as

$$F_k(\alpha) \leq G_{M_X N_R}(\beta_k\eta\bar{\gamma}_0/2M_X), \tag{5.12}$$

where the function $G_n(\cdot)$ is as defined in (4.25)

$$G_n(c) = \frac{1}{2}\left[1 - \mu(c)\sum_{k=0}^{n-1}\binom{2k}{k}\left(\frac{1-\mu^2(c)}{4}\right)^k\right], \mu(c) = \sqrt{\frac{c}{1+c}}. \tag{5.13}$$

The expression in (5.12) is further bounded by the Chernoff inequality given by

$$F_k(\alpha) < \tfrac{1}{2}\left(1 + \beta_k \eta \bar{\gamma}_0 / M_X\right)^{-M_X N_R}. \tag{5.14}$$

The Chernoff bound in (5.14) clearly shows that the full diversity order $M_X N_R$ is achieved for TAS/STBC systems. The diversity order achievable is determined by the total number of transmit and receive antennas, while independent of the number of transmit antennas chosen for STBC transmission.

5.3.2 Exact BEP Analysis for TAS Systems

5.3.2.1 System with Single Receive Diversity when $N_R = 1$

In some communication scenario, it is difficult to deploy multiple antennas at the receiver side, e.g., due to the size of receiver. This is often the case with downlinks in a communication system. In this section, we derive a closed-form BEP expression for TAS STBC systems with single receive antenna, so that the spatial diversity is provided by the transmit side. With $N_R = 1$, each $\hat{\gamma}_i$ in (5.4) has a Rayleigh distribution. The problem now becomes choosing the maximum M_T from M_X Rayleigh random variables. According to the results in [86], the MGF of the estimated combined SNR is

$$\begin{aligned} M_{\hat{\gamma}_{GSC}}(s) &= (1 - s\bar{\gamma})^{-M_T+1} \prod_{n=M_T}^{M_X}\left(1 - \frac{s\bar{\gamma}M_T}{n}\right)^{-1} \\ &= (1 - s\bar{\gamma})^{-M_T+1} \sum_{n=0}^{M_X - M_T} \frac{(-1)^n \binom{M_X}{M_T}\binom{M_X - M_T}{n}}{1 + \frac{n}{M_T} - s\bar{\gamma}}. \end{aligned} \tag{5.15}$$

from which the mean estimated output SNR can be derived as as

$$\bar{\gamma}_{out} = M_T\bar{\gamma}\left(1 + \sum_{n=M_T+1}^{M_X}\frac{1}{n}\right). \tag{5.16}$$

The p.d.f is obtained by inverse Laplace transformation of 5.15

$$\begin{aligned} f_{\gamma_{TAS}}(\gamma) = \binom{M_X}{M_T}\Bigg[\frac{\gamma^{M_T-1}e^{-\gamma/\bar{\gamma}}}{\bar{\gamma}^{M_T}(M_T-1)!} + \frac{1}{\bar{\gamma}}\sum_{n_1=1}^{M_X-M_T}\Bigg((-1)^{M_T+n_1-1}\binom{M_X-M_T}{n_1} \\ \cdot\left(\frac{M_T}{n_1}\right)^{M_T-1}e^{-(\gamma/\bar{\gamma})}\left[e^{-(n_1\gamma/M_T\bar{\gamma})} - \sum_{n_2=0}^{M_T-2}\frac{1}{n_2!}\left(\frac{-n_1\gamma}{M_T\bar{\gamma}}\right)^{n_2}\right]\Bigg)\Bigg]. \end{aligned} \tag{5.17}$$

Substituting (5.17) into (5.3), one gets the BEP function as

$$\begin{aligned} F_k(\alpha) = \binom{M_X}{M_T}\Bigg[G_{M_T}(c_1) + \sum_{n_1=1}^{M_X-M_T}(-1)^{M_T+n_1-1}\binom{M_X-M_T}{n_1}\left(\frac{M_T}{n_1}\right)^{M_T-1} \\ \cdot\left(\frac{M_T}{n_1+M_T}G_1(c_2) - \sum_{n_2=0}^{M_T-2}\left(\frac{-n_1}{M_T}\right)^{n_2}G_{n_2+1}(c_1)\right)\Bigg], \end{aligned} \tag{5.18}$$

where $c_1 = \beta\bar{\gamma}/2, c_2 = \beta M_T\bar{\gamma}/[2(n_1+M_T)]$ and $G_n(c)$ is as defined in (5.13). When SNR is high enough so that $\bar{\gamma} \gg 1$, we have a high-SNR approximation for (5.18) as

$$F_k(\alpha) \simeq \frac{(2M_X-1)!!}{2M_T^{M_X-M_T}M_T!}\left(\frac{1}{\beta\bar{\gamma}}\right)^{M_X}, \tag{5.19}$$

which is obtained by expanding (5.18) into a polynomial series and dropping those higher order moments. This approximation shows that the full diversity order M_X is achieved asymptotically for any number of selected antennas, which is consistent with the conclusion drawn from the upper bound in (5.14).

5.3.2.2 System with Dual Transmit Diversity when $M_X = 2, M_T = 1$

According to the preliminary numerical results in section 5.4, it will be found that TAS with conventional 1Tx transmission outperforms the STBC with the same number of transmit antennas without TAS. We derive a closed-form BEP expression for a com-

munication system with multiple receive and two transmit antennas, from which one is chosen for data transmission, i.e., $M_X = 2$ and $M_T = 1$. Following (5.4) to (5.7), the p.d.f. of the maximum $\hat{\gamma}_{1:M_X}$ is

$$f_{\hat{\gamma}_{1:M_X}}(\gamma) = \frac{2N_R}{(N_R-1)!\bar{\gamma}} e^{-\frac{N_R\gamma}{\bar{\gamma}}} \left(\frac{N_R\gamma}{\bar{\gamma}}\right)^{N_R-1} \left[1 - e^{-\frac{N_R\gamma}{\bar{\gamma}}} \sum_{n=0}^{N_R-1} \frac{1}{n!} \left(\frac{N_R\gamma}{\bar{\gamma}}\right)^n\right]. \quad (5.20)$$

The MGF of the (5.20) is

$$M_{\hat{\gamma}_{1:N_R}}(s) = 2\left[\left(1 - \frac{s\bar{\gamma}}{N_R}\right)^{-N_R} - \sum_{n=0}^{N_R-1} \binom{N_R+n-1}{n} \frac{1}{2^{N_R+n}} \left(1 - \frac{s\bar{\gamma}}{2N_R}\right)^{-N_R-n}\right]. \quad (5.21)$$

The BEP function is then evaluated as

$$P(\alpha) = 2G_{N_R}(\frac{\beta\bar{\gamma}}{2N_R}) - \sum_{n=0}^{N_R-1} \binom{N_R+n+1}{n} 2^{-N_R-n+1} G_{N_R+n}(\frac{\beta\bar{\gamma}}{4N_R}). \quad (5.22)$$

When $\bar{\gamma} \gg 1$, this BEP function can be approximated as

$$P(\alpha) \simeq \frac{N_R^{2N_R-1} \prod_{n=1}^{2N_R} (2n-1)}{2N_R!(N_R-1)!} \left(\frac{1}{\beta\bar{\gamma}}\right)^{2N_R}. \quad (5.23)$$

Consistent with (5.19), (5.23) again shows that the diversity order achievable for a TAS system is determined by the total number of transmit and receive antennas available.

5.4 Numerical Results and Discussion

The BEP performance results are illustrated in Fig. 5.2-5.9. The system parameters are chosen as $L_f = 10$ and $L_p = 3$. With $E_P = E_0$ and $P \simeq M_T$, as one pilot block is inserted into the data stream every ten blocks, there is an around-10% loss in bandwidth efficiency. The BEP is thus plotted against $\gamma_b = (10/9)\bar{\gamma}_0/\log_2 M$ for compensation. Fig. 5.2 and Fig. 5.3 shows the performance gain with transmit selection as the number of available transmit antenna increases from the necessary M_T. BEP performances of TAS with Alamouti's STBC are shown in Fig. 5.2. BEP performances with perfect CSI are

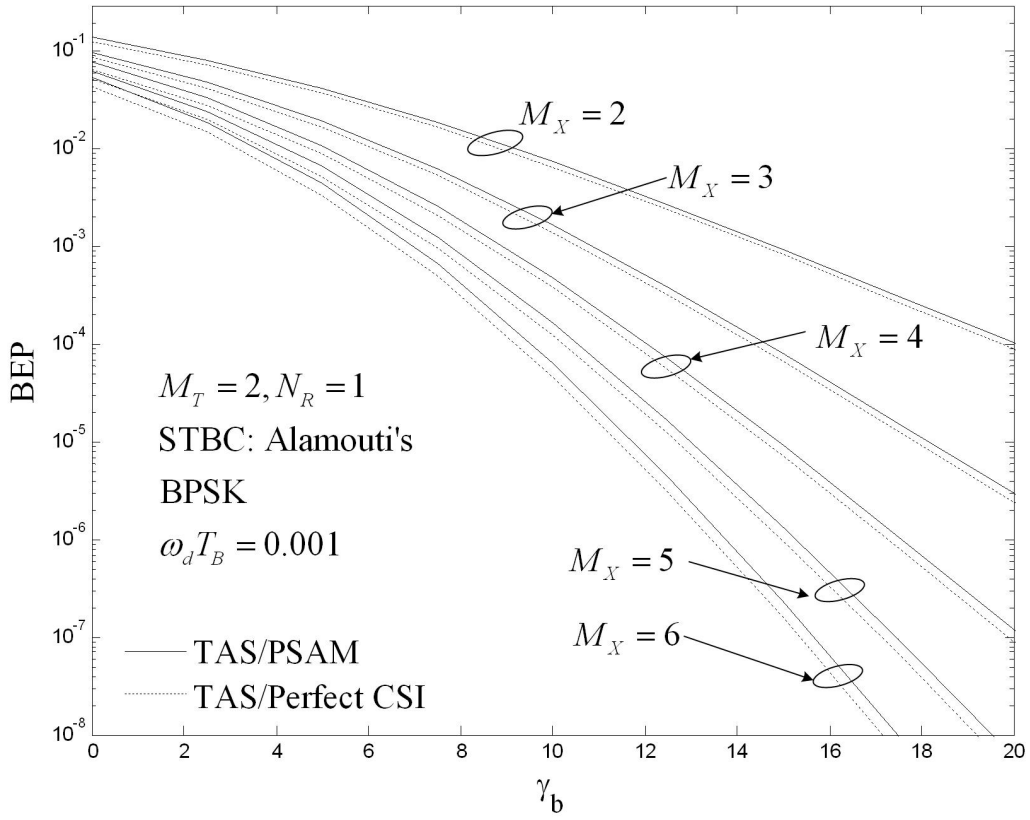

Fig. 5.2: Performance of Alamouti's STBC with transmit antenna selection

also plotted for comparison by setting $\sigma_e^2 = 0$. As the number of transmit antennas increases from two to three to provide a redundant antenna for TAS, considerable gain is achieved. Specifically, more than 5-dB gain is provided by the extra antenna at BEP level 10^{-4}. Further gain can be obtained by increasing the number of transmit antennas. However, the gain also tends to diminish with M_X. The 4×4, rate-3/4 STBC design in [47, 48] is used for illustration in Fig. 5.3. Similar to Fig. 5.2, maximum gain is achieved when there is one additional transmit antenna to choose from, i.e., $M_X = 5, M_T = 4$, but the gain is not as large as that with Alamouti's STBC. The gain is around 3dB at BEP level 10^{-6}. As M_X increases, although the transmitter has more antennas to

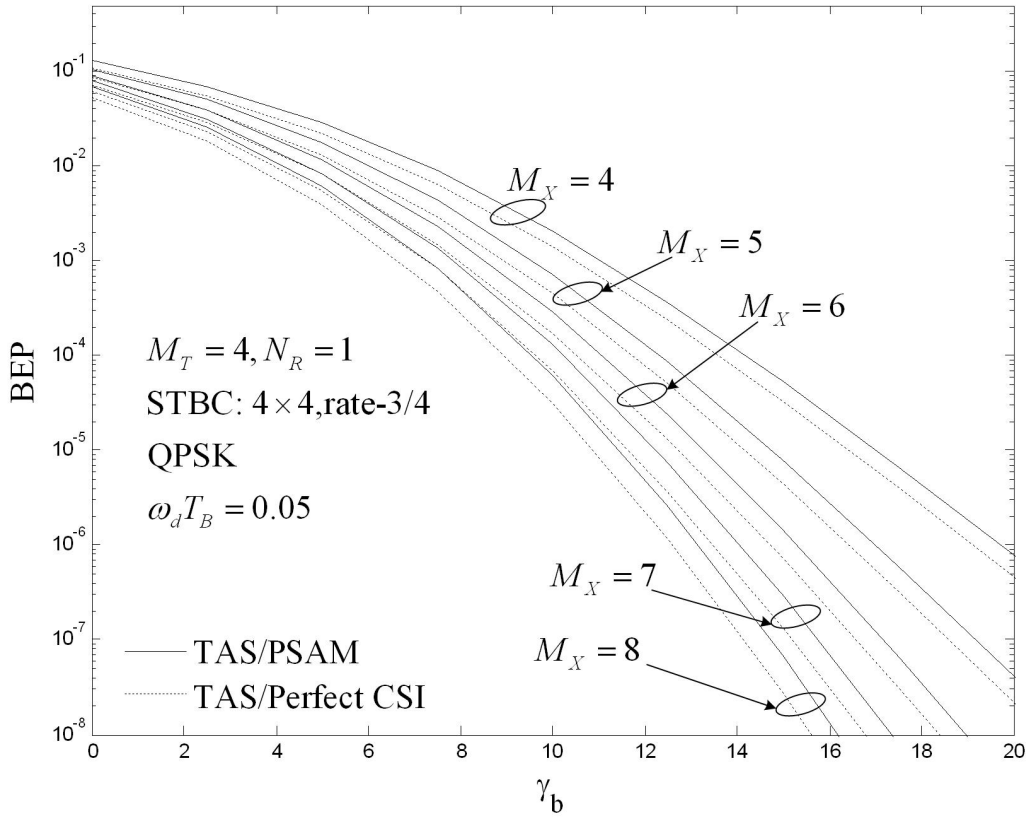

Fig. 5.3: Performance of the 4×4*, rate* $3/4$ *STBC with transmit antenna selection*

choose from, the gain becomes more and more limited.

In practice, the total number of transmit antenna cannot be arbitrarily large. We compare the BEP performances of different STBC's in Fig. 5.4 when the number of transmit antennas is fixed to four, while in Fig. 5.5 when the number of transmit antennas is fixed at eight. It is interesting to find that in both scenarios, the less active transmit antennas chosen, the better the performances would be. In another word, 1Tx transmission is the optimum choice as it injects all transmission energy into the best channel, while STBC's allocate the energy (almost) uniformly onto each channel. The phenomenon in Fig. 5.4 and Fig. 5.5 indicates that the transmit antenna selection is a

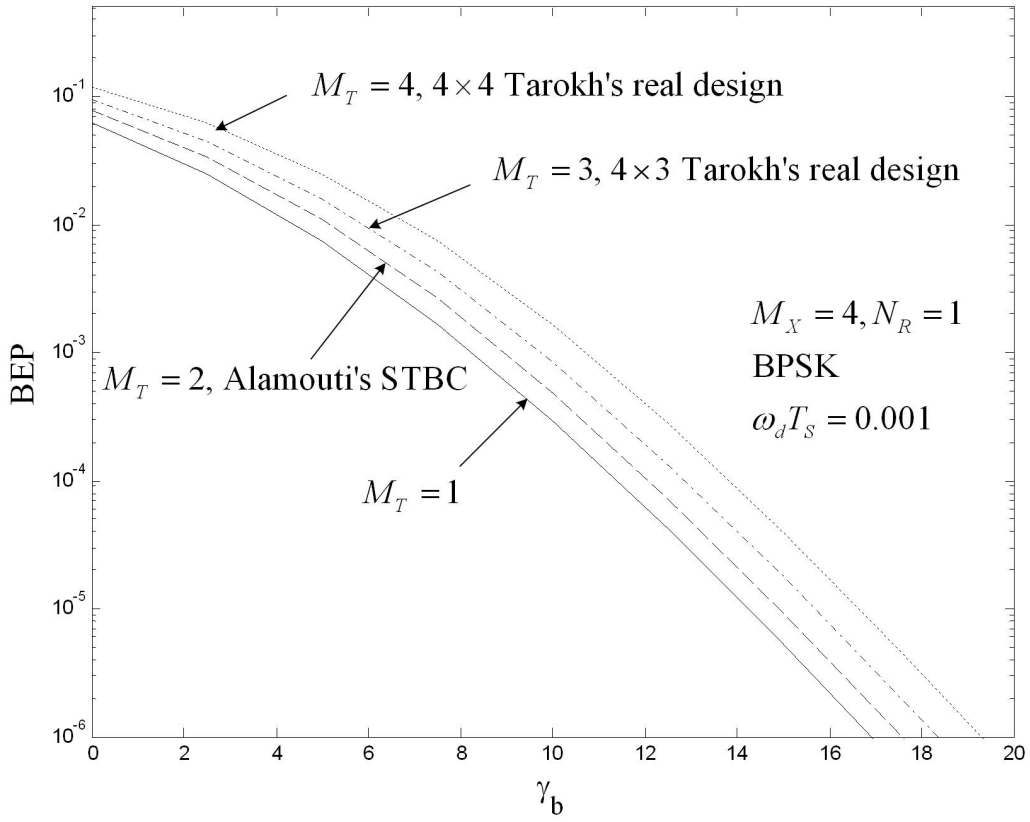

Fig. 5.4: Performance comparison among different STBC's with four transmit antennas for selection

more efficient way to utilize the transmit diversity as long as the reverse link is available.

As the conventional system with one active transmit antenna is shown to be theoretically the best choice for TAS system and it is indicated in Figs. 5.2-5.4 that one extra antenna for selection gives the largest gain, we plot the theoretical performance with two available and one active transmit antenna. The theoretical performances of Alamouti's STBC without TAS are also plotted for comparison. It is shown that as the number of receive antennas increases, the gain from non-TAS system becomes more and more limited. The approximation (5.23) shows good match to the BEP performance under high SNR.

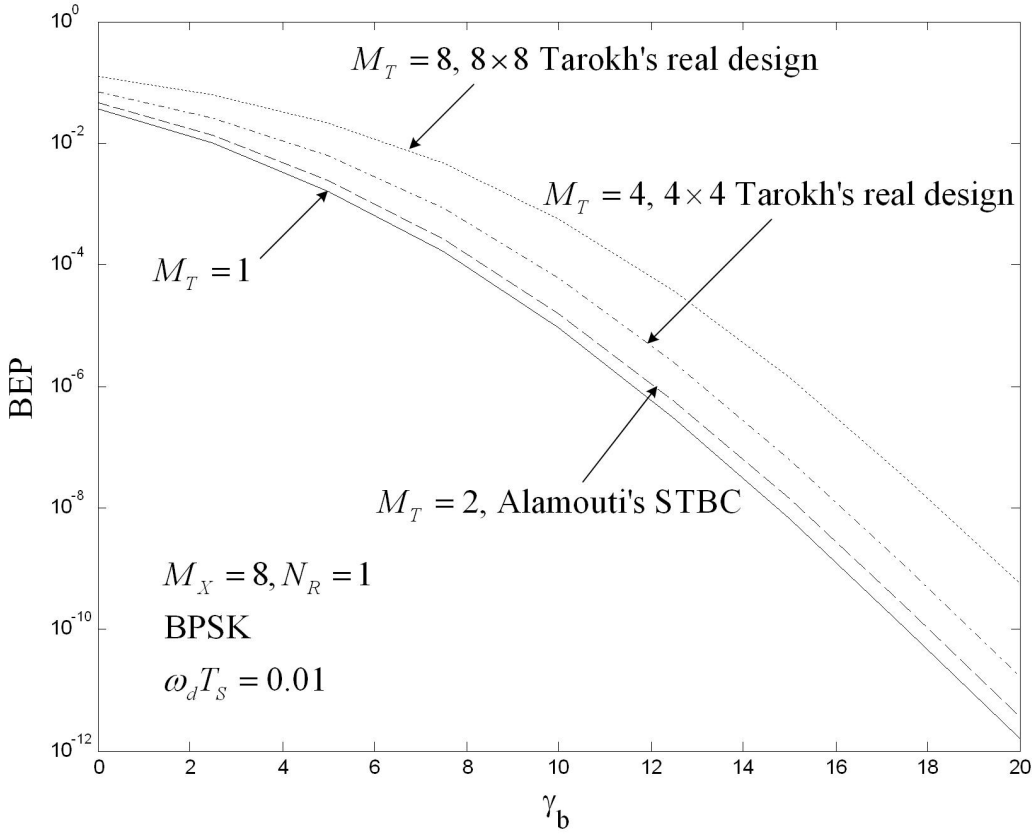

Fig. 5.5: Performance comparison among different STBC's with eight transmit antennas for selection

However, we have made two assumptions in our analysis. First, the channels are assumed to be block-wise constant; and secondly, we assume the TAS decisions are from the same PSAM channel estimation used for decoding. As addressed in the previous section, compared to the channel estimates for decoding, the channel estimation for TAS is less accurate and thus it is more likely to make mistakes on antenna selection, which eventually lowers the output SNR at the receiver and degrades the BEP performance. It would be of interest to know how the performance would degrade in practice when the two assumptions are invalid. The performance of Alamouti's STBC with four available antennas for transmit and one receive antenna are plotted in Fig.5.7. The theoretical

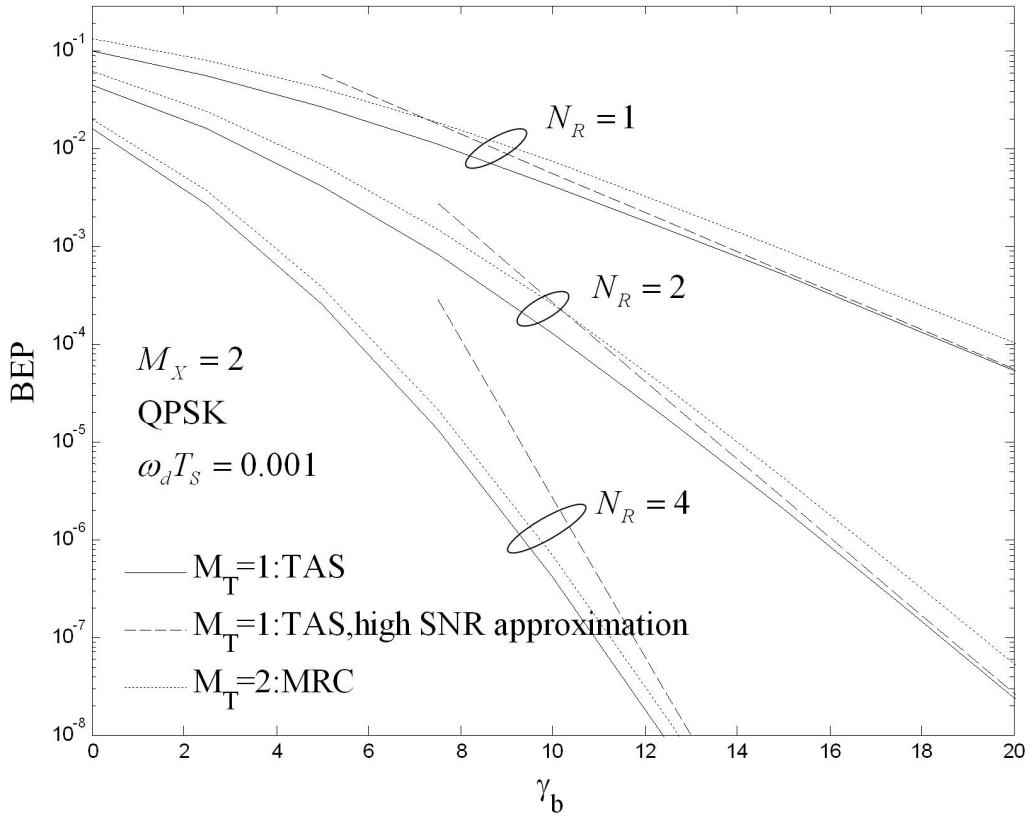

Fig. 5.6: Performance comparison between 1Tx/TAS and 2Tx/MRC systems with two transmit antennas

performances are calculated with the normalized block fade rate $\omega_d T_B = 0.002$. It is shown that the theoretical performance is very close to the one when perfect CSI is available. The upper bound is around 2-dB above the actual theoretical performance, and the high-SNR approximation given in (5.19) gives a asymptotic upper limit of the BEP performance and matches the theoretical BEP performance very well for $\gamma_b > 15$dB. Simulation results under both symbol-wise constant channel with $\omega_d T_S = 0.001$ and symbol-wise constant channel with $\omega_d T_B = 0.002$ are presented to show how the two assumptions affect the theoretical prediction from actual one. As the channel fluctuates from symbol to symbol, the orthogonality of received signal is disturbed. Therefore the

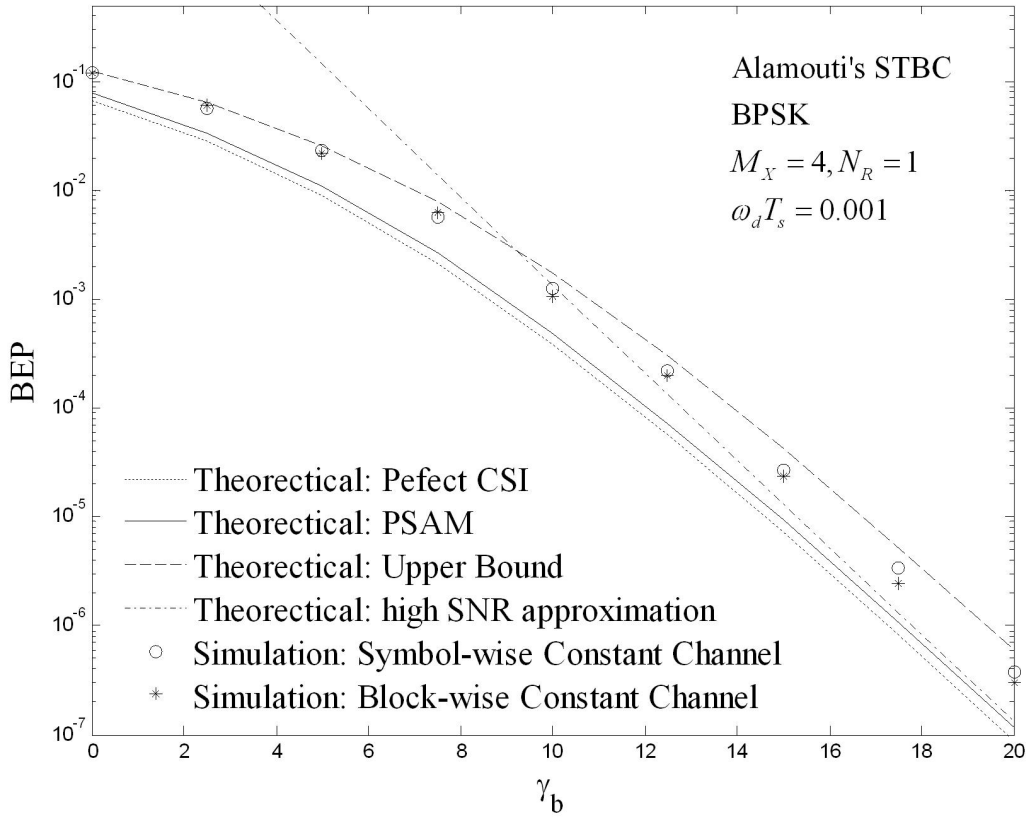

Fig. 5.7: Theoretical and simulation performances of Alamouti's STBC with four transmit antennas and one receive antenna

performance would be worse than that under a block-wise constant channel. However, under a slow fading channel $\omega_d T_S = 0.001$, the performance loss of symbol-wise constant channel from the performance of block-wise constant channel is minor and within half-dB. Hence the around 1-dB gap between the simulation with block-wise constant and theoretical prediction is due to the error decision on antenna selection. However, the theoretical BEP still gives a good prediction of the actual performance with a no more than 2-dB error.

Fig.5.8 shows the theoretical and simulation performances for a system with two transmit antennas. Two schemes are adopted for comparison, 1Tx/TAS that chooses the

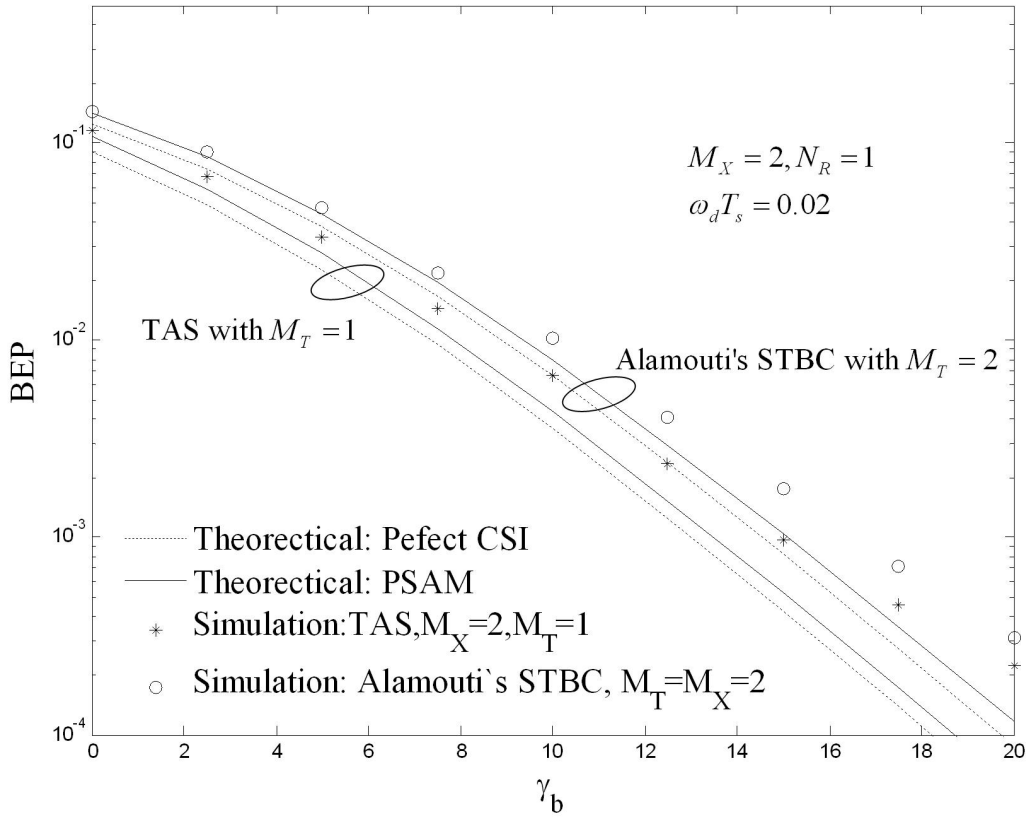

Fig. 5.8: Performances comparison of TAS and STBC with two available transmit antennas

better link for transmission, and Alamouti's STBC without TAS. The simulations are conducted under a relatively fast symbol-wise constant fading channel with $\omega_d T_S = 0.02$. The actual BEP performance of the 1Tx/TAS system tends to deviate from theoretical prediction more and more as the SNR increases, which indicates that the error due to erroneous TAS is dominant under high SNR. However, the 1Tx/TAS still exhibits better performance than the 2-Tx STBC system while having a simpler receiver structure. This validates the conclusion that in a TAS system, the less dispersed energy allocated onto the available links, the better the performance would be.

We extend our simulation to a system with four available transmit antennas under

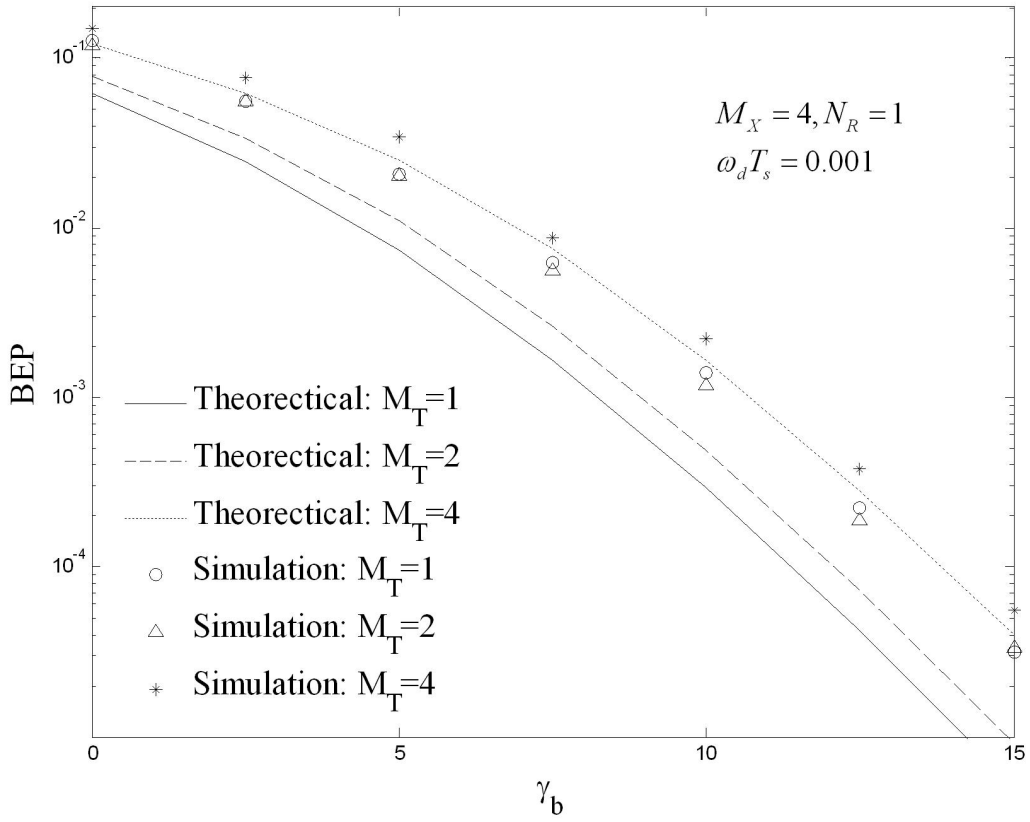

Fig. 5.9: Performances comparison of TAS and STBC with four available transmit antennas

slow fading environments in Fig. 5.9. The simulation results show that using $M_T = 1$ with TAS is around 1-dB better than that using 4-Tx STBC without TAS. Different from Fig.5.8, now using Alamouti's 2-Tx STBC with TAS is no worse than that with 1-Tx transmission. This can be explained from two causes. First, it has been shown in both Chapter 3 and Fig. 5.7 that a fading channel with normalized fade rate $\omega_d T_s = 0.001$ is slow enough to be called block-wise constant fading, i.e., the continuously changing channel does not disturb the orthogonality of received STBC much, so that the Alamouti's STBC does not suffer much loss from the symbol-wise fading channel. Second, compared to Fig.5.8, the 1-Tx system now has two more antennas to select from. How-

ever, it is also more likely for the system to make TAS mistake by not selecting the most significant antenna. With Alamouti's STBC, the system chooses the best two antennas out of four for transmission. Even if the channel estimator interchanges the order of the best two branches, the resultant performance would be unchanged. It is less likely to make decision mistakes compared to 1-Tx system with TAS, which explains why the 2-Tx/TAS system is even slightly better than 1-Tx/TAS system when M_X increases to four. However, it is shown the performances are almost identical with a gap less than half a dB, i.e., these two systems have comparable performances. The 1-Tx/TAS system is still preferable in practice as it has simpler system structure and is more robust against fast-fading channel.

5.5 Summary

In this chapter, we presented the performance analysis for STBC with transmit antenna selection. The selection rule is based on the estimated SNR obtained from channel estimation. As the channel estimation is imperfect, the BEP results are dependent on both SNR and estimation MSE. Exact closed-form BEP expressions are derived for generalized orthogonal STBC. The numerical results show that when the transmitter is informed which subset of transmit antennas to choose for transmission, one active transmit antenna exhibits better performance than that of STBC's.

Chapter 6

Constellation Design for Unitary Space-Time Modulation

In Chapter 2, we surveyed the channel capacity in an MIMO system. In this chapter, we first investigate the optimal constellation properties that achieve capacity, which in turn leads to the concept of unitary space-time modulation (USTM). In USTM, every data block is treated as one constellation and can be decoded both with or without channel state information as long as the channel is piece-wise constant. We then focus our work on the constellation design problem for differential USTM (DUSTM). We propose two new algorithms to improve the DUSTM constellation over the cyclic codes initially proposed for DUSTM.

6.1 Unitary Space-Time Modulation

6.1.1 Constellations that Achieve Capacity

Consider the system over P symbol periods. Each receiver antenna responds to each transmitter antenna through a statistically independent fading coefficient that is

constant. We assume that the fading coefficient changes to a new independent realization every P symbol periods. The transmission equation then is as presented in (2.5). The conditional probability density of the received signals given the transmitted signal is:

$$p\left(\boldsymbol{R}|\boldsymbol{S}\right) = \frac{\exp\left(-Tr\left\{\left[\boldsymbol{I}_P + \left(\rho/M_T\right)\boldsymbol{S}\boldsymbol{S}^H\right]^{-1}\boldsymbol{R}\boldsymbol{R}^{\boldsymbol{H}}\right\}\right)}{\pi^{PN_R}\det^{N_R}\left[I_P + \left(\rho/M_T\right)\boldsymbol{S}\boldsymbol{S}^H\right]}, \tag{6.1}$$

where $\boldsymbol{I}_P$ denotes the $P \times P$ identity matrix and "Tr" denotes "trace".

The channel is completely described by this conditional probability density. Note that the propagation coefficients do not appear in this expression. Although the received signals are conditionally Gaussian, the transmitted signals only affect the covariance of the received signals, in contrast to the classical additive Gaussian noise channel where the transmitted signals affect the mean of the received signals.

Further, let $\boldsymbol{\Phi}$ and $\boldsymbol{\Psi}$ be $P \times P$ and $M_T \times M_T$ unitary matrices, we get some properties as below:

$$p\left(\boldsymbol{R}|\boldsymbol{S}\boldsymbol{\Psi}^H\right) = p(\boldsymbol{S})\ p(\boldsymbol{\Phi}\boldsymbol{R}|\boldsymbol{\Phi}\boldsymbol{S}) = p(\boldsymbol{R}|\boldsymbol{S}). \tag{6.2}$$

In the system above, each channel use (consisting of a block of P transmitted symbols) is independent of every other, and (6.1) is the conditional probability density of the output $\boldsymbol{R}$, given $\boldsymbol{S}$. Thus, data can theoretically be transmitted reliably at any rate less than the channel capacity, where the capacity is the least upper bound on the mutual information between $\boldsymbol{R}$ and $\boldsymbol{S}$, or

$$C = \sup_{p(\boldsymbol{S})} I\left(\boldsymbol{R};\boldsymbol{S}\right) \tag{6.3}$$

subject to the average power constraint (2.4), and where

$$I(\boldsymbol{R};\boldsymbol{S}) = E\log\frac{p(\boldsymbol{R}|\boldsymbol{S})}{p(\boldsymbol{R})} = \int d\boldsymbol{S}\ p(\boldsymbol{S})\int d\boldsymbol{R}p(\boldsymbol{R}|\boldsymbol{S})\log\left\{\frac{p(\boldsymbol{R}|\boldsymbol{S})}{\int d\tilde{\boldsymbol{S}}p(\tilde{\boldsymbol{S}})p(\boldsymbol{R}|\tilde{\boldsymbol{S}})}\right\}. \tag{6.4}$$

Thus, C is measured in bits per block of P symbols. And it is always convenient to normalize C by dividing by P.

In [25], Hochwald etc. came to such conclusion:

Proposition 6.1 *The signal matrix that achieves capacity can be written as* $\boldsymbol{S} = \boldsymbol{\Phi V}$*, where* $\boldsymbol{\Phi}$ *is a* $P \times P$ *isotropically distributed unitary matrix, and* $\boldsymbol{V}$ *is an independent* $P \times M_T$ *real, nonnegative, diagonal matrix. Furthermore, we can choose the joint density of the diagonal elements of* $\boldsymbol{V}$ *to be unchanged by rearrangements of its arguments.*

There is no point in making the number of transmitter antennas greater than the length of the coherence interval. In a very real sense, the ultimate capacity of a multiple-antenna wireless link is determined by the number of symbol periods between fades. This is somewhat disappointing since it severely limits the ultimate capacity of a rapidly fading channel. For example, in the extreme case where a fresh fade occurs every symbol period, only one transmitter antenna can be usefully employed. Strictly speaking, one could increase capacity indefinitely by employing a large number of receiver antennas, but the capacity appears to increase only logarithmically in this number—not a very effective way to boost capacity.

The transmitted signals that achieve capacity are mutually orthogonal with respect to time among the transmit antennas. The constituent orthonormal unit vectors are isotropically distributed and statistically independent of the signal magnitudes. This result provides insight for the design of efficient signaling schemes, and it greatly simplifies the task of determining capacity, since the dimensionality of the optimization problem is equal only to the number of transmitter antennas.

When the coherence interval becomes large compared to the number of transmit antennas, the normalized capacity approaches the capacity obtained as if the receiver knew the propagation coefficients. The magnitudes of the time-orthogonal signal vectors become constants that are equal for all transmitter antennas. In this regime, all of the signaling information is contained in the directions of the random orthogonal vectors, the receiver learns the propagation coefficients, and the channel becomes similar to the classical Gaussian channel.

6.1.2 Unitary Space-Time Modulation

The conclusion in the previous section indicates that when the duration of the coherence interval is significantly greater than the number of transmitter antennas ($P >> M_T$), setting the diagonal elements of $\boldsymbol{V}$ to: $v_1 = v_2 = \cdots = v_{M_T} = \sqrt{P}$ attains capacity.

Taking all these results, we define *unitary space-time modulation* to be the transmission of $\boldsymbol{S} = \sqrt{P}\boldsymbol{\Phi}$, where $\boldsymbol{\Phi}^H\boldsymbol{\Phi} = \boldsymbol{I}$ [26]. And it is also proved that unitary space-time modulation is also optimal for any fixed $P > M_T/2$, as $\rho \to \infty$. And now the system model (2.5) can be re-written as:

$$\boldsymbol{R} = \sqrt{\frac{\rho}{M_T}}\boldsymbol{S}\boldsymbol{H} + \boldsymbol{N} = \sqrt{\frac{\rho P}{M_T}}\boldsymbol{\Phi}\boldsymbol{H} + \boldsymbol{N}. \tag{6.5}$$

6.1.2.1 ML Receiver for USTM

Now consider the ML reception of a constellation of L signals employing unitary space-time modulation,

$$\boldsymbol{S}_l = \sqrt{P}\boldsymbol{\Phi}_l \; l = 1, \ldots, L, \tag{6.6}$$

where $\{\boldsymbol{\Phi}_l, l = 1, \ldots, L\}$ are $P \times M_T$ complex matrices satisfying $\boldsymbol{\Phi}^H\boldsymbol{\Phi} = \boldsymbol{I}$.

Channel Unknown to the Receiver Recall the conditional probability density function of received signal (6.1), then the maximum-likelihood decoding becomes [28]:

$$\boldsymbol{\Phi}_{ml} = \arg \max_{\Phi_l \in \{\Phi_1, \ldots, \Phi_L\}} p\left(\boldsymbol{R}|\boldsymbol{\Phi}_l\right) = \arg \max_{\Phi_l \in \{\Phi_1, \ldots, \Phi_L\}} tr\{\boldsymbol{R}^H\boldsymbol{\Phi}_l\boldsymbol{\Phi}_l^H\boldsymbol{R}\}. \tag{6.7}$$

The ML receiver seeks to maximize the energy contained in the $M_T N_R$ inner products that comprise $\boldsymbol{\Phi}_l^H\boldsymbol{R}$.

Channel Known to the Receiver When $\boldsymbol{H}$ is known to the receiver

$$p(\boldsymbol{R}|\boldsymbol{S},\boldsymbol{H}) = \frac{1}{\pi^{PN_R}} \exp\left(-tr\{(\boldsymbol{R} - \sqrt{\rho/M_T}\boldsymbol{S}\boldsymbol{H})(\boldsymbol{R} - \sqrt{\rho/M_T}\boldsymbol{S}\boldsymbol{H})^H\}\right) \tag{6.8}$$

and the maximum-likelihood decoding becomes

$$\boldsymbol{\Phi}_{ml} = \arg \min_{\boldsymbol{\Phi}_l \in \{\boldsymbol{\Phi}_1,...,\boldsymbol{\Phi}_L\}} \mathrm{Tr}\left\{(\boldsymbol{R} - \sqrt{\rho P/M_T}\boldsymbol{\Phi}_l\boldsymbol{H})(\boldsymbol{R} - \sqrt{\rho P/M_T}\boldsymbol{\Phi}_l\boldsymbol{H})^H\right\}. \tag{6.9}$$

6.1.3 Differential Unitary Space-Time Modulation

Although channel state information is not necessary, the unitary space-time modulation discussed in the previous chapter assumes a piece-wise constant channel to work properly. It is natural to extend this scheme to a differential one to adapt to a continuously changing channel, just like the differential PSK in single-antenna unknown-channel systems.

6.1.3.1 System Model

Recall the system set up in section 2.1.1. We further normalize the complex baseband notation as: at time p we transmit the complex symbols s_{pi} on antennas $i = 1, ..., M_T$, and we receive r_{pl} on receiver antennas $l = 1, ..., N_R$. The action of the channel is modeled by

$$r_{pl} = \sqrt{\rho}\sum_{i=1}^{M_T} h_{il}s_{pi} + n_{pl} \; p = 0, 1, ...P; n = 1, ..., N_R. \tag{6.10}$$

Here h_{il} is the complex-valued fading coefficient between the i-th transmitter antenna and the l-th receiver antenna at time p. The fading coefficients are assumed to be independent with respect to i and l, and are $CN(0,1)$ -distributed. The additive noise at time p and receiver antenna l is denoted by n_{pl}, and is independently, identically $CN(0,1)$ distributed , with respect to both p and l.The realizations of h_{il}, $i = 1, ..., M_T$, $l = 1, ..., M_T$, are known neither to the transmitter nor the receiver. The transmitted

symbols are normalized to obey:

$$\mathrm{E}\left[\sum_{m=1}^{M_T} |s_{pi}|^2\right] = 1, \tag{6.11}$$

where E denotes expectation. Equations (6.10) and (6.11) ensure that ρ is the expected SNR at each receiver antenna, independently of the number of transmitter antennas M_T. Equivalently, the total transmitted power does not depend on M_T.

We assume that the fading coefficients change continuously according to a model such as Jakes' [34]. While the exact model for the continuous fading is unimportant, we require the fading coefficients to be approximately constant for overlapping blocks of $P \geq 2$ symbol periods. We have some freedom to choose P, but it generally cannot be larger than the approximate coherence time (in symbols) of the fading process.

6.1.3.2 Differential Transmission and Reception

Assume a data sequence of integers $z_1, z_2, \ldots$ with $z_t \in \{0, \ldots, L-1\}$ is to be transmitted. Each z_t corresponds to a constellation matrix from the constellation set $\{\boldsymbol{\Phi}_l\}$, $l = 0, \ldots, L-1$.The transmitter sends the symbol stream $\boldsymbol{S_1}, \boldsymbol{S}_2, \ldots$, which is determined by the following fundamental differential encoding rule [29],

$$\boldsymbol{S}_t = \boldsymbol{\Phi}_{\boldsymbol{z}_t} \boldsymbol{S}_{t-1} \qquad t = 1, 2, \ldots, \tag{6.12}$$

where $\boldsymbol{S}_0 = \boldsymbol{I}_{M_T}$.

At the receiver, the demodulator receives a stream $\boldsymbol{R}_0, \boldsymbol{R}_1, \boldsymbol{R}_2 \ldots$ where $\boldsymbol{R}_t$ is an $M_T \times N_R$ matrix. The consecutive received signal matrices can be written as

$$\boldsymbol{R}_{t-1} = \sqrt{\rho} \boldsymbol{S}_{t-1} \boldsymbol{H} + \boldsymbol{N}_{t-1} \tag{6.13}$$

$$\boldsymbol{R}_t = \sqrt{\rho} \boldsymbol{S}_t \boldsymbol{H} + \boldsymbol{N}_t. \tag{6.14}$$

Since the noise matrices remain invariant statistically after multiplying by unitary matrices, equation (6.14) can be written as

$$\boldsymbol{R}_t = \boldsymbol{\Phi}_{z_t}\boldsymbol{R}_{t-1} + \sqrt{2}\boldsymbol{N'}_t, \tag{6.15}$$

where $\boldsymbol{N'}_t$ is an $M_T \times N_R$ matrix of additive independent $CN(0,1)$ noise. Equation (6.15) shows the 3-dB performance loss in effective SNR compared to the coherent detection. The maximum-likelihood detector for differential space-time modulation is given by

$$\hat{z}_t = \arg \min_{l=0,\ldots,L-1} ||\boldsymbol{R}_t - \boldsymbol{\Phi}_l \boldsymbol{R}_{t-1}||, \tag{6.16}$$

where $||\cdot||$ is the Frobenius norm which is defined as $||\boldsymbol{A}|| = \sqrt{tr(\boldsymbol{A}^H\boldsymbol{A})}$. The Chernoff upper bound on the pairwise probability of error $P_{ll'}$ is given by

$$\begin{aligned} P_{ll'} &= \{choose\ \boldsymbol{\Phi}_{l'} | \boldsymbol{\Phi}_l\ transmitted\} \\ &\leq \tfrac{1}{2} \prod_{m=1}^{M_T} \left[1 + \tfrac{\rho^2}{1+2\rho}\sigma_m(\boldsymbol{\Phi}_l - \boldsymbol{\Phi}_{l'})\right]^{-N_R}, \end{aligned} \tag{6.17}$$

where $\sigma_m(\boldsymbol{\Phi}_l - \boldsymbol{\Phi}_{l'})$ is the m-th singular value of $(\boldsymbol{\Phi}_l - \boldsymbol{\Phi}_{l'})$. Then the constellation design rule is to maximize the diversity product ζ

$$\zeta = \min_{0\leq l\leq l'\leq L-1} \zeta_{ll'} = \frac{1}{2} \min_{0\leq l\leq l'\leq L-1} |\det(\boldsymbol{\Phi}_l - \boldsymbol{\Phi}_{l'})|^{1/M_T}. \tag{6.18}$$

We will elaborate on this diversity product rule in section 6.1.4.

6.1.3.3 Constellation Design for DUSTM (Cyclic Code)

In [29], a simple scheme to generate a group-structure constellation, which is called cyclic codes, has been proposed. The cyclic code is defined as:

$$\boldsymbol{\Phi}_l = diag\left[e^{j\theta_L k_1 l}, e^{j\theta_L k_2 l}, \ldots, e^{j\theta_L k_{M_T} l}\right]\ \ l = 0, 1, \ldots L, \tag{6.19}$$

where $\theta_L = 2\pi/L$. By doing exhaustive search, values of $\{k_1, k_2, \ldots, k_{M_T}\}$ are found to maximize the diversity product. Since this constellation is group structured, i.e., the product of two constellation signals is also within the constellation set, we have

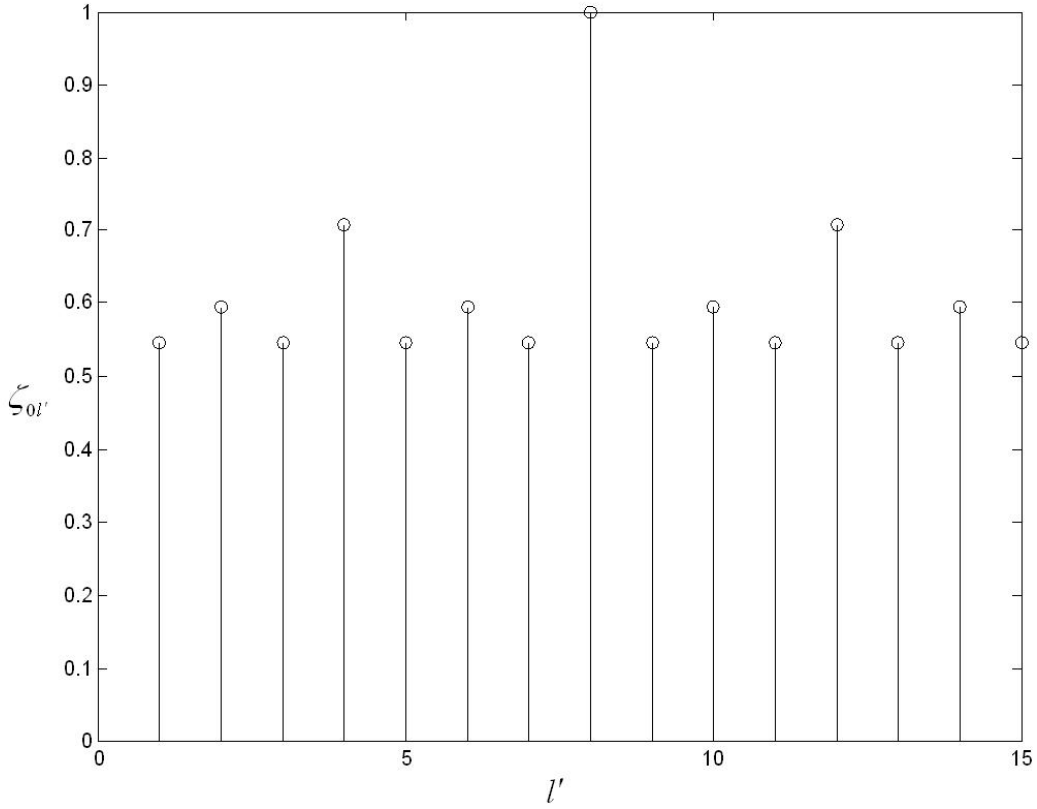

Fig. 6.1: Diversity product sample $\zeta_{0l'}$ when $M_T = 4, L = 16$

$\zeta_{0l'} = \zeta_{l(l+l')}$. Thus, instead of computing all the $L(L-1)\zeta_{ll'}$ s, only $(L-1)$ are needed. A sample of $\zeta_{0l'}$ is shown in Figure 6.1.

Because of the group-structure property, the encoding at the transmitter becomes very easy, since only summation of the constellation subscript is needed to calculate the transmitting matrix.

Another characteristic of a cyclic code is that it is diagonal, i.e., only one antenna transmits at any given time. One power amplifier can be switched among the antennas. But this amplifier must deliver M_T -times the power it would otherwise deliver if there were an array of M_T amplifiers simultaneously driving the other antennas. Consequently,

this amplifier needs to have a larger linear operating range than an amplifier array would. Amplifiers with a larger linear range are often expensive to design and build. It may therefore occasionally be desirable to have all M_T antennas transmitting simultaneously at low power.

6.1.4 Constellation Design Criteria for DUSTM

In single-antenna systems, the constellation is designed to maximize the minimum distance between the two signals. For the unitary space-time modulation, the constellation signals are no longer as simple as complex values, e.g. the MPSK constellations, but complex matrices. The distance definition between two matrices is not unique. For example, the Euclidean distance between matrices $\boldsymbol{A}$ and $\boldsymbol{B}$ of the same size $M_T \times N_R$ is defined by:

$$d = ||\boldsymbol{A} - \boldsymbol{B}|| = \sqrt{tr[(\boldsymbol{A} - \boldsymbol{B})^H (\boldsymbol{A} - \boldsymbol{B})]} = \sqrt{\sum_{m=1}^{M_T} \sum_{n=1}^{N_R} |a_{mn} - b_{mn}|^2}, \tag{6.20}$$

where $||\cdot||$ is denoted as Frobenius norm or Euclidean norm.

Next, we will derive a criterion for optimal constellation design for differential unitary space-time modulation discussed in the previous section.

The pairwise probability $P_{l,l'}$ of mistaking $\boldsymbol{V}_l$ for $\boldsymbol{V}_l'$ $(\forall l, l' \in \boldsymbol{Z}_L, l \neq l')$ or vice versa for the ML demodulator has a closed-form expression of [26, 29]:

$$\begin{aligned} &P_{l,l'} = \mathrm{P}\{ \text{ choose } \boldsymbol{V}_{l'} | \boldsymbol{V}_l \text{ transmitted } \} \ = \mathrm{P}\{ \text{ choose } \boldsymbol{V}_l | \boldsymbol{V}_{l'} \text{ transmitted } \} \\ &= \frac{1}{2\pi} \int_0^{\pi/2} \prod_{m=1}^{M_T} \left[\frac{\cos^2\theta + 1 - \mathrm{sgn}(\sigma_m^2)}{\cos^2\theta + \frac{\rho^2}{4(1+2\rho)}\sigma_m^2 + 1 - \mathrm{sgn}(\sigma_m^2)} \right]^{N_R} d\theta, \end{aligned} \tag{6.21}$$

where $\sigma_m \overset{def}{=} \sigma_m(\boldsymbol{V}_l - \boldsymbol{V}_{l'})$ represents the m-th singular value of the $M_T \times M_T$ difference matrix $\boldsymbol{V}_l - \boldsymbol{V}_{l'}$ for $m = 1, 2..., M_T$, and the function sgn() is the signum function. Then

the pairwise probability of error $P_{l,l'}$ has the Chernoff upper bound [26, 29]:

$$P_{l,l'} \leq \frac{1}{2} \prod_{m=1}^{M_T} \left[1 + \frac{\rho^2 \sigma_m^2}{4(1+2\rho)} \right]^{-N_R}. \tag{6.22}$$

We assume that the L transmitted unitary signals are equally probable *a priori*. Then, the performance of a general constellation consisting of unitary space-time signals can be measured by the following Chernoff union bound on the block probability of error P_e [28, 29],

$$\begin{aligned} P_e &= \tfrac{1}{L} \sum_{l=0}^{L-1} \text{prob}\{\text{error}|V_l \text{transmitted}\} \leq \tfrac{2}{L} \sum_{l=0}^{L-2} \sum_{l'=l+1}^{L-1} P_{ll'} \\ &\leq \tfrac{1}{L} \sum_{l=0}^{L-2} \sum_{l'=l+1}^{L-1} \prod_{m=1}^{M_T} \left[1 + \tfrac{\rho^2 \sigma_m^2}{4(1+2\rho)} \right]^{-N_R} = \tfrac{1}{L} \sum_{l=0}^{L-2} \sum_{l'=l+1}^{L-1} \left[1 + \sum_{m=1}^{M_T} \tilde{\rho}^m E_m \right]^{-N_R}, \end{aligned} \tag{6.23}$$

where

$$\tilde{\rho} \stackrel{def}{=} \frac{\rho^2}{4(1+2\rho)} \tag{6.24}$$

and

$$E_m = E_m(\boldsymbol{V}_l - \boldsymbol{V}_{l'}) \stackrel{def}{=} \sum_{1 \leq i_1 < \cdots < i_m \leq M_T} \prod_{k=1}^{m} \sigma_{i_k}^2 (\boldsymbol{V}_l - \boldsymbol{V}_{l'}) \tag{6.25}$$

for $m = 1, 2, \ldots, M_T$. It is seen from (6.23) that the Chernoff bound on the pairwise probability of error $P_{l,l'}$ is small when the terms E_m for all $m = 1, 2, \ldots, M_T$ are large. The Chernoff bound (6.23) on the block probability of error P_e is small when the terms $E_m(\boldsymbol{V}_l - \boldsymbol{V}_{l'})$ are large for all $m = 1, 2, \ldots, M_T$ and for all $0 \leq l < l' \leq L-1$. Now, we want to introduce some quantities that are closely related to the evaluation of the pairwise probability of error and the block probability of error.

For any two $M_T \times M_T$ unitary matrices $\boldsymbol{V}_1$ and $\boldsymbol{V}_2$, we define M_T quantities that reflect the dissimilarity between the two matrices as follows [102]:

$$D_m(\boldsymbol{V_1}, \boldsymbol{V}_2) = \frac{1}{2} \left(\frac{E_m(\boldsymbol{V}_1 - \boldsymbol{V}_2)}{\binom{M_T}{m}} \right)^{1/(2m)}. \tag{6.26}$$

For any given $M_T \times M_T$ unitary signal constellation $\boldsymbol{V}$ of size L, namely, $\boldsymbol{V} = \left\{\boldsymbol{V}_l | V_l^H \boldsymbol{V}_l = \boldsymbol{I}_{\boldsymbol{M}_T}, l \in \boldsymbol{Z}_L\right\}$, we may define the following M_T quantities that reflect the minimum dissimilarity between any two different unitary signals in $\boldsymbol{V}$ as follow:

$$\xi_m(L, \boldsymbol{V}) = \min_{0 \le l < l' \le L-1} D_m(\boldsymbol{V}_l, V_{l'}) \; m = 1, 2, \ldots, M_T. \tag{6.27}$$

In the extreme cases of $m = 1$ and $m = M_T$, the quantities $\xi_m(L, \boldsymbol{V})$ are, respectively,

$$\delta(L, \boldsymbol{V}) \stackrel{def}{=} \xi_1(L, \boldsymbol{V}) = \frac{1}{2\sqrt{M_T}} \min_{0 \le l < l' \le L-1} \left(\sum_{m=1}^{M_T} \sigma_m^2(\boldsymbol{V}_l - \boldsymbol{V}_{l'}) \right)^{1/2} \tag{6.28}$$

and

$$\varsigma(L, \boldsymbol{V}) \stackrel{def}{=} \xi_{M_T}(L, \boldsymbol{V}) = \frac{1}{2} \min_{0 \le l < l' \le L-1} \left(\prod_{m=1}^{M_T} \sigma_m^2(\boldsymbol{V}_l - \boldsymbol{V}_{l'}) \right)^{1/2M_T}. \tag{6.29}$$

In [29], the quantity $\varsigma(L, \boldsymbol{V})$ is called the *diversity product* of the constellation $\boldsymbol{V}$, which is represented in terms of the minimum among the products of the squared singular values for all difference signal matrices. Analogously, we may call $\delta(L, \boldsymbol{V})$ the *diversity sum* of constellation $\boldsymbol{V}$, since it is represented in terms of the minimum among the sums of the squared singular values for all difference signal matrices.

In [102], the M_T quantities defined by (6.27) are shown to possess the following properties:

Proposition 6.2 *For any given $M_T \times M_T$ unitary signal constellation $\boldsymbol{V}$ of size L, the nonnegative quantities $\xi_m(L, \boldsymbol{V})$ given by (6.27) for $m = 1, 2, \ldots, M_T$ and $L \ge 2$ satisfy the following conditions.*

- *For each $m = 1, 2, \ldots, M_T - 1$, $\xi_m(L, \boldsymbol{V}) \ge \xi_{m+1}(L, \boldsymbol{V})$*

  and for each $m = 2, \ldots, M_T - 1$, $\xi_m^{2m}(L, \boldsymbol{V}) \ge \xi_{m+1}^{m+1}(L, \boldsymbol{V}) \xi_{m-1}^{m-1}(L, \boldsymbol{V})$

- *If $2 \le L \le 2{M_T}^2 + 1$, then $\xi_m(L, \boldsymbol{V}) \le \sqrt{\frac{L}{2(L-1)}}$ for all $m = 1, 2, \ldots, M_T$*

In the case $m = 1$, the above inequality holds with equality if and only if any two distinct matrices in $\boldsymbol{V}$ have the same normalized Euclidean distance and that the sum of all the L signal matrices in $\boldsymbol{V}$ is an $M_T \times M_T$ all-zero matrix.

- *If $2{M_T}^2 + 1 \leq L \leq 4{M_T}^2$, then $\xi_m(L, \boldsymbol{V}) \leq \frac{1}{\sqrt{2}}$ for all $m = 1, 2, \ldots, M_T$*

- *If $L > 4{M_T}^2$, then $\xi_m(L, \boldsymbol{V}) < \frac{1}{\sqrt{2}}$ for all $m = 1, 2, \ldots, M_T$*

Proposition 6.2 actually gives an upper bound for both the diversity sum and diversity product.

According to (6.23) and (6.26), the Chernoff bound on the pairwise probability of error $P_{ll'}$ is small when the dissimilarity quantities $D_m(\boldsymbol{V}_1, \boldsymbol{V}_2)$ for all $m = 1, 2, \ldots, M_T$ are large. Therefore, when the minimum-dissimilarity quantities $\xi(L, \boldsymbol{V})$ of the signal constellation $\boldsymbol{V}$, defined by (6.27), are large for all $m = 1, 2, \ldots, M_T$, the Chernoff bound (6.23) on the block probability of error P_e becomes small correspondingly, at any SNR ρ. Moreover, it is easy to see that the diversity product, i.e., $\xi(L, \boldsymbol{V})$, is crucial for the performance of the unitary space–time constellations at high-SNR ρ, while the diversity sum, i.e., $\xi(L, \boldsymbol{V})$, is at low-SNR ρ (see also [29, 64]). For the sake of simplicity, we shall only consider to design the unitary signal constellation $\boldsymbol{V}$ with diversity sum (6.28) and diversity product (6.29) as large as possible. If the unitary signal constellation $\boldsymbol{V}$ has the *largest possible* diversity product (6.29), we call it a *diversity-product-optimal* constellation. Respectively, when a constellation has largest possible diversity sum (6.28), then it is *diversity-sum-optimal* constellation. And if the diversity product and the diversity sum converges, which means all the M_T quantities $\xi_m(L, \boldsymbol{V})$ are identical, then we say that the constellation is *sub-optimal*. And when all the M_T quantities $\xi_m(L, \boldsymbol{V})$ achieve the upper bound in Proposition 6.2, we can safely say the constellation is optimal.

For the convenience of analysis, we define a diversity product function as:

$$\varsigma_{l,l'} \stackrel{def}{=} \frac{1}{2}\left(|\det(\boldsymbol{V}_l - \boldsymbol{V}_{l'})|\right)^{1/M_T} = \frac{1}{2}\left(\prod_{m=1}^{M_T} \sigma_m^2(\boldsymbol{V}_l - \boldsymbol{V}_{l'})\right)^{1/2M_T} \tag{6.30}$$

and respectively, diversity sum function:

$$\delta_{l,l'} \stackrel{def}{=} \frac{1}{2\sqrt{M_T}}||\boldsymbol{V}_l - \boldsymbol{V}_{l'}||_F = \frac{1}{2\sqrt{M_T}}\left(\sum_{m=1}^{M_T} \sigma_m^2(\boldsymbol{V}_l - \boldsymbol{V}_{l'})\right)^{1/2}. \tag{6.31}$$

In the following, we focus on methods to find optimized constellation with criteria of diversity product.

6.1.5 A Revisit of Cyclic Designs

Recall the cyclic design in (6.19). With the simple diagonal cyclic design, the quantity $|\det(\boldsymbol{\Phi}_l - \boldsymbol{\Phi}_{l+\Delta l})|$ can be readily evaluated as

$$|\det(\boldsymbol{\Phi}_l - \boldsymbol{\Phi}_{l+\Delta l})| = \left|\prod_{m=1}^{M_T} (e^{jlk_{1m}\theta_L} - e^{j(l+\Delta l)k_{1m}\theta_L})\right| = 2^{M_T}\prod_{m=1}^{M_T} |\sin(\Delta l k_{1m}\theta_L/2)|. \tag{6.32}$$

Then the diversity function is simplified to

$$\zeta_{l,l+\Delta l} = \frac{1}{2}|\det(\boldsymbol{\Phi}_l - \boldsymbol{\Phi}_{l+\Delta l})|^{1/M_T} = \prod_{m=1}^{M_T} |\sin(\Delta l k_{1m}\pi/L)|^{1/M_T}. \tag{6.33}$$

It is clear from (6.33) that the diversity product function depends only on Δl, i.e.,

$$\zeta_{l,l+\Delta l} = \zeta_{l',l'+\Delta l} = \zeta_{\Delta l}. \tag{6.34}$$

Furthermore, we have the symmetry property

$$\zeta_{\Delta l} = \prod_{m=1}^{M_T} |\sin(\Delta l k_{1m}\pi/L)|^{1/M_T} = \prod_{m=1}^{M_T} |\sin(k_{1m}\pi - \Delta l k_{1m}\pi/L)|^{1/M_T} = \zeta_{L-\Delta l}. \tag{6.35}$$

When $\Delta l = L/2$ and $k_{1m} = even$, we have $\zeta_{L/2} = 0$, so that k_{1m} can only take the odd values from 0 to $(L-1)$. The exhaustive search of maximum diversity product now can be significantly simplified. Assume L is a even number. Then from 0 to $(L-1)$, there are

$\frac{L}{2}$ odd integers in total; and $(\frac{L}{2}-1)$ iterations of comuputation of (6.33) are needed due to the symmetry property. According to the diversity product function expression (6.33), the problem now is to choose M_T elements from a set of size L to form a non-ordered set $\{k_{1m}\}_{m=1}^{M_T}$.

We denote the algorithm complexity by the number of real multiplications, which is the dominant part when comparing to summation computation. A complex multiplication is equivalent to four real multiplications. To compute the diversity product in (6.33) for an eligible constellation set, $(\frac{L}{2}-1)(M_T-1)$ real multiplications must be performed. We adopt the following algorithm to go through all the non-ordered sets with size M_T, whose element is chosen from the size- $L/2$ set:

Improved algorithm for cyclic constellation search:
for $k_{11} = 1 : 2 : \text{Ł}$
  for $k_{12} = k_{11} : 2 : \text{Ł}$
    ...
      for $k_{1M_T} = k_{1(M_T-1)} : 2 : \frac{L}{2}$
        Calculate the diversity product;
        ...

The improved complexity is now $(\frac{L}{2}-1)(M_T-1)Q(M_T, L/2)$, where

$$Q(M_T, L) = \sum_{n_1=1}^{L} \sum_{n_2=1}^{n1} \cdots \sum_{n_{M_T}=1}^{n_{M_T-1}} n_{M_T}. \tag{6.36}$$

6.2 Constellation Design for Unitary Space-Time Modulation

So far we have reviewed the constellation design criterion for DUSTM. Also introduced is the cyclic constellation design brought forward by Hochwald [29] in their original paper on DUSTM. The cyclic constellation enjoys the simplicity of both encoder and decoder due to its group structure. However, its diagonal structure also suggests that only one antenna is working at any given time slot. This indicates that the cyclic codes

may not be efficient at exploiting the space and time diversities. In the following, we will propose two new constellation design algorithms that outperform the cyclic code while with limited increase in computational complexity.

6.2.1 DUSTM Constellation Designs Based on Rotation Matrices (Scheme I)

6.2.1.1 Constellation Construction

In this section, a differential unitary space time modulation scheme with M_T transmit and N_R receive antennas is considered. $L = 2^p$ is the size of unitary signal constellation and $j = \sqrt{-1}$ is the imaginary unit. θ_L is defined as $\theta_L = 2\pi/L$.

For a given set of integers $\boldsymbol{K} = \{k_{11}, k_{12}, \ldots, k_{1M_T}; k_2\} \in Z$, we construct the constellation as follows:

$$\boldsymbol{\Phi}_l = \begin{pmatrix} e^{j\theta_L k_{11}} & \cdots & 0 \\ \vdots & \ddots & \vdots \\ 0 & \cdots & e^{j\theta_L k_{1M_T}} \end{pmatrix}^l [R_{pq}(k_2\theta_L)]^l, l = 0...L-1, \tag{6.37}$$

where $\boldsymbol{R_{pq}}(\theta)$ is a rotation matrix defined as:

Definition 6.1 *A matrix is defined as a rotation matrix when: the (p,p) and (q,q) elements of* $\boldsymbol{R}_{pq}(\theta)$ *are equal to* $\cos\theta$ *for* $p \neq q$*, and all other diagonal elements are unity, and the (p,q) element is equal to* $\sin\theta$*, the (q,p) element is equal to* $-\sin\theta$*, and all other off-diagonal elements are zero.*

For example, when $M_T = 2$:

$$\boldsymbol{R}_{12}(\theta) = \begin{pmatrix} \cos\theta & \sin\theta \\ -\sin\theta & \cos\theta \end{pmatrix} \tag{6.38}$$

when $M_T = 4$, $p = 1$, $q = 3$

$$\boldsymbol{R}_{13}(\theta) = \begin{pmatrix} \cos\theta & 0 & \sin\theta & 0 \\ 0 & 1 & 0 & 0 \\ -\sin\theta & 0 & \cos\theta & 0 \\ 0 & 0 & 0 & 1 \end{pmatrix}. \tag{6.39}$$

Clearly, there are $M_T(M_T - 1)$ possible rotation matrices with different (p, q).

Proposition 6.3 *A rotation matrix as defined in Definition 6.1 has the properties below:*
i) $\boldsymbol{R}^l(\theta) = \boldsymbol{R}(l\theta)$
ii) $\boldsymbol{R}(\theta + \pi) = -\boldsymbol{R}(\theta), \boldsymbol{R}_{pq}(-\theta) = \boldsymbol{R}_{\boldsymbol{q}p}(\theta) = \boldsymbol{R'}_{pq}(\theta)$
iii) $\boldsymbol{R}(\theta) \cdot \boldsymbol{R}(\theta) = \boldsymbol{I}_{\boldsymbol{M_T}}$

In implementation, we randomly choose a possible rotation matrix. For any given constellation size of L, we search for a certain set of values $\boldsymbol{K} = \{k_{11}, k_{12}, \ldots, k_{1M_T}; k_2\}$ which maximizes the diversity product ζ. When $k_2 = 0$, it is exactly the same with the diagonal cyclic scheme proposed in [29]. And for the $M_T = 2$ case, the resulting diversity products are the same with the scheme presented in [102, 103].

6.2.1.2 Simplification to the Search Algorithm

Let's take a more detailed look at the algorithm. A constellation signal takes the form as below, assuming $p = 1, q = 2$ for the rotation matrix without loss of generality:

$$\begin{aligned} \boldsymbol{\Phi}_l &= \operatorname{diag}\left[e^{jk_{11}\theta_L}, e^{jk_{12}\theta_L}, ..., e^{jk_{1M_T}\theta_L}\right]^l \cdot [\boldsymbol{R}_{\boldsymbol{pq}}(k_2\theta_L)]^l \\ &= \begin{pmatrix} e^{jlk_{11}\theta_L}\cos(lk_2\theta_L) & e^{jlk_{11}\theta_L}\sin(lk_2\theta_L) & \cdots & \cdots & 0 \\ -e^{jlk_{12}\theta_L}\sin(lk_2\theta_L) & e^{jlk_{12}\theta_L}\cos(lk_2\theta_L) & \ddots & \ddots & \vdots \\ \vdots & \ddots & e^{jlk_{13}\theta_L} & \ddots & \vdots \\ \vdots & \ddots & \ddots & \ddots & \vdots \\ 0 & \cdots & \cdots & \cdots & e^{jlk_{1M_T}\theta_L} \end{pmatrix}. \end{aligned} \tag{6.40}$$

Thus:

$$\begin{aligned}
&|\det(\mathbf{\Phi}_l - \mathbf{\Phi}_{l+\Delta l})| \\
&= \left|e^{jl\theta_L(k_{11}+k_{12})}[1-(e^{j\Delta l\theta_L k_{11}}+e^{j\Delta l\theta_L k_{12}})\cos k_2\Delta l\theta_L + e^{j\Delta l\theta_L(k_{11}+k_{12})}]\right| \\
&\cdot \left|\prod_{m=3}^{M_T}(e^{jlk_{1m}\theta_L} - e^{j(l+\Delta l)k_{1m}\theta_L})\right| \\
&= \left|[1-(e^{j\theta_{\Delta l}k_{11}}+e^{j\theta_{\Delta l}k_{12}})\cos k_2\theta_{\Delta l} + e^{j\theta_{\Delta l}(k_{11}+k_{12})}]\right| \cdot 2^{M_T-2}\prod_{m=3}^{M_T}|\sin(\theta_{\Delta l}k_{1m}/2)|.
\end{aligned} \tag{6.41}$$

And then the diversity product function could be written as:

$$\begin{aligned}
&\zeta_{l,l+\Delta l} = \tfrac{1}{2}|\det(\mathbf{\Phi}_l - \mathbf{\Phi}_{l+\Delta l})|^{1/M_T} \\
&= \left|[1-(e^{j\theta_{\Delta l}k_{11}}+e^{j\theta_{\Delta l}k_{12}})\cos k_2\theta_{\Delta l} + e^{j\theta_{\Delta l}(k_{11}+k_{12})}]\right|^{1/M_T} 2^{1-\frac{2}{M_T}}\prod_{m=3}^{M_T}|\sin(\theta_{\Delta l}k_{1m}/2)|^{1/M_T},
\end{aligned} \tag{6.42}$$

where $\theta_{\Delta l} = \Delta l\theta_L$. We can see that the diversity product only affects the subscript difference of two constellations Δl. That is:

$$\zeta_{l,l+\Delta l} = \zeta_{l',l'+\Delta l} = \zeta_{\Delta l}. \tag{6.43}$$

Thus only (L-1) computations of diversity product function are needed to find the diversity product. Furthermore, we have:

$$\begin{aligned}
\zeta_{\Delta l} &= 2^{-\frac{2}{M_T}}\left|[1-(e^{j\Delta l\theta_L k_{11}}+e^{j\Delta l\theta_L k_{12}})\cos k_2\Delta l\theta_L + e^{j\Delta l\theta_L(k_{11}+k_{12})}]\right| \cdot \left|\prod_{m=3}^{M_T}|\sin(\Delta l\theta_L k_{1m}/2)|^{1/M_T}\right| \\
&= 2^{-\frac{2}{M_T}}\left|[1-(e^{j\Delta l\theta_L k_{11}}+e^{j\Delta l\theta_L k_{12}})\cos k_2\Delta l\theta_L + e^{j\Delta l\theta_L(k_{11}+k_{12})}]^*\right| \cdot \left|\prod_{m=3}^{M_T}|\sin(\Delta l\theta_L k_{1m}/2)|^{1/M_T}\right| \\
&= 2^{-\frac{2}{M_T}}\left|[1-(e^{-j\Delta l\theta_L k_{11}}+e^{-j\Delta l\theta_L k_{12}})\cos k_2\Delta l\theta_L + e^{-j\Delta l\theta_L(k_{11}+k_{12})}]\right| \\
&\qquad\qquad \cdot \left|\prod_{m=3}^{M_T}|\sin(\pi - \Delta l\theta_L k_{1m}/2)|^{1/M_T}\right| \\
&= 2^{-\frac{2}{M_T}}\left|[1-(e^{j(L-\Delta l)\theta_L k_{11}}+e^{j(L-\Delta l)\theta_L k_{12}})\cos k_2(L-\Delta l)\theta_L + e^{j(L-\Delta l)\theta_L(k_{11}+k_{12})}]\right| \\
&\qquad\qquad \cdot \left|\prod_{m=3}^{M_T}|\sin((L-\Delta l)\theta_L k_{1m}/2)|^{1/M_T}\right| \\
&= \zeta_{L-\Delta l}.
\end{aligned} \tag{6.44}$$

This indicates that the diversity product function is symmetric, same as the property of cyclic codes we have discussed. The computations of diversity product function is further reduced to $(\frac{L}{2}-1)$ just as in the cyclic designs.

And if $\Delta l = L/2$ and $k_{1m}, m = 3...L-1$ is an even integer, the second term of (6.42), $\left|\prod_{m=3}^{M_T}(1-e^{j\Delta l k_{1m}\theta_L})\right|$, will become zero. The diversity product function equals to zero means the two constellation signals are the same. For generality, we restrict all $k_{1m}, m = 1...L-1$ to be odd integers. With this assumption, we find that when $\Delta l = \frac{L}{2}, k_2 = odd$, (6.42) becomes:

$$\begin{aligned}\zeta_{l,l+\Delta l} &= 2^{-\frac{2}{M_T}}\left|[1-(e^{j\Delta l\theta_L k_{11}}+e^{j\Delta l\theta_L k_{12}})\cos k_2\Delta l\theta_L + e^{j\Delta l\theta_L(k_{11}+k_{12})}]\right|^{1/M_T} \\ &\qquad\qquad \cdot\prod_{m=3}^{M_T}|\sin(\Delta l\theta_L k_{1m}/2)|^{1/M_T} \\ &= 2^{-\frac{2}{M_T}}\left|[1-(e^{j\pi k_{11}}+e^{j\pi k_{12}})\cos k_2\pi + e^{j\pi(k_{11}+k_{12})}]\right|^{1/M_T}\cdot\prod_{m=3}^{M_T}|\sin(\Delta l\theta_L k_{1m}/2)|^{1/M_T} \\ &= 0.\end{aligned} \tag{6.45}$$

To calculate the diversity product for an eligible constellation set according to (6.42), $(\frac{L}{2}-1)(M_T+3)$ real-number multiplications are needed. By adopting a similar algorithm to that presented in page 119, there are totally $\left(\frac{L}{2}^3\right)$ possible combinations of k_{11}, k_{12} and k_2; $Q(M_T-2, L/2)$ possible combinations for $k_{13}, k_{14}, ...k_{1M_T}$. So the total number of necessary multiplications is $2\left(\frac{L}{2}\right)^4(M_T+3)Q(M_T-2, L/2)$.

6.2.1.3 Comparison with Space-Time Block Codes

The main characteristic of this Scheme I is that it has non-group constellation structure. Most constellation designs such as the cyclic codes presented in [64] and [29] have group constellation structure. The orthogonal STBC designs proposed in [18] and [19] also have non-group constellation structure. Take the well-known Alamouti's STBC

M	L	orthogonal designs	cyclic codes	Scheme I
2	4	0.7071	0.7071	0.7071
	8	-	0.5946	0.7071
	16	0.5000	0.3827	0.5946
	32	-	0.2494	0.3827
	64	0.2706	0.1985	0.3090
	128	-	0.1498	0.2606
	256	-	0.0988	0.1898
	512	-	0.0697	0.1510
4	4	-	0.7071	0.7071
	8	-	0.5946	0.6484
	16	0.5000	0.5453	0.5562
	32	-	0.3827	0.4447
8	4	-	0.7071	0.7071
	8	-	0.5946	0.6209
	16	-	0.5453	0.5453
	32	-	0.5221	0.5221

Table 6.1: Diversity products of different constellation design schemes

when $M_T = 2$ for example, the signal constellation can be written as in [15, 17]

$$\varphi = \left\{ \begin{pmatrix} x_1 & x_2 \\ x_2^* & -x_1^* \end{pmatrix} | x_1, x_2 \in \{ \frac{1}{\sqrt{2}} e^{2jk\pi/m} | k = 0, \ldots, m \} \right\}, \tag{6.46}$$

where each signal is a m-PSK signal. Then the diversity product could be written as:

$$\begin{aligned} \zeta &= \min_{l,l'} \tfrac{1}{2} \left| \det(\boldsymbol{V}_l - \boldsymbol{V}_{l'}) \right|^{1/M_T} \\ &= \min_{l,l'} \tfrac{1}{2} \left| \det \left[\begin{pmatrix} x_1 & x_2 \\ x_2^* & -x_1^* \end{pmatrix} - \begin{pmatrix} x_3 & x_4 \\ x_4^* & -x_3^* \end{pmatrix} \right] \right|^{1/2} \\ &= \min_{l,l'} \tfrac{1}{2} \left(|x_1 - x_3|^2 + |x_2 - x_4|^2 \right)^{1/2} = \tfrac{1}{\sqrt{2}} \sin\left(\tfrac{\pi}{m}\right) \end{aligned} \tag{6.47}$$

.

And for this orthogonal case, $L = m^2$ since each signal matrix contains two m-PSK signals. Some of the diversity products of different schemes are illustrated in Table 6.1.

6.2.2 DUSTM Constellation Designs Based on Full-Rotation Matrices (Scheme II)

6.2.2.1 Constellation Construction

We introduce another matrix to make the diversity product function $\zeta_{ll'}$ to distribute more evenly. First, we define a full-rotation matrix for an arbitrary even number M_T as follows:

$$\boldsymbol{R}F_{\boldsymbol{M_T}}(\theta) = \begin{pmatrix} \boldsymbol{R}F_{\boldsymbol{2}}(\theta) & \cdots & 0 \\ \vdots & \ddots & \vdots \\ 0 & \cdots & \boldsymbol{R}F_{\boldsymbol{2}}(\theta) \end{pmatrix}_{M_T \times M_T} . \tag{6.48}$$

The $\boldsymbol{R}F_{\boldsymbol{M_T}}(\theta)$ still keeps some properties of the rotation matrix such as:

i) $\boldsymbol{R}F^{l}_{M_T}(\theta) = \boldsymbol{R}F_{\boldsymbol{M_T}}(l\theta)$

ii) $\boldsymbol{R}F_{\boldsymbol{M_T}}(\theta+\pi) = -\boldsymbol{R}F_{\boldsymbol{M_T}}(\theta), \boldsymbol{R}F_{\boldsymbol{M_T}}(-\theta) = \boldsymbol{R}F'_{\boldsymbol{M_T}}(\theta)$

iii) $\boldsymbol{R}F_{\boldsymbol{M_T}}(\theta) \cdot \boldsymbol{R}F_{\boldsymbol{M_T}}(\theta) = \boldsymbol{I}_{\boldsymbol{M_T}}$

Similarly, we re-define our DUSTM constellations as:

$$\boldsymbol{\Phi}_l = \begin{pmatrix} e^{j\theta_L k_{11}} & \cdots & 0 \\ \vdots & \ddots & \vdots \\ 0 & \cdots & e^{j\theta_L k_{1M_T}} \end{pmatrix}^{l} \cdot [\boldsymbol{R}F_{\boldsymbol{M_T}}(k_2\theta_L)]^l,\ l = 0 \ldots L-1. \tag{6.49}$$

For any given constellation size of L, we search for a certain set of value $\boldsymbol{K} = \{k_{11}, k_{12}, \ldots, k_{1M_T}; k_2\}$ which maximizes the diversity product ζ. When $k_2 = 0$, it is exactly the same as the diagonal cyclic scheme proposed in [29].

6.2.2.2 Simplification to the Search Algorithm

Similar to what we have discussed in previous sections, in this case, the diversity product function could be finally written as:

$$\begin{aligned}&\varsigma_{l,l+\Delta l} = \tfrac{1}{2}|\det(\mathbf{\Phi}_l - \mathbf{\Phi}_{l+\Delta l})|^{1/M_T} \\ &= \prod_m [1 - (e^{j\Delta l\theta_L k_{1m}} + e^{j\Delta l\theta_L k_{1(m+1)}})\cos k_2\Delta l\theta_L + e^{j\Delta l\theta_L(k_{1m}+k_{1(m+1)})}] \\ &\text{where } 0 \le m \le L-1, m = \text{even},\end{aligned} \tag{6.50}$$

which indicates that $\zeta_{l,l+\Delta l} = \zeta_{l',l'+\Delta l} = \zeta_{\Delta l}$. Similar to the proposed Scheme I, only $(L-1)$ computation of diversity product function needed to find the diversity product ζ for a general candidate constellation rather than $\frac{L(L-1)}{2}$. Again, we can prove that $\zeta_{\Delta l} = \zeta_{L-\Delta l}$. For the selection of k_{1m} and k_2, we have:

Proposition 6.4 *If L is an even number, $\boldsymbol{K} = \{k_{11}, k_{12}, \ldots, k_{1M_T}; k_2\}$ must take either of following form to yield a positive diversity product:*
i) $\{k_{1m} = even, k_2 = odd\}$
ii) $\{k_{1m} = odd, k_2 = even\}$ where $m = 1, 2, ..., M_T$.

According to (6.50), $\left(\frac{L}{2}\right) 8^{M_T-1}$ real multiplications are needed to find the diversity product for a eligible constellation set. From Proposition 6.4, we can conclude that only $\left(\frac{L}{2}\right)\left(\frac{5L}{2}-1\right)$ real multiplications are needed to find the diversity product for a eligible constellation. And there are $2\left(\frac{L}{2}\right)^{M_T+1}$ possible combinations for $k_{11}, ..., k_{1M_T}; k_2$. The algorithm complexity becomes $2\left(\frac{5L}{2}-1\right)\left(\frac{L}{2}\right)^{M_T+2}$. Compared to the former designs, the computation complexity increases considerably as M_T is now in the exponent.

In practice, we also find that if the algorithm is further simplified to the following form, it can still yields the optimal diversity product:

$$\begin{aligned}\mathbf{\Phi}_l = diag[&e^{j\theta_L k_{11} l}, e^{j\theta_L(k_{11}+2)l}, \ldots, e^{j\theta_L(k_{11}+M_T-2)l}, e^{j\theta_L k_{12} l}, e^{j\theta_L(k_{12}+2)l}, \ldots, e^{j\theta_L(k_{12}+M_T-2)l}] \\ &\cdot [\boldsymbol{R} F_{\boldsymbol{M_T}}(l k_2 \theta_L)],\end{aligned} \tag{6.51}$$

M	L	Cyclic Code	Scheme II
2	3	0.8660	0.8660
	4	0.7071	0.7071
	5	0.7477	0.7906
	6	0.5000	0.6124
	7	0.5824	0.6323
	8	0.5946	0.7071
	9	0.4689	0.6124
	16	0.3827	0.5946
	32	0.2494	0.3827
	64	0.1985	0.3070
4	4	0.7071	0.7071
	8	0.5946	0.7071
	16	0.5453	0.6153
	32	0.3827	0.5453
	64	0.3399	0.4055
	128	0.2594	0.3574
6	4	0.7071	0.7071
	8	0.5946	0.7071
	16	0.5066	0.5946
	32	0.4483	0.5069
8	4	0.7071	0.7071
	8	0.5946	0.7071
	16	0.5453	0.5946
	32	0.5221	0.5453
	64	0.4231	0.5221

Table 6.2: Comparison of Diversity products of Scheme II against cyclic codes

where k_{11} and k_{12} are restricted to odd integers, and k_2 is an even integer ranging from 0 to $L/2$. Thus only 3 parameters are included and the complexity of algorithm is now significantly reduced to $\frac{L^4}{32}\left(\frac{5L}{2}-1\right)$, which is no longer dependent on M_T.

But when the constellation number is odd, unfortunately, we have to check all the possible $\boldsymbol{K} = \{k_{11}, k_{12}, \ldots, k_{1M_T}; k_2\}$ combinations.

6.2.2.3 Comparison with Former Designs

Comparison of diversity products between proposed and cyclic-codes is presented in Table 6.2.

In Proposition 6.2, an upper bound has been proposed for all the M_T quantities defined in (6.26), among which the diversity sum defined in (6.28) is the largest. The

M	L	Diversity product	Diversity sum	Optimal	Sub-Optimal	Diversity-Sum Optimal
2	2	1	1	√	√	√
	3	0.8660	0.8660	√	√	√
	4	0.7071	0.7071		√	
	5	0.7906	0.7906	√	√	√
	6	0.6124	0.6124		√	
	7	0.6323	0.6323		√	
	8	0.7071	0.7071		√	
	9	0.6124	0.7500			√
	16	0.5946	0.7071			
	32	0.3827	0.3827			
	64	0.3070	0.4016			
4	4	0.7071	0.7071		√	
	8	0.7071	0.7071		√	
	16	0.6153	0.7071			
	32	0.5453	0.7071			
	64	0.4055	0.4661			
	128	0.3574	0.3827			
6	4	0.7071	0.7071		√	
	8	0.7071	0.7071		√	
	16	0.5946	0.7071			
	32	0.5069	0.5581			
	128	0.4483	0.5882			
8	4	0.7071	0.7071		√	
	8	0.7071	0.7071		√	
	16	0.5946	0.7071			
	32	0.5453	0.7071			
	64	0.5221	0.7071			

Table 6.3: Diversity product and diversity sum of the proposed constellation

diversity sums of the proposed constellations are shown in Table 6.3.

Fig. 6.2 gives sample comparisons of the diversity product function for cyclic codes and the proposed method. Due to the symmetric property, only half of the distributions are plotted.

With our new method, the diversity product function distribution becomes more even and thus make the diversity product larger. Optimally, we would like the distribution to be uniform. However, as there is no systematic approach to construct uniformly spaced sub-space, we can only try to make the distribution as flat as possible.

Moreover, the improved Scheme II in 6.51 reduces the complexity of search algorithm so much, such that it is faster than the improved cyclic search process, especially

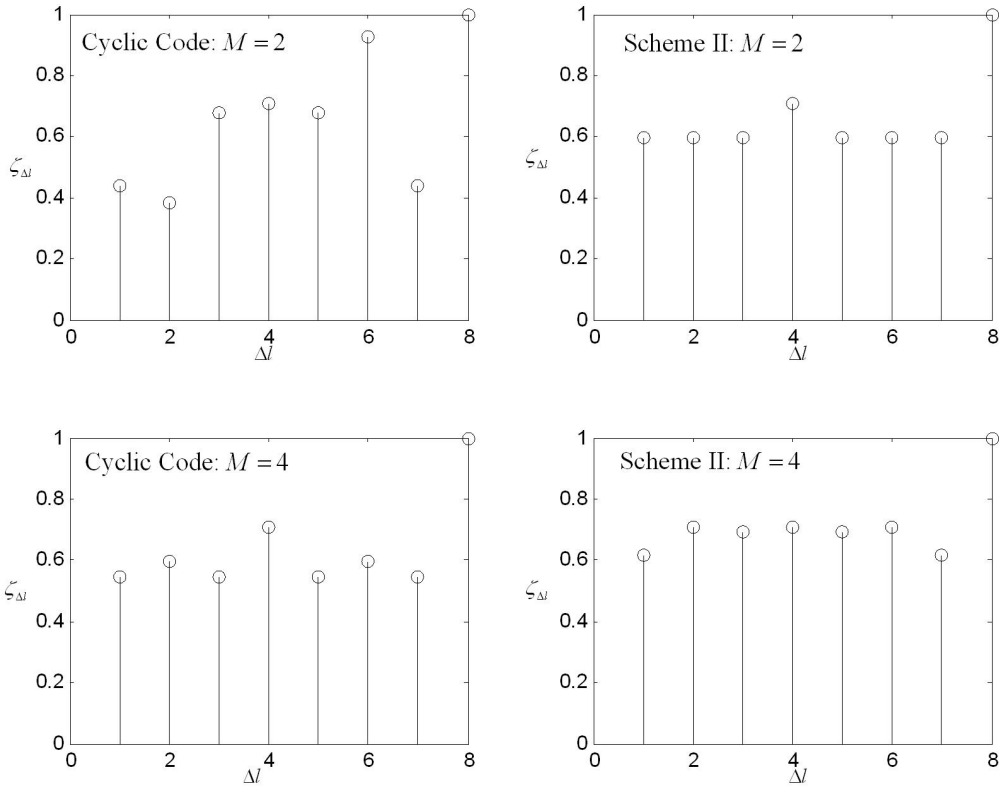

Fig. 6.2: Diversity product function distribution with constellation size $L = 16$

when M_T gets large. Fig. 6.3 clearly shows the complexity marked by the number of real multiplications for all the algorithms mentioned in this chapter. Before simplification, Scheme II is the most complex. However, the improved algorithm in 6.51 gives the least complexity and simpler than the cyclic code with respect to both M_T and L. Especially it is immune to the increase of M_T while others keep exponential dependence on M_T. Although we take the number of real multiplication as the criterion of algorithm complexity, it is not so accurate as there are summation and comparison operations involved. In Table 6.4, we give a more intuitional comparison in the form of searching time on computer. It is clearly shown that Scheme II provides both the shortest run-times

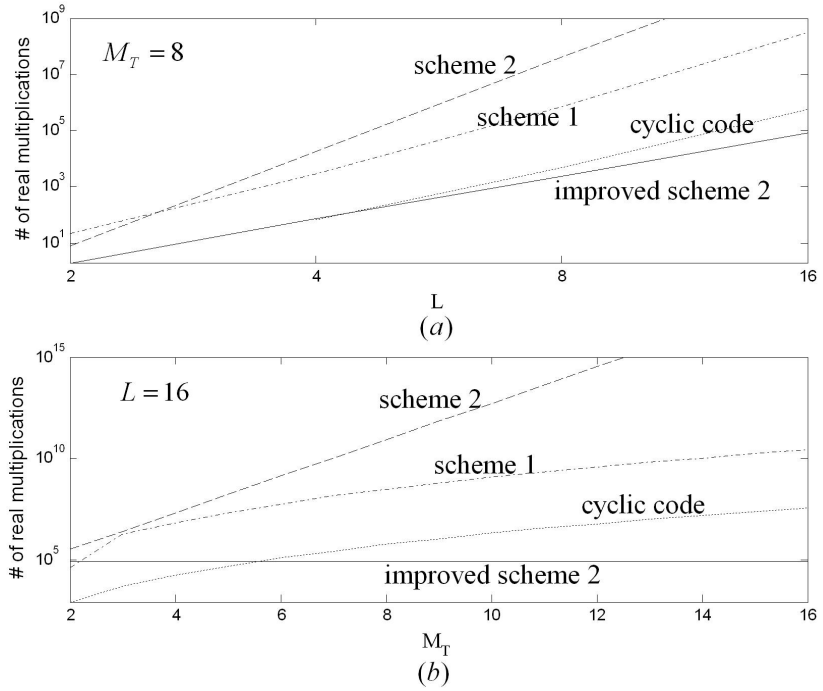

Fig. 6.3: Demonstration of algorithm complexities

M	L	Cyclic Code	Scheme I	Improved Scheme II
2	32	0.01	0.03	0.02
	64	0.01	0.16	0.08
	128	0.01	1.08	0.53
	256	0.01	7.73	3.78
	512	0.03	53.05	24.82
	1024	0.17	398.31	187.21
4	32	0.02	1.96	0.01
	64	0.18	37.03	0.16
	128	2.28	898.74	0.96
	256	34.18	24798.47	6.79
	512	-	-	46.63
	1024	-	-	359.18
8	16	0.11	4.41	0.02
	32	8.24	552.23	0.06
	64	1451.2	-	0.31

Table 6.4: Run-time comparison of algorithms (All data are in seconds and based on Matlab simulations using a P4 2.4G desktop with 512M RAM)

and the best diversity products. Especially when M_T and L become relatively large, Scheme II costs at most several minutes while the other two need hours or even days to complete the search. It is noted that Table 6.4 only gives a measure of the complexity of different algorithms. The detailed run-time data depends on the computer specification and efficiencies in the Matlab programming.

It can be found from the diversity product plots that the mutual distance between two constellation matrices are different. Normally if an error occurs under high SNR condition, the transmitted signal is most likely to be decoded as those constellations nearest to it. It is then natural to set partition for all the constellation into groups. By adopting the idea of gray coding or trellis coded modulation (TCM) , coding gain can be attained for BEP performances. As this is not the main interest of our work, we neglect the possible gain from such TCM/DUSTM systems. Related works can be found in [104, 105] and the references therein. We only focus on the symbol error probability (SEP) performance in the next section.

6.3 Numerical Results and Discussion

The newly proposed schemes have been shown to have smaller diversity products over the cyclic constellations. In this section, we will illustrate the performance gain of the newly proposed schemes over the cyclic one. Rayleigh fading channels with Jakes' model are adopted for fading simulation. We assume the fading process is symbol-wise constant in a realistic sense. Also as Scheme II always generates the same or better diversity product results compared to the Scheme I, we concentrate our simulations on Scheme II only.

As the theory of USTM/DUSTM requires the channel to be block-wise constant, we then first illustrate the SEP performance under slow fading channels with $\omega_d T_s = 0.001$. As Scheme II generates the same constellation results as the cyclic codes when $M =$

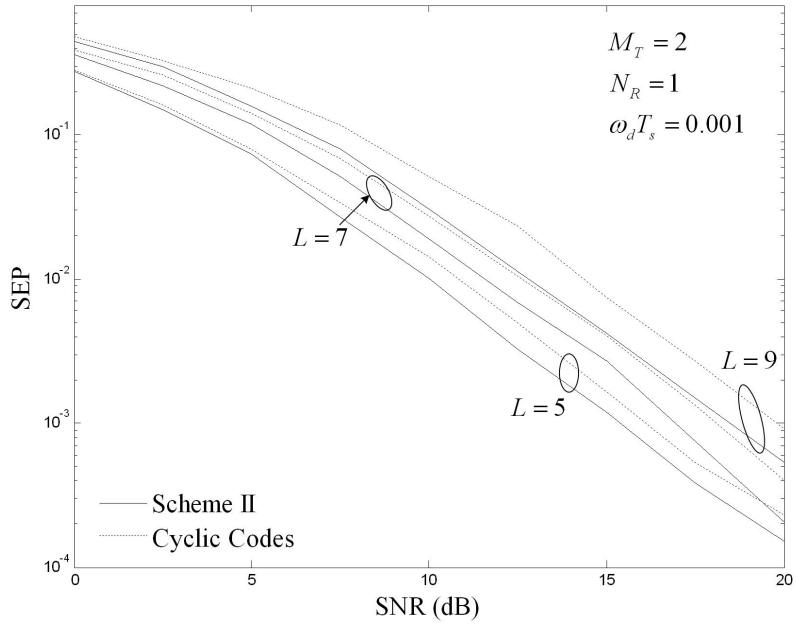

Fig. 6.4: SEP of DUSTM with $M_T = 2$ and $L = 5, 7, 9$

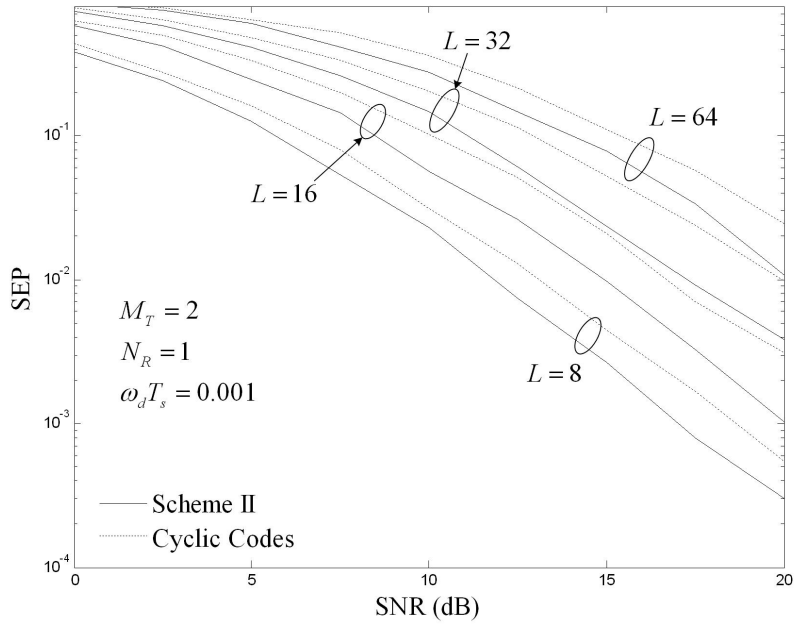

Fig. 6.5: SEP of DUSTM with $M_T = 2$ and $L = 8, 16, 32, 64$

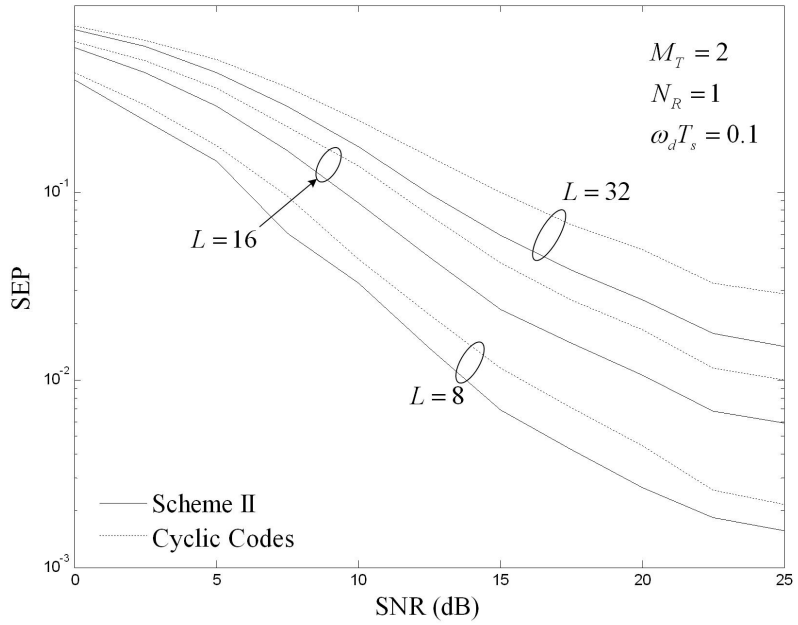

Fig. 6.6: SEP of DUSTM with $M_T = 2$ under fast fading

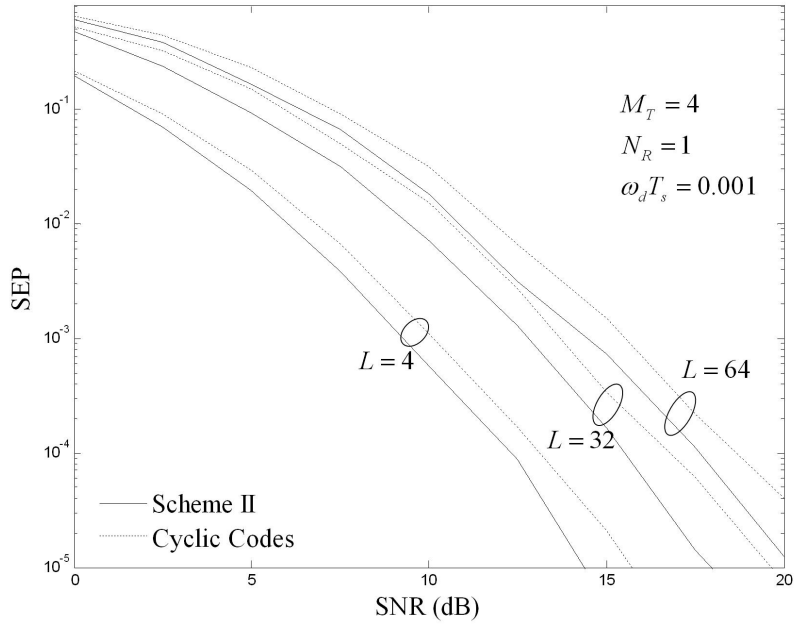

Fig. 6.7: SEP of DUSTM with $M_T = 4, L = 4, 32, 64$

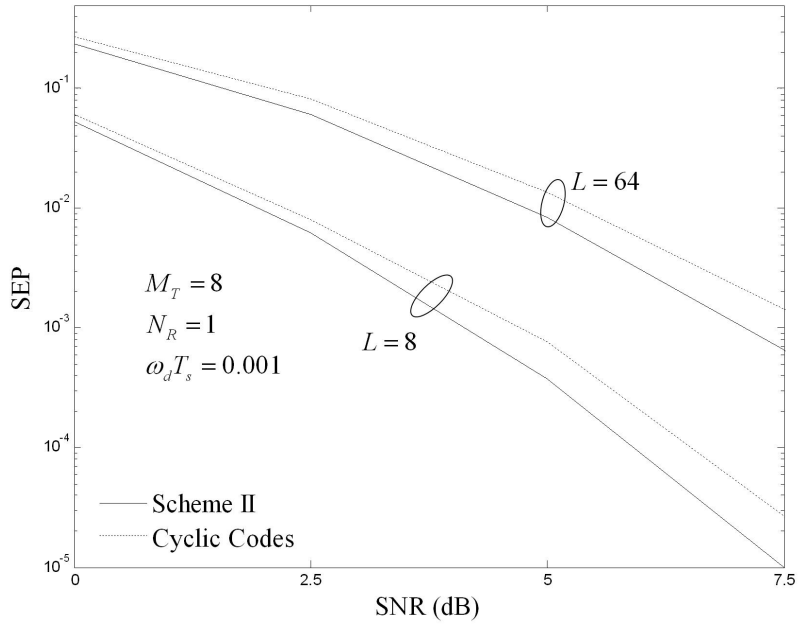

Fig. 6.8: SEP of DUSTM with $M_T = 8, L = 8, 32, 64$

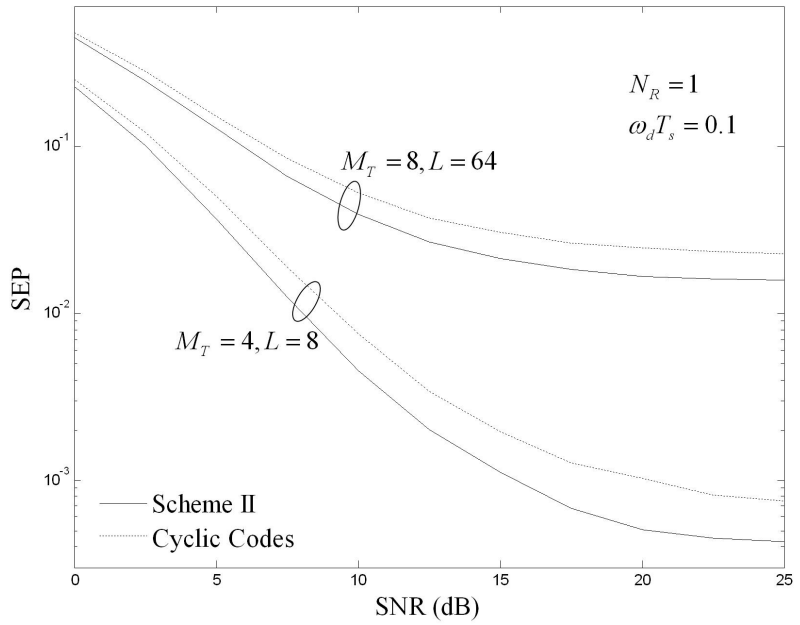

Fig. 6.9: SEP of DUSTM with $L = 64$ under fast fading

$2, L = 3, 4$, thus the performances would be the same. So that plotted in Fig. 6.4 and Fig. 6.5 are the SEP performance with constellation size greater than four. It is clear from both figures that the proposed new constellations attain 1-3dB gain against the cyclic code with SNR around 20dB. The best 3-dB gain is achieved when $M = 2, L = 16, 32$. As the SNR increases, this gain becomes more and more obvious. This validates the proposition that the diversity product design criterion is high-SNR oriented while the diversity sum design criterion is low-SNR oriented. With the diversity product list in Table 6.2, it can be also concluded that a slight increase in diversity product may result in a relatively significant improvement in performance. The search procedure for better constellation designs is worthwhile.

Fig. 6.6 demonstrates the performance when the channel fades as rapidly as $\omega_d T_s = 0.1$. As DUSTM adopts differential detection and assumes block-wise constant channel, both conditions are not met under fast-fading channel. We can expect that the performance would seriously degrade under such a fast-fading channel. Obvious performance floors are observed as SNR increases. As the new Scheme II has a lower floor, the gain is quite significant under high SNR.

Plotted in Fig. 6.7 and Fig. 6.8 are the SEP performance with four and eight transmit antennas, respectively. Similarly, 1-3dB gains are achieved for all cases.

As demonstrated in Chapter 3, the most significant limitation of space-time coding is that it requires longer coherence time as the number of transmit antennas increases, and USTM is not an exception. Especially for differential encoding and decoding, theoretically this coherence time is required to be doubled to enable differential decoding. We expect that under a fast-fading scenario, the less transmit antennas, the better the performance would be. Fig. 6.9 demonstrates the performances of DUSTM with $M_T = 4$ and $M_T = 8$ under a fade-rate of $\omega_d T_s = 0.1$. For the sake of fairness, the constellation sizes are chosen to be $L = 8$ and $L = 64$, respectively, so that both schemes transmit six bits over eight symbol periods. It is clear in Fig. 6.9 that the performances of $M_T = 4$

case are far better than those of $M_T = 8$. Not only it has a lower error floor, but the floor appears later than that of $M_T = 8$ case. In both cases, the SEP value of floor is halved by adopting the proposed Scheme II.

6.4 Summary

In this chapter, we first introduce the development of coherent and differential unitary space-time modulation. Based on the orthogonal structure of signal matrices, we then introduce the derivation of its constellation design criteria. As there are no systematic ways to achieve optimality in general, people normally choose to use some sub-optimal easy-to-construct yet efficient constellation for implementations. In the original paper where USTM/DUSTM was proposed, the author also put forward a simple code called cyclic code for constellation generation. As the signal matrix is always diagonal for all possible constellation, i.e., only one antenna is active at one time, cyclic code is obviously not the best solution for USTM/DUSTM. Based on this cyclic code, we propose two constellation schemes that outperform the cyclic one in diversity product criteria. We studied the diversity product properties in detail and then simplified the constellation search process significantly while achieving higher diversity products. Simulations are carried out to show the performance gain of the newly proposed schemes over the cyclic codes.

Chapter 7

Conclusions and Proposals for Future Research

7.1 Conclusions

The research work in this dissertation includes: performance analysis of MIMO communication systems with imperfect channel estimation, and constellation designs for unitary space-time modulation.

MIMO systems that employ multiple antennas at both transmit and receive sides have been a hot topic for the past few years. Some recent techniques like turbo coding have brought the utilization of a single link very close to Shannon limits of channel capacity. To achieve more capacity required by the next generation communication, one must create multiple links between a terminal and a base station, which is fulfilled by MIMO systems. Among those MIMO techniques, STBC has attracted much research interest for its simple receiver structure using only linear processing.

As channel state information is necessary at the receiver for coherent STBC decoding, joint channel estimation and STBC detection must be performed in implementation. In our work, we proposed a MMSE channel estimation-based STBC receiver structure,

which can be applied to either decision-directed estimation or pilot-symbol assisted modulation. Based on the receiver structure, we derived the optimum maximum-likelihood STBC decoder. However, as the optimum receiver is too computationally complex, we then proposed a sub-optimal simple receiver structure, where each symbol in the STBC can be decoupled and decoded independently. With the receiver structure and channel models, we analyzed the BEP performance of such STBC systems. Exact closed-form BEP expressions are obtained for generalized orthogonal STBC systems, which show direct dependence on the MSE of the channel estimation and signal-to-noise ratio. Extensive simulations have been carried out for the proposed system. Simulation results show that our theoretical results give a very good prediction.

We then extend our work to STBC systems with selection combining at the receiver with imperfect channel estimation. Selection combining has long been known as an effective diversity technique which can reduce the power consumption at receiver when doing decoding. Based on the channel estimation available at the receiver, the decoder chooses received signal from the best one or several antennas with maximum estimated SNR for decoding. BEP performances are derived in closed-form for such STBC systems with channel estimation and selection combining. Moreover, we also contribute to adaptive transmit antenna selection with STBC. By setting up a reverse link, the receiver can indicate to the transmitter which antennas have the best link qualities for transmission based on channel estimation. BEP performances in exact closed-form are developed for such systems. Both theoretical and simulation results show that selection combining and transmit selection techniques are efficient yet simple in implementation while achieving the full diversity order of the MIMO systems.

Contribution has also been made to constellation designs for differential unitary space-time modulation. A simple constellation search algorithm was proposed to look for code designs that outperform the existing cyclic design for unitary space-time modulation.

In summary, our works focus on the MIMO application perspective where channel estimation is necessary for coherent space-time decoding. All the systems proposed are implementation-feasible and can easily be integrated with other coding or modulation techniques such as: turbo-coding, OFDM, and UWB, etc., for the next-generation communication systems.

As MIMO is a bandwidth-efficient technique compatible with most other emerging communication techniques, it is predictable that most high-speed wireless application will use MIMO in the future.

7.2 Proposals for Future Research

The performance analysis of MIMO systems using STBC presented in this dissertation basically assumes the channels are i.i.d Rayleigh fading channel. One straight found extension is to employ other channel models such as Nakagami-m model. One would also be interested in the STBC performance when the channels are independent but not identically distributed, or even correlated. So far, there are quite a lot works that have been done in this area, but most of these works leads to SEP expressions with unsolvable integrals, where numerical means must be taken. Although a closed-form BEP expression is not likely to be obtainable for every scenario, we can still extend the STBC performance analysis.

Previously in this dissertation, we have extended the preliminary work on BEP performance analysis with MRC in Chapter 3 by introducing selection combining and transmit selection into the system in Chapter 4 and Chapter 5, respectively. The results therein show that both selection combing and transmit selection are efficient ways to employ transmit and receive diversities, while independent of STBC. It is also found that so far not much work has been done for STBC system with selection combining or transmit selection. It is still worthwhile to explore more on this topic. Possible directions

are as follows. First, we can improve or simplify the selection rule. Since we use the estimated SNR as the selection criterion, channel estimations must be performed before the transmission or before the data decoding, even for those channels not selected. It is of interest to know how much loss would be involved if we choose to use some less-optimal schemes such as switch diversity or threshold-testing technique. Second, in Chapter 4 and Chapter 5, we have assumed i.i.d. channel model. If the channels are non-i.i.d or even correlated, what is the optimum transmitter and receiver structure to minimize the BEP? We expect such a problem would result in a power-allocation strategy at the transmitter, and weighted summation of the received signals at the receiver to form the decoding metric. Then, what is the optimum (or sub-optimum if optimum is not applicable) rule to determine the tap weights in both problems? How much can the performance be improved so that such systems are desirable? All these questions are still open and worthy of further investigation.

Seven years have passed since the debut of space-time coding in 1998. The space-time coding technique is entering its maturing phase. Now people are keen on what we can really do with space-time. The research interests are shifting from physical layer design to cross-layer design for MIMO. A hot topic now is MIMO in wireless networks. The cross-layer design tends to optimize the MIMO system together with the data-link, network layers, or even up to the application layer as a whole. It tries to make use of MIMO for packet scheduling, QoS controlling, or constructing a cooperative network, and so on.

In a wireless network, there are multiple nodes capable of both transmitting and receiving signals. Different from the conventional wired network, they share the same free space and same bandwidth for transmission. The transmissions must be carefully scheduled to minimize interference. What we currently do is, as shown in Fig. 7.1(a), when a source node wants to transmit, it first mutes all the adjacent antennas, and then transmits. A question that has attracted quite a lot of research interests is: can

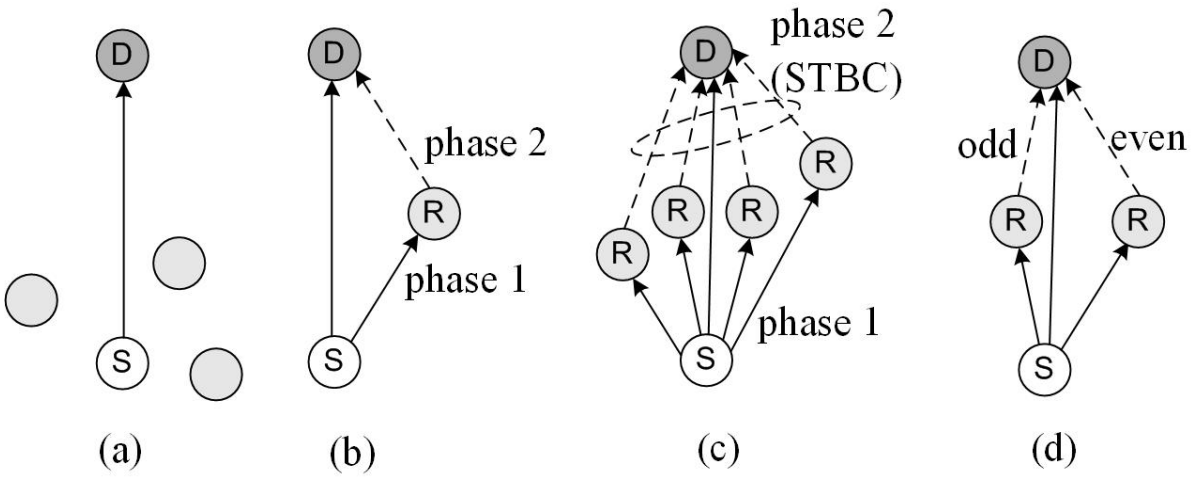

Fig. 7.1: Examples of relay diversity: (a) No relay; (b) Half-rate scheme with one relay node; (c) Half-rate scheme with multiple relay nodes; (d) Full-rate scheme with two relay nodes.

we use those silent nodes to help the source, so that we can get some gain from such cooperations? This leads to the concept of cooperative networks, and we term the gain obtained as relay gain, which is a particular kind of diversity gain. Early investigations on relay diversity topic include those of Sendonaris [106–108]and those of Laneman [109, 110]. Some examples of relay diversity are illustrated in Fig. 7.1(b)-(d), where we assume a node can be either receiving or transmitting, but not simultaneously. Normally the relay transmission is divided into two phases, like in scheme (b)[109–111]. During the first phase, the source transmits and both the relay and destination listen. And during the second phase, the relay re-transmits the received signals received in the first phase in either a decode-and-forward or an amplify-and-forward manner. Alternatively, if more idle relay nodes are available, they can help to transmit the same message or even cooperate to use space-time block coding, as in (c). Of course, STBC transmission would require negotiation and accurate synchronization among all the relay nodes. The cost for both schemes (b) and (c) is that the data rate is halved since the transmission is split into two phases. A full-rate scheme is shown as in (d)[112]. Two relay nodes are used, relay one listens at even slots and re-transmits at odd slots; similarly, relay two listens at

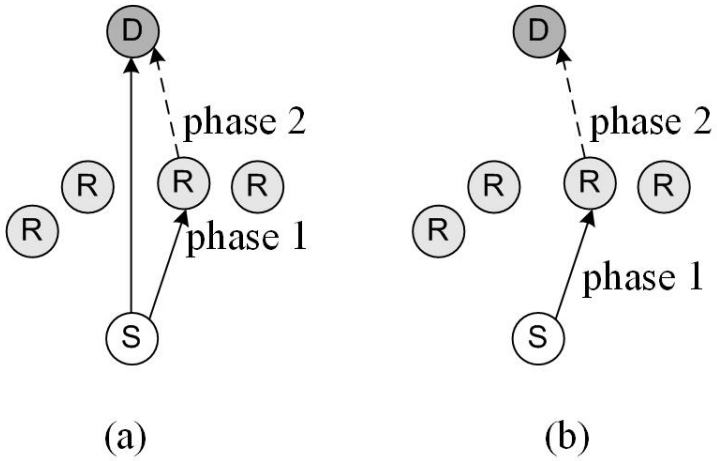

Fig. 7.2: Selection relay diversity: (a) Synchronized two-phase transmission; (b) Multi-hop selection transmission with power schedule or beamforming.

odd while transmit at even time slots. Thus the system is like what we have mentioned in Chapter 1, the delay diversity. But clearly this relay scheme would perform better than delay diversity, since the delayed copies are by turns from two different nodes, so that more diversity gain is expected.

All those schemes (b)-(d) in Fig. 7.1 need the nodes to be accurately synchronized for cooperation. Based on the result we have, I would like to propose a selection relay scheme as in Fig. 7.2, where the best relay is chosen from a bunch of them for cooperation with the source. Some foreseeable advantages are that, first, it allows simpler transmit-receive structure compared to STBC system while with comparable performance as we have seen in Chapter 5. Secondly, it does not need the accurate synchronization as in Fig. 7.1. If the source-to-relay channel is good, we can even reduce the transmission power at phase 1. In other words, in phase one, the source can be dedicated to the transmission to relay and ignore the destination; and the destination decodes only based on the information from the relay node and treats the received signal in phase 1 as interference. An antenna array can also be deployed at the transmitter to allow STBC transmission. Then the result we obtained in Chapter 5 can be directly applied

to such systems. Alternatively, the antenna array at the source can also be used for beamforming. In phase 1, the source dedicates most of its transmission power towards the selected relay node. Then the source-to-destination channel can be ignored as in (b), and the problem becomes a routing problem. The selected relay node can even adopt a "store-and-forward" strategy so that synchronization is almost unnecessary, just like the conventional multi-hop packet network. The cost of such a network is, channel state information of all the links inside the network must be broadcast to all possible source nodes (as we can intentionally add relay nodes to the network to improve the throughput, some nodes can be pure relay nodes), so that the source can independently generate an optimal route for the data transmission. This CSI spreading can be done by either a TDD or an FDD system. In [113], the authors discussed this problem and make some comparisons between the two systems. They suggested a FDD system using analog modulation to quickly feed back the information. This technique can be also used to spread the CSI to the whole network. All those problems discussed in this section are still developing; people are trying to find different ways to exploit the so-called relay diversity for different scenarios. MIMO from a network view is a hot topic for the time being, and without doubt, there are still plenty of things to be explored.

Bibliography

[1] J. Winters, "On the capacity of radio communication systems with diversity in a rayleigh fading environment," *Journal on Selected Areas in Communications, IEEE*, volume SAC-5, pp. 871–878, Jun. 1987

[2] A. Wittneben, "Basestation modulation diversity for digital simulcast," *Proc. Vehicular Technology Conf. (VTC), IEEE*, pp. 848–853, 1991

[3] ——, "A new bandwidth efficient transmit antenna modulation diversity scheme for linear digital modulation," *Proc.International Conf. on Communication (ICC), IEEE*, volume 3, pp. 1630–1634, 1993

[4] N. Seshadri and J.H. Winters, "Two signaling schemes for improving the error performance of frequency-division-duplex (FDD) transmission systems using transmitter antenna diversity," *Proc. Vehicular Technology Conf. (VTC), IEEE*, pp. 508–511, 1993

[5] G.J. Foschini, "Layered space-time architecture for wireless communication in fading environment when using multi-element antennas," *Bell Labs. Tech. J.*, volume 1, no. 2, pp. 41–59, 1996

[6] G.J. Foschini and M.J. Gans, "On limits of wireless communication in a fading environment when using multiple antennas," *Wireless Personal Commun.*, Mar 1998

[7] P.W.Wolniansky, G.J. Foschini, G.D. Golden and R.A. Valenzuel, "V-BLAST: An architecture for realising very high data rates over the rich-scattering wireless channel," *Proc. ISSSE'98*, Sept. 1998

[8] V. Tarokh, N. Seshadri and A. R. Calderbank, "Space-time codes for high data rate wireless communication: Performance criterion and code construction," *Trans. Inform. Theory, IEEE*, volume 44, no. 2, pp. 744–765, 1998

[9] V. Tarokh, A. Naguib, N. Seshadri and A.R. Calderbank, "Space-time codes for high data rate wireless communication: Performance criteria in the presence of channel estimation errors, mobility, and multiple paths," *Trans. Commun., IEEE*, volume 47, no. 2, pp. 199–207, Feb. 1999

[10] M.P. Fitz and J.V. Krogmeier, "Further results on space-time codes fro Rayleigh fading," *Proc. Allerton*, pp. 391–400, Sept. 1998

[11] Q. Yan and R.S. Blum, "Optimum space-time convolutional codes for quasi-static slow fading channels," *Proc. Wireless Communicaitons and Networking Conf. (WCNC), IEEE*, pp. 1351–1355, Sept. 2000

[12] S. Baro, G. Bauch and A. Hansman, "Improved codes for space-time trellis-coded modulation," *Commun. Lett., IEEE*, volume 1, pp. 20–22, 2000

[13] A.R. Hammons and H.E. Gamal, "On the theory of space-time codes for PSK modulaiton," *Trans. Inform. Theory, IEEE*, volume 46, pp. 524–542, Mar. 2000

[14] Y. Liu, M.P. Fitz and O.Y. Takeshita, "A rank criterion for QAM space-time codes," *Proc. IEEE Int.Symp. Information Theory*, pp. 3062–3079, Dec. 2000

[15] S.M. Alamouti, "A simple transmitter diversity scheme for wireless communications," *Journal on Selected Areas in Communications, IEEE*, volume 16, pp. 1451–1458, Oct. 1998

[16] V. Tarokh, H. Jafarkhani and A.R. Calderbank, "Space-time block coding for wireless communications: Performance results," *Journal on Selected Areas in Communications, IEEE*, volume 17, no. 3, pp. 451–460, Mar. 1999

[17] ——, "Space-time block codes from orthogonal design," *Trans. Inform. Theory, IEEE*, volume 45, pp. 1456–1467, Jul. 1999

[18] V. Tarokh and H. Jafarkhani, "A differential detection scheme for transmit diversity," *Journal on Selected Areas in Communications, IEEE*, volume 18, no. 7, pp. 1169–1174, Jul. 2000

[19] H. Jafarkhani and V. Tarokh, "Multiple transmit antenna differential detection from generalized orthogonal designs," *Trans. Commun., IEEE*, volume 47, no. 6, pp. 2626–2631, Sept. 2001

[20] G. Ganesan and P. Stoica, "Differential modulation using space-time block codes," *Signal Processing Lett., IEEE*, volume 9, no. 2, pp. 57–60, Feb. 2002

[21] X. Shao and J. Yuan, "A new differential space-time block coding scheme," *Commun. Lett., IEEE*, volume 7, pp. 437 – 439, 2003

[22] C. Hwang, S.H. Nam, J. Chung and V. Tarokh, "Differential space time block codes using nonconstant modulus constellations," *Trans. Signal Processing, IEEE*, volume 51, pp. 2955 – 2964, Nov. 2003

[23] Z. Liu, G.B. Giannakis and B.L. Hughes, "Double differential space-time block coding for time-selective fading channels," *Trans. Commun., IEEE*, volume 49, no. 9, pp. 1529–1539, Sept. 2001

[24] R. Schober and L. H.-J. Lampe, "Noncoherent Receivers for Differential Space-Time Modulation," *Trans. Commun., IEEE*, volume 50, pp. 768–777, May 2002

[25] T.L. Marzetta and B.M. Hochwald, "Capacity of a mobile multiple-antenna communication link in Rayleigh flat fading," *Trans. Inform. Theory, IEEE*, volume 45, no. 1, pp. 139–157, 1999

[26] B.M. Hochwald and T.L. Marzetta, "Unitary space-time modulation for multiple-antenna communication in Rayleigh flat fading," *Trans. Inform. Theory, IEEE*, volume 46, no. 2, pp. 543–564, 2000

[27] Yardena Arar, "Wireless Networking:Faster! Farther!" *PC World magazine*, Aug. 2005

[28] B.M. Hochwald, T.L. Marzetta, T. Richardson, W. Sweldens and T. Urbanke, "Systematic design of unitary space-time constellation," *Trans. Inform. Theory, IEEE*, volume 46, no. 6, pp. 1962–1973, 2000

[29] B.M. Hochwald and W. Sweldens, "Differential unitary space-time modulation," *Trans. Commun., IEEE*, volume 48, no. 12, pp. 2041–2052, 2000

[30] P.A. Bello and B.D. Nelin, "The influence of fading spectrum on the binary error probabilities of incoherent and differentially coherent matched filter receivers," *IEEE Trans. Commun. Syst.*, volume 10, pp. 160–168, Jun. 1962

[31] N.C. Beaulieu, "On the performance of digital detectors with dependent samples," *Trans. Commun., IEEE*, volume 36, pp. 1248–1253, Nov. 1988

[32] B. Anderson and J. B. Moore, *Optimal Filtering*, Englewood Cliffs, NJ: Prentice-Hall, 1979

[33] R. Clarke, "A statistical theory of mobile-radio reception," *Bell Syst. Tech. J.*, volume 47, p. 957C1000, Jul.CAug. 1968

[34] W.C. Jakes, *Microwave Mobile Communications*, New York: Wiley, 1974

[35] P. Dent, G.E. Bottomley and T.Croft, "Jakes fading model revistied," *Electron. Lett., IEEE*, volume 29, no. 13, pp. 1162–1163, Jun. 1993

[36] M. Patzold and F. Laue, "Statistical properties of Jakes' fading channel simulator," *Proc. Vehicular Technology Conf. (VTC), IEEE*, pp. 712–718, 1998

[37] Y.X. Li and X. Huang, "The generation of independent Rayleigh faders," *Proc.International Conf. on Communication (ICC), IEEE*, pp. 41–45, 2000

[38] Y.B. Li and Y.L. Guan, "Modified Jakes model for simulating multiple uncorrelated fading waveforms," *Proc.International Conf. on Communication (ICC), IEEE*, pp. 46–49, 2000

[39] M.F. Pop and N.C. Beaulieu, "Limitations of sum-of-sinusoids fading channel simulators," *Trans. Commun., IEEE*, volume 49, pp. 699–708, Apr. 2001

[40] C. Xiao, Y.R. Zheng and N.C. Beaulieu, "Second-order statistical properties of the WSS Jakes' fading channel simulator," *Trans. Commun., IEEE*, volume 50, pp. 888–891, Jun. 2002

[41] Y.R. Zheng and C. Xiao, "Improved models for the generation of multiple uncorrelated Rayleigh fading waveform," *Commun. Lett., IEEE*, volume 6, no. 6, pp. 256–258, Jun. 2002

[42] ——, "Simulation models with correct statistical properties for Rayleigh fading channels," *Trans. Commun., IEEE*, volume 51, pp. 920–928, Jun. 2003

[43] E. Telatar, "Capacity of multi-antenna Gaussian channels," *AT&T Bell Labs Internal Technical Memo.*, 1995

[44] V. Tarokh, H. Jafarkhani and A.R. Calderbank, "Correction to 'Space-time block codes from orthogonal design," *Trans. Inform. Theory, IEEE*, volume 46, p. 314, 2000

[45] Z.A. Khan and B.S. Rajan, "A generalization of some existence results on orthogonal designs for STBCs," *Trans. Inform. Theory, IEEE*, volume 50, no. 1, pp. 218–219, Jan. 2004

[46] X.-B. Liang and X.-G. Xia, "On the nonexistence of rate-one generalized complex orthogonal designs," *Trans. Inform. Theory, IEEE*, volume 49, no. 11, pp. 2984 – 2988, Nov. 2003

[47] G. Ganesan and P. Stioca, "Space-time block codes: A maximum SNR approach," *Trans. Inform. Theory, IEEE*, pp. 1650–1656, Apr. 2001

[48] O. Tirkkonen and A. Hottinen, "Square-matrix embeddable space-time block codes for complex signal constellations," *Trans. Inform. Theory, IEEE*, volume 48, pp. 1122–1126, Feb. 2002

[49] W. Su and X.-G. Xia, "Two generalized complex orthogonal space-time block codes for rates 7/11 and 3/5 for 5 and 6 transmit antennas," *Trans. Inform. Theory, IEEE*, volume 49, pp. 313–316, Jan. 2003

[50] X.-B. Liang, "A high-rate orthogonal space-time block code," *Commun. Lett., IEEE*, volume 7, pp. 222–223, May. 2003

[51] C. Xu, Y. Gong and K. B. Letaief, "High-rate complex orthogonal space-time block codes for high number of transmit antennas," *Proc.International Conf. on Communication (ICC), IEEE*, volume 2, pp. 20–24, Jun. 2004

[52] H. Wang and X.-G. Xia, "Upper bounds of rates of space-time block codes from complex orthogonal designs," *Trans. Inform. Theory, IEEE*, volume 49, pp. 2788–2796, Oct. 2003

[53] W. Su, X.-G Xia and K.J. Ray Liu, "A systematic design of high-rate complex orthogonal space-time block codes," *Commun. Lett., IEEE*, volume 8, pp. 380–382, Jun. 2004

[54] W. Su and X.-G. Xia, "Quasi-orthogonal space-time block codes with full diversity," *Proc. Global Telecommunications Conf.. (GLOBECOM), IEEE*, volume 2, pp. 1098 – 1102, Nov. 2002

[55] M. Uysal and C.N. Georghiades, "Non-orthogonal space-time block codes for 3Tx antennas," *Electron. Lett., IEEE*, volume 38, pp. 1689–1691, Dec. 2002

[56] G. Wang, W. Su and X.-G. Xia, "Orthogonal-like space-time coded CPM with fast demodulation for three and four transmit antennas," *Proc. Global Telecommunications Conf.. (GLOBECOM), IEEE*, pp. 3321–3325, 2003

[57] R. Ran, J. Hou and M.H. Lee, "Triangular non-orthogonal space-time block code," *Proc. Vehicular Technology Conf. (VTC), IEEE*, volume 1, pp. 292–295, Apr. 2003

[58] Z. Li and G. Hu, "Space-time block codes based on coordinate symmetric orthogonal designs," *Electron. Lett., IEEE*, volume 39, pp. 670–671, Apr. 2003

[59] J. Hou, M.H. Lee and J.Y. Park, "Matrices analysis of quasi-orthogonal space-time block codes," *Commun. Lett., IEEE*, volume 7, pp. 385–387, Aug. 2003

[60] A. Boariu and D.M. Ionescu, "A class of nonorthogonal rate-one space-time block codes with controlled interference," *Trans. Wireless Commun., IEEE*, volume 2, pp. 270–276, Mar. 2003

[61] C. Yuen, Y.L. Guan and T.T. Tjhung, "Orthogonal space-time block code from amicable complex orthogonal design," *Proc. Int. Conf., Acoustics, Speech, and Signal Processing (ICASSP), IEEE*, volume 4, pp. 469–472, 2004

[62] P.Y. Kam, "Optimal detection of digital data over the nonselective Rayleigh fading channel with diversity reception," *Trans. Commun., IEEE*, volume 39, pp. 214–219, Feb. 1991

[63] B.L. Hughes, "Space-time group codes," *Conference Record of the Thirty-Fourth Asilomar Conference on Signals, Systems and Computers*, volume 1, pp. 699–704, Oct. 2000

[64] ——, "Differential space-time modulation," *Trans. Inform. Theory, IEEE*, volume 46, no. 7, pp. 2567–2578, Nov. 2000

[65] C. Cozzo and B.L. Hughes, "Joint channel estimation and data symbol detection in space-time communications," *Proc.International Conf. on Communication (ICC), IEEE*, pp. 287–291, Jun. 2000

[66] Y. Li, C. N. Georghiades and G. Huang, "Sequence estimation for space-time coded systems," *Trans. Commun., IEEE*, volume 49, pp. 948–951, Jun. 2001

[67] Z. Baranski and A.M. Haimovich, "EM-based iterative receiver for space-time coded modulation with noise variance estimation," *Proc. Global Telecommunications Conf.. (GLOBECOM), IEEE*, volume 1, pp. 355–359, 2002

[68] C. Gao, A. Haimovich and D. Lao, "Bit error probability for space-time block code with coherent and differential detection," *Proc. Vehicular Technology Conf. (VTC), IEEE*, Sept. 2002

[69] J. Yuan, "On the performance of space-time block codes on slow rayleigh fading channels," *Proc. Personal, Indoor and Mobile Radio Communications (PIMRC), IEEE*, volume 2, pp. 1688–1692, Sept. 2003

[70] H. Shin, and J. H. Lee, "Performance analysis of space-time block codes over keyhole Nakagami-m fading channels," *Trans. Vehicular Tech., IEEE*, volume 53, no. 2, pp. 351–362, Mar 2004

[71] G. R. Mohammad-Khani, V. Meghdadi, J. P. Cances and L. Azizi, "Maximum likelihood docoding rules for STBC generalized framework for detection and derivation of accurate upperbounds," *Proc.International Conf. on Communication (ICC), IEEE*, volume 5, pp. 2578–2583, Jun. 2004

[72] P. Garg, R.K. Mallik and H.A. Gupta, "Performance analysis of space-time coding with imperfect channel estimation," *Personal Wireless Communications, 2002 IEEE International Conference on*, pp. 71–75, Dec. 2002

[73] H. Cheon and D. Hong, "Performance analysis of space-time block codes in time-varying Rayleigh fading channels," *Proc. Int. Conf., Acoustics, Speech, and Signal Processing (ICASSP), IEEE*, volume 3, pp. 2357–2360, 2002

[74] Z. Liu, X. Ma and G.B. Giannakis, "Space-time coding and Kalman filtering for time-selective fading channels," *Trans. Commun., IEEE*, volume 50, pp. 183–186, Feb. 2002

[75] P.Y. Kam and C.H. Teh, "An adaptive receiver with memory for slowly fading channels," *Trans. Commun., IEEE*, volume 32, pp. 654–659, Jun. 1984

[76] J.K. Cavers, "An analysis of pilot symbol assisted modulation for Rayleigh fading channel," *Trans. Vehicular Tech., IEEE*, volume 40, no. 4, pp. 686–693, Nov. 1991

[77] P.Y. Kam and C.H. Teh, "Reception of PSK signals over fading Channels via Quadrature Amplitude Estimation," *Trans. Commun., IEEE*, volume 31, pp. 1024–1027, Aug. 1983

[78] G. Tarrico and E. Biglieri, "Decoding space-time coding with imperfect channel estimation," *Proc.International Conf. on Communication (ICC), IEEE*, Jun. 2004

[79] J. G. Proakis, *Digital Communication*, McGraw-Hill, 3rd edition, 1995

[80] P.J. Lee, "Computation of the bit error rate of coherentM-ary PSK with Gray code bit mapping," *Trans. Commun., IEEE*, volume COM-34, pp. 488–491, May 1986

[81] M. Schwartz, W.R. Bennett and S. Stein, *Communication Systems and Techniques*, New York: McGraw-Hill, 1996

[82] G.L. Stuber, *Principles of Mobile Communication*, Boston:Kluwer Academic, 1996

[83] T. Eng, N. Kong and L.B. Milstein, "Comparison of diversity combining techniques for Rayleigh-fading channels," *Trans. Commun., IEEE*, volume 44, pp. 1117–1129, Sept. 1996

[84] N. Kong and L.B. Milstein, "Average SNR of a generalized diversity selection combining scheme," *Commun. Lett., IEEE*, volume 3, pp. 57–59, Mar. 1999

[85] ——, "A closed form expression for the average SNR when combining an arbitrary number of diversity branches with non identical Rayleigh fading statistics," *Proc.International Conf. on Communication (ICC), IEEE*, volume 3, pp. 1864–1868, Jun. 1999

[86] M-S. Alouini and M.K. Simon, "An MGF-based performance analysis of generalized selection combining over Rayleigh fading channels," *Trans. Commun., IEEE*, volume 48, pp. 401–415, Mar. 2000

[87] M.K. Simon and M-S. Alouini, "Performance analysis of generalized selection combining with threshold test per branch (T-GSC)," *Trans. Vehicular Tech., IEEE*, volume 51, pp. 1018–1029, Sept. 2002

[88] A. Annamalai and C. Tellambura, "A new approach to performance evaluation of generalized selection diversity receivers in wireless channels," *Proc. Vehicular Technology Conf. (VTC), IEEE*, volume 4, pp. 2309–2313, Oct. 2001

[89] Y. Ma and C.C. Chai, "Unified error probability analysis for generalized selection combining in Nakagami fading channels," *Journal on Selected Areas in Communications, IEEE*, volume 18, pp. 2198–2210, Nov. 2000

[90] M.K. Simon and M-S. Alouini, "A unified performance analysis of digital communication with dual selective combining diversity over correlated Rayleigh and Nakagami-m fading channels," *Trans. Commun., IEEE*, volume 47, pp. 33–43, Jan. 1999

[91] C.M. Lo and W.H. Lam, "Approximate BER performance of generalized selection combining in Nakagami-m fading," *Commun. Lett., IEEE*, volume 5, pp. 254–256, Jun. 1999

[92] H. Fu and P.Y. Kam, "Performance comparison of selection combining schemes for binary DPSK on nonselective Rayleigh-fading channels with interference," *Trans. Wireless Commun., IEEE*, volume 4, pp. 192–201, Jan. 2005

[93] L. Xiao and X. Dong, "Effect of imperfect channel estimation on the performance of selection combining in Rayleigh fading channels," *Proc. Global Telecommunications Conf.. (GLOBECOM), IEEE*, volume 6, pp. 3641–3645, Dec. 2004

[94] S.W. Kim and E.Y. Kim, "Optimum receive antenna selection minimizing error probability," *Proc. Wireless Communicaitons and Networking Conf. (WCNC), IEEE*, volume 1, pp. 441–447, Mar. 2003

[95] X. N. Zeng and A. Ghrayed, "Performance bounds for space-time block codes with receive antenna selection," *Trans. Inform. Theory, IEEE*, volume 50, pp. 2130–2137, Sept. 2004

[96] M.K. Simon and M.S. Alouini, *Digital communication over fading channels - a unified approach to performance analysis*, Wiley&Sons, Inc., 2000

[97] S. Zhang, P.Y. Kam and P. Ho, "Performance of pilot-symbol-assisted-modulation with transmit-receive diversity in nonselective Rayleigh fading channels," *Proc. Vehicular Technology Conf. (VTC), IEEE*, volume 3, pp. 1840–1844, Sept. 2004

[98] D.A. Gore and A.J. Paulraj, "MIMO antenna subset selection with space-time coding," *Trans. Signal Processing, IEEE*, volume 50, no. 10, pp. 2580–2588, Oct. 2002

[99] Z. Chen, J. Yuan, B. Vucetic and Z. Zhou, "Performance of Alamouti scheme with transmit antenna selection," *Proc. Personal, Indoor and Mobile Radio Communications (PIMRC), IEEE*, volume 2, pp. 1135–1141, Sept. 2004

[100] ——, "Performance analysis of space-time trellis codes with transmit antenna selection in Rayleigh Fading Channels," *Proc. Wireless Communicaitons and Networking Conf. (WCNC), IEEE*, volume 4, pp. 2456–2462, Mar. 2004

[101] A. Ghrayeb and T.M. Duman, "Performance analysis of MIMO systems with antenna selection over quasi-static fading channels," *Trans. Vehicular Tech., IEEE*, volume 52, pp. 281–288, Mar. 2003

[102] X. Liang and X. Xia, "Unitary signal constellations for differential space-time modulation with two transmit antennas: Parametric codes, optimal designs, and bounds," *Trans. Inform. Theory, IEEE*, volume 48, no. 8, pp. 2291–2322, Aug. 2002

[103] ——, "Some unitary signal constellations for differential space-time modulation," *Conference Record of the Thirty-Fourth Asilomar Conference on Signals, Systems and Computers*, volume 1, pp. 716–720, 2000

[104] Z. Sun and T. T. Tjhung, "On performance analysis and design criteria for trellis coded differential unitary space-time modulation," *Proc.International Conf. on Communication (ICC), IEEE*, volume 5, pp. 3477–3481, May 2003

[105] M. Tao and R.S. Cheng, "Trellis-coded differential unitary space-time modulation over flat fading channels," *Trans. Commun., IEEE*, volume 51, pp. 587–596, Apr. 2003

[106] A. Sendonaris, E. Erkip and B. Aazhang, "Increasing uplink capacity via user cooperation diversity," *"Proc. of 1998 IEEE Inter. Symp. on Inform. Theory"*, p. 156, Aug. 1998

[107] ——, "User cooperation diversity - Part I: System description," *Trans. Commun., IEEE*, volume 51, no. 11, pp. 1927–1938, Nov. 2003

[108] ——, "User cooperation diversity - Part II: Implementation aspects and performance analysis," *Trans. Commun., IEEE*, volume 51, no. 11, pp. 1939–1948, Nov. 2003

[109] J. Laneman and G. Wornell, "Distributed space-time coded protocols for exploiting cooperative diversity in wireless networks," *Trans. Inform. Theory, IEEE*, volume 49, no. 10, pp. 2415–2425, Oct. 2003

[110] J. Laneman, D. Tse and G. Wornell, "Cooperative Diversity in Wireless Networks: Efficient Protocols and Outage Behavior," *Trans. Inform. Theory, IEEE*, volume 50, no. 12, pp. 3062–3080, Dec. 2004

[111] P. Mitran, H. Ochiai and V. Tarokh, "Space-time diversity enhancements using collaborative communications," *Trans. Inform. Theory, IEEE*, volume 51, no. 6, pp. 2041–2057, Jun. 2005

[112] T.J. Oechtering and A. Sezgin, "A new cooperative transmission scheme using the space-time delay code," *Smart Antennas, 2004. ITG Workshop on*, pp. 41–48, 2004

[113] T.L. Marzetta and B.M. Hochwald, "Fast transfer of channel state information in wireless systems," *Submitted to IEEE Transactions on Signal Processing*

List of Publications

[1] **Cheng Shan**, P.Y. Kam, A. Nallanathan, "Theoretical Performance of Space-Time Block Coded Systems with Channel Estimation", *Global Telecommunications Conference, 2004. GLOBECOM '04. IEEE,* vol. 6, pp. 3666-3670, 29 Nov.-3 Dec., 2004

[2] **Cheng Shan**, P.Y. Kam, A. Nallanathan, "On the Performance of Space-Time Block Coded Systems with Channel Estimation", *IEEE Vehicular Technology Conference, 2004. VTC2004-Fall,* vol.4, pp. 2439-2443, Sept. 2004

[3] H. Tan, P. Ho, P. Y. Kam and **Cheng Shan**, "An Adaptive Coherent Receiver for MPSK/MDPSK over the Nonselective Rayleigh Fading Channel with Unknown Characteristics," to appear on *IEEE Transation on Wireless Communications* Nov. 2005.

[4] **Cheng Shan**, A. Nallanathan, P.Y. Kam, "A New Class of Signal Constellations for Differential Unitary Space-Time Modulation (DUSTM)," *Communications Letters, IEEE*, Vol. 8, Issue 1, Jan. 2004, pp. 1-3

[5] **Cheng Shan**, A. Nallanathan, P.Y. Kam, "Signal constellations for differential unitary space-time modulation with multiple transmit antennas," *IEEE Vehicular Technology Conference*, 2003. *VTC 2003-Spring*, vol.1, pp. 713-716, 22-25 April 2003

[6] **Cheng Shan**, P.Y. Kam, A. Nallanathan, "A Symbol-by-Symbol Channel Estimation Receiver for Space-Time Block Coded Systems and Its Performance Analysis," submitted to *IEEE Trans.Commun.*

[7] **Cheng Shan**, P.Y. Kam, A. Nallanathan, "Selection combining in the presence of imperfect channel estimation for space-time block codes," under preparation for submission to *IEEE Trans. Vehicular Techn.*.

[8] **Cheng Shan**, P.Y. Kam, A. Nallanathan, "Space-time block coded system with transmit selection and channel estimation," under preparation for submission to *IEEE Transation on Wireless Communications*.